Sveučilište u Rijeci
POMORSKI FAKULTET U RIJECI
FACULTY OF MARITIME STUDIES RIJEKA
University of Rijeka

University of Zagreb
Faculty of Transport
and Traffic Sciences

Royal Institute of Navigation
Science Technology Practice

ISSN 1849-7306

10th Annual Baška GNSS Conference

PROCEEDINGS

Baška, Krk Island, Croatia
8 – 10 May 2016

Sveučilište u Rijeci
POMORSKI FAKULTET U RIJECI
FACULTY OF MARITIME STUDIES RIJEKA
University of Rijeka

University of Zagreb
Faculty of Transport
and Traffic Sciences

Royal Institute of Navigation
Science Technology Practice

ISSN 1849-7306

10th Annual Baška GNSS Conference

PROCEEDINGS

Baška, Krk Island, Croatia
8 – 10 May 2016

Published by:
University of Rijeka, Faculty of Maritime Studies Rijeka, Rijeka, Croatia
The Royal Institute of Navigation, London, UK

For the Publisher:
Associate Professor Alen Jugović, Ph. D., Dean, Faculty of Maritime Studies, Rijeka, Croatia

Publishing Associates:
Captain James B. Taylor, OBE RN, President, The Royal Institute of Navigation
Captain Peter Chapman-Andrews, LVO MBE RN, Director, The Royal Institute of Navigation

Editors:
Full Professor Serdjo Kos, Ph. D., FRIN, Faculty of Maritime Studies Rijeka
Associate Professor Renato Filjar, Ph. D., FRIN, Faculty of Maritime Studies Rijeka
Assistant Professor David Brčić, Ph. D., Faculty of Maritime Studies Rijeka

Front-page photo credits:
Associate Professor Renato Filjar, Ph. D., FRIN, Faculty of Maritime Studies Rijeka

Text formatting:
Tempora, Rijeka

Print:
AKD d.o.o. Zagreb

Address:
Faculty of Maritime Studies Rijeka
Studentska 2
51000 Rijeka
Croatia
Phone: +385 (0)51 338 411
Fax: +385 (0)51 336 755
URL: http://www.pfri.uniri.hr/
E-mail: dekanat@pfri.hr

ISSN 1849-7306

CONTENTS

PREFACE

Navigation is a science, a skill, but principally the way of life.

Enhanced with the ingenious invention of the late Sir Arthur C Clarke, it is mostly practiced as the satellite one in modern times. Still, the satellite navigation is prone to many error sources and the other causes of satellite navigation performance and operation disruptions, rendering satellite navigation, now a global enabling technology, particularly vulnerable.

Recognising a raising problem with potentially disastrous effects on technology and business, a group of satellite navigation specialists and enthusiasts gathered ten years ago in Baška, Krk Island, Croatia to discuss the challenges and prepare the answers. This gathering originated what was called GNSS Vulnerabilities and Solutions Conference series, later re-branded to the Annual Baška GNSS Conference.

Organised on behalf of The Royal Institute of Navigation (RIN, London, UK), the conference series has immediately found its place on the global map of GNSS activities, along with the names of Washington, Moscow, Beijing, San Francisco, Bruxelles, Portland, Sankt Petersburg and Shanghai – to name just a handful. A tiny little town on the Adriatic island of Krk, former sailors' village and now a famous holiday resort, has started to attract GNSS specialists, scientists, engineers, technology and business developers, policy and strategy developers, users, students, media representatives and general audience. And those who came for the first time have continued to do so.

Prof J David Last, FRIN (then-President) and Gp Capt David Broughton, FRIN (then-Director) of The Royal Institute of Navigation, London, UK had established the conference series by setting up its substance, aim and course. The tradition has continued with provision of unlimited support to conference series organisation from all the succeeding Presidents (including the current President Capt James B Taylor, FRIN, and the past President Roger A McKinley, FRIN) and Directors Capt Peter Chapman-Andrews and Mr John R Pottle, FRIN). The huge energy flying effortlessly from the 1 Kensington Gore RIN HQ in London has been met in Croatia by a small, but devoted local team of organisers led by Professors Serdjo Kos of Faculty of Maritime Studies, University of Rijeka, Tomislav Kos of Faculty of Electrical Engineering and Computing, University of Zagreb, and Hrvoje Gold of Faculty of Transport and Traffic Sciences, University of Zagreb. Local community has appreciated a world-class event organised every year in Baška with its traditional hospitality immersed in the unique beauty of the Baška Valley and its Mediterranean atmosphere.

Ms Djurdja Daljevac (and later Ms Ivana Topić, her successor) of Hoteli Baška, Ms Majda Šale of Krk Tourist Office, Baška's Mayor Mr Toni Juranić, and Klapa Tramuntana have always done their best in organising fantastic accommodation, supporting social programmes and making every event in the conference series memorable.

GNSS operators have recognised the importance of the Annual Baška GNSS Conference series, thus allowing every single one of the events to start with the plenary outlining the most recent developments in GPS, GLONASS, Beidou and Galileo/EGNOS system, presented by top officials. It is with honour and delight to remember presentations given by long-standing contributors Mr Robert Crane (USA), Prof Grigory Stupak (Russia), Prof Jingnong Weng (China), Ms Marta Kriwanis-Brzostowska (EU GSA) and many others.

With a real global outreach and aiming at development of international co-operation on joint actions on tackling GNSS vulnerabilities and resilient GNSS development, the conference soon attracted the attention of the UN International Committee on GNSS. On behalf of the UN OOSA in Vienna, Austria, Ms Sharafat Gadimova provided a continuous support to the conference organisation and its steering towards the most important subjects at the time. Ms Gadimova's boundless energy devoted to the conference organisation, her informative presentations, and affable personality have opened the room for even larger and more successful international co-operation, and expanded the number highly-qualified contributors to the Annual Baška GNSS Conference.

Space weather and ionospheric disturbances have already been recognised as the most serious threats to satellite navigation. Dr Ljiljana Cander of the Rutherford Appleton Laboratory, Chilbolton, UK brought to the conference's stage a number of space weather scientists, rendering the conference a multi-disciplinary event capable of tackling increasingly complex subjects.

Ten years have passed quickly. The conference is now mature, but still evolving towards more enjoyable, informative and result-rich gatherings. It is encouraging and delightful to observe that numerous young GNSS specialists join the conference, with some of them to appear soon in the regular conference proceedings not only as authors, but as the capable and confident experts at the conference's helm, steering it again to Baška. Every year. As usual.

The rest is the history, as recorded in proceedings such as this one, you are just reading.

We look forward for both the privilege and pleasure of meeting you in Baška in the years to come.

Editors

Sveučilište u Rijeci
POMORSKI FAKULTET U RIJECI
FACULTY OF MARITIME STUDIES RIJEKA
University of Rijeka

University of Zagreb
Faculty of Transport
and Traffic Sciences

Royal Institute of Navigation
Science Technology Practice

10th Annual Baška GNSS Conference

PROCEEDINGS

THE NAVIGATION OF NAVIGATION

Professor David Last

Royal Institute of Navigation
Past-President

We professionals in the navigation business are the stewards of an exceptionally successful technology. Satellite navigation has been one of the outstanding technical achievements of the late twentieth and early twenty-first centuries. Among science-based industries, it has been a star. It does not pollute the atmosphere, cause global warming, or involve fracking; everybody loves GNSS!

But satellite navigation has now raised challenges that navigation professionals – and especially their governments – appear unable to meet.

Life used to be so simple: proper navigators were all professionals. They wore uniforms and they had beards! Sailors knew nothing about navigating an airliner and the technologies of roads and land vehicles were different again. Matching government departments administered these quite separate activities and helped achieve international cooperation and standardisation. But those modes of transport remained apart.

God was in his Heaven and all was well until along came this wretched satellite navigation and spoiled it! Soon, a

single technology served us across all modes of transport. And then it escaped from us navigators and became a tool for many professions, and finally, heaven forbid, a consumer product.

The report in Figure 1, by the UK's Royal Academy of Engineering, struggled to find a single area of transportation, of commerce, of industry or of telecommunications that does not now employ satellite navigation.

Figure 1

My government, your government, governments around the world were completely unprepared to respond to this single technology on which depended, and from which profited, activities as diverse as missiles, farming and the stock market. Governments had separate ministries for each of those things: not only for the traditional modes of transport – land, air and sea – but also for industry and trade and communications. Absolutely no-one was responsible for setting national policy in navigation: there simply was no clear plan for the navigation of navigation!

Yet such leadership had become essential, especially outside the United States as governments came to realise that this GPS, this technology on which so much in their economies depended, was controlled not only by a foreign power – the US – but ultimately by its military!

Figure 2

In response, those countries – or regions like Europe – that could afford to, set up their own satellite navigation systems (Figure 2). So GPS, which much earlier had inspired GLONASS, now begat Beidou and QZSS, Galileo and IRNSS. Plus a host of augmentation systems: WAAS and EGNOS and other funny names.

Soon, these new "GNSS" became invested with immense national pride. Their vast cost had to be justified by claims of technical superiority. In reality, we engineers know that their designers had no choice but to make them largely compatible with GPS, since GPS was decades ahead and the world standard. And these new systems had to squeeze alongside GPS into the narrow radio bands allocated to navigation. Not surprisingly – indeed happily – all our GNSS turned out to look very like GPS: versions of the same technology – with just a hint of garlic here, a whiff of curry there! This similarity is obvious to engineers and to navigators, but rarely to politicians.

And now each of these new systems is following a similar trajectory to that of GPS. For its first decade, GPS was seen as the way to meet every significant navigation need; to replace all older aids across land, sea and air. That was the clear view of the US Government Accountability Office, and is now the view of Galileo in Europe. And why not? The growth of GPS did indeed result in the demise of Omega, Decca Navigator and a host of national systems you have

never heard of, that simply couldn't compete technically or commercially. But this triumph of satellite navigation bred a certain hubris: overbearing pride.

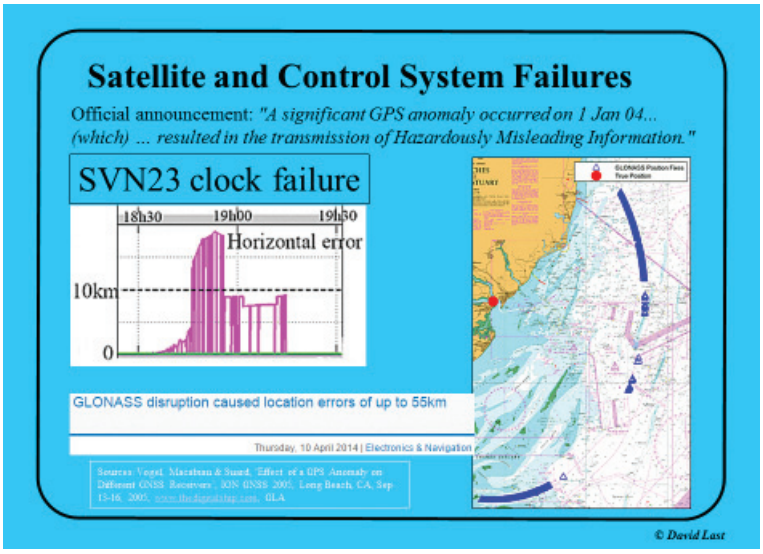

Figure 3

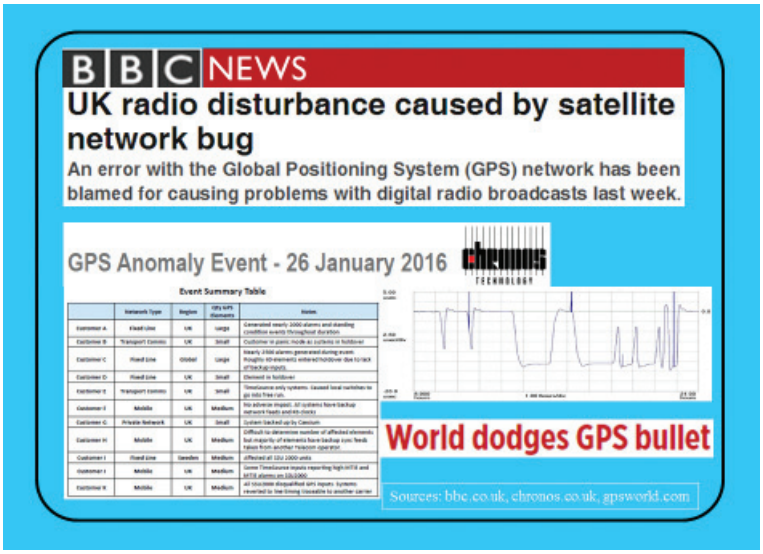

Figure 4

Unexpected events and vulnerabilities began to shake confidence in GPS. As Figure 3 shows, the final atomic clock in satellite SVN23 failed, causing large position errors. Then we had a double failure of GLONASS – suddenly, errors of 55 kilometres. Then on 26 January this year a failure of GPS timing (Figure 4) took broadcasting systems off the air and affected communications worldwide for many hours.

On the day shown in Figure 5, the Sun emitted radio noise so intense that GPS receivers stopped working across the entire sunlit side of the Earth. In another event – until recently denied – GPS navigation was lost, accidentally, and without warning for two hours, across the San Diego area. Many mobile cell-phone sites using GPS timing were affected.

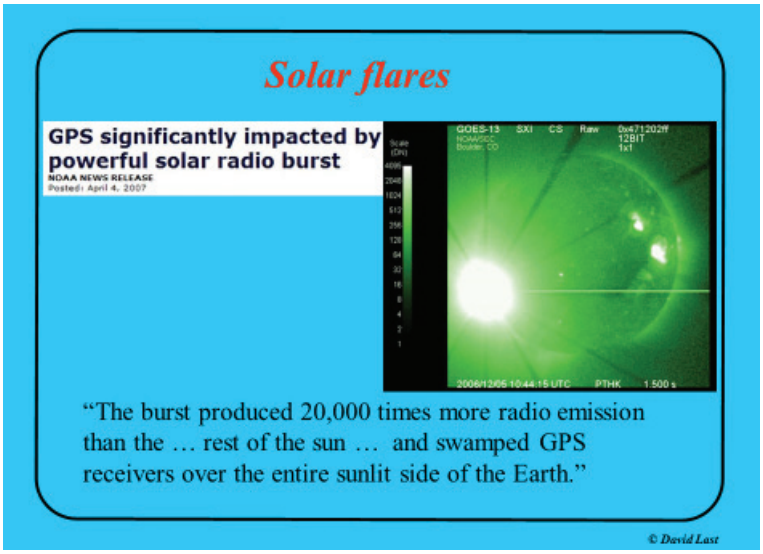

Figure 5

And then intentional jamming appeared on the scene. A low-power jamming device tested at a British lighthouse (Figure 6, upper left) disrupted GPS throughout the red zone shown there, out across the North Sea to the horizon at 30 km. The blue line (Figure 6, upper right) is the track of a vessel: in the main jamming beam it loses GPS entirely. But either side the jammer caused all the false positions shown; other ships appeared to track over land.

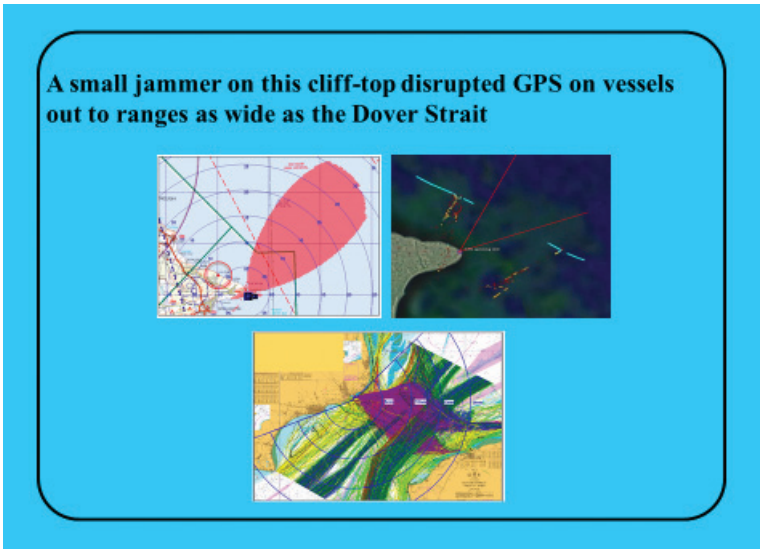

Figure 6

Figure 7

The effect of jamming on a ship is dramatic, as shown in Figure 7. A jammer of less than one thousandth of a watt aboard this vessel caused false positions on the chart displays; the autopilot would steer the ship quietly off course; and the

ship reported those false positions via AIS to other ships nearby and to the shore; it lost satellite communications; the distress system that raises alarms and guides in rescuers failed; even the ship's clocks went wrong. And when the officers sensibly reverted to radar and gyrocompass, to their surprise they found those affected too. Ships nowadays – like many of our critical systems ashore – have multiple GPS receivers embedded in multiple systems in ways no-one understands. When one receiver fails, they all fail.

Again this year we have seen a sovereign state launch prolonged high-powered GPS jamming attacks on its neighbour, impacting maritime navigation, aviation, cell-phones and critical military capabilities.

Figure 8

The little hand-held jammer in Figure 8, sold world-wide, is hundreds of times more powerful than early ones. It has been carefully designed to block all the new GPS frequencies, plus all the frequencies of Galileo plus Beidou plus QZSS. It also jams all our augmentations, like EGNOS, as well.

Terrorists can buy or build a jammer powerful enough to affect large areas of a major city from a publically-accessible location. But in many parts of the world – maybe yours – there are now a powerful local myth: that our version of GNSS is immune to GPS jamming.

In the United States 15 years ago, growing concern among navigation professionals culminated the Volpe Report of the Department of Transportation. This clearly and officially recognised the multiple threats posed by the vulnerability of GPS – and recommended independent backup systems. Since then, interference and jamming events have multiplied in all our countries. A detector on a UK highway close to the threshold of a UK regional airport gets up to 200 jamming hits a month. Similar data has been reported in France and the USA. Mariners report GPS outages. There is no question: there are plenty of jammers out there.

Figure 9

Now there is this new threat of "spoofing": that is, transmitting false GNSS signals that take over a receiver. Researchers used a laptop and spoofer to lead the super-yacht shown In Figure 9 silently off course. There was no alarm on the bridge to tell the crew they were sailing into danger. In the future, when criminals hijack a truck, a spoofer will make its on-board tracker show it remaining on schedule, when really they have diverted and robbed it. And researchers have now demonstrated how to shift precise GPS timing. This opens the door to fraud, spoofing the automated systems of banks and stock exchanges with their million trades a second. It may also allow the disruption of power grids. Low-cost spoofers (Figure 9) have now appeared; any competent hacker can build a

spoofer for a few hundred dollars and take over GNSS receivers. I watched a spoofer demonstrated recently in an English country pub!

So, what can we do about this vulnerability of satellite navigation, to: jamming, spoofing, interference, solar weather or equipment failure? Well, first, we must recognise the problem and face up to the need for Resilient Position, Navigation and Timing. Almost without exception, engineers and practising navigators now do so. Almost without exception, politicians do not.

Of course, as Professor Brad Parkinson has argued, we must protect and harden our technology. We will use these intelligent adaptive receiving antennas that favour satellite signals over interferers. The military already do that, and the very top of the civil market will. But they are only a remote possibility for the mass of vulnerable users already out there.

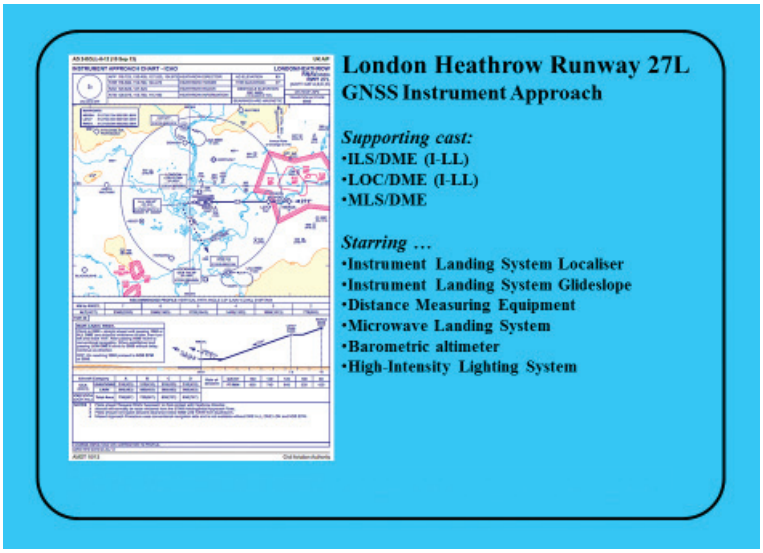

Figure 10

We will integrate satellite navigation with other technologies: dead-reckoning in land vehicles, atomic clocks for precise telecomms timing. But the powerful solutions are navigation and timing technologies independent of GNSS yet complementary to it. Aviation is rich in these. It has maintained multiple independent and compatible technologies. So, London Heathrow runway 27 Left now has the GNSS Instrument Approach shown in Figure 10. But it is supported

by an ILS, an MLS, DME, VOR, ADF, inertial navigation, radar and baro altimeters and magnetic compasses. And that aviation GNSS has mandatory RAIM and WAAS and compulsory reversion to a legacy system as soon as GNSS is less than perfect. What a contrast with maritime or land practice!

The Volpe Report mentioned above prompted the US Federal Aviation Administration to propose and demonstrate Enhanced Loran (eLoran) (Figure 11). By applying GPS digital techniques to the obsolete Loran C low-frequency technology, they created a new system that met the accuracy, integrity, availability and continuity standards of certain aircraft instrument approaches plus the demanding port entrance requirements of shipping. And it could deliver timing of GPS quality to support telecommunications. A high-level study group of industry leaders concluded that this was the only cost-effective substitute for US needs.

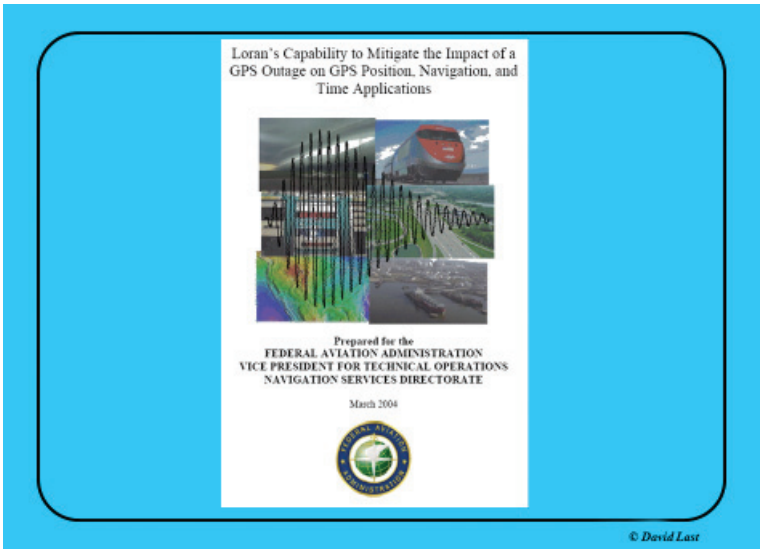

Figure 11

The US Department of Homeland Security announced the adoption of eLoran as the US national backup to GPS – and then completely failed to implement it! Delivering a navigation system that benefits multiple areas of national life has turned out to be beyond the capabilities of governments. In Washington, no single department owned either civil GPS, or this powerful new backup. So when it came to cost-benefit analyses there was simply no-one to aggregate the

benefits across the whole of government, industry and commerce. Each department feared being landed with the costs. Before that dilemma was resolved, a budget cut closed down the obsolete Loran-C system recently modernised for the move to eLoran!

In response to the US announcement on eLoran, the United Kingdom and Ireland took the concept and created a prototype system, re-using obsolete Loran-C infrastructure from the north of Norway to the south of France, and adding a brand new station. It achieved Initial Operational Capability with 10-metre accuracy and full compliance with IMO standards at those 7 major UK ports shown in yellow in Figure 12. Ship-borne equipment switched automatically and seamlessly to eLoran when GPS was lost. Separately, a high-precision version of the technology was demonstrated by the maritime pilots at Rotterdam, Europe's largest port.

Figure 12

So, has Europe recognised GNSS vulnerability and adopted an insurance policy? No! Those prototype systems were terminated at New Year, when Norway, Denmark, Germany and France switched off their stations. Europe simply has no viable plan to respond to the vulnerability of GNSS – why, who needs a plan when Europe has Galileo and EGNOS?! There has never been a Volpe Report on vulnerability in Europe or anywhere outside the US.

What appears to be happening now is interesting: in both the US and Europe industry looks likely to take over the Loran infrastructure, with plans to sell the eLoran service to users. These will firstly be in telecommunications and broadcasting, industries that now see the need for resilient timing, and also to individual government departments. The market – and good old greed! – will provide the mechanism for realising those benefits, paying the costs and making a profit.

What this example of GNSS vulnerability and eLoran has clearly shown is the lack of any informed debate on this matter in many countries. Thirty-eight years after the launch of the first GPS satellite, there is still little recognition by governments anywhere in the world, of how essential resilient Position, Navigation and Timing have become to the critical infrastructure of their nations. Our immensely successful navigation industry has simply out-stripped our systems of government.

Figure 13

Our world is changing fast: we now have all the constellations of satellites shown in Figure 2. But I suggest that we are approaching the end of the "Era of Constellations". To clarify: those who operate GPS, GLONASS, Beidou or Galileo each have a view of their own constellation, consisting of satellites, control systems, receivers, applications and users. All these are overseen by a

national or regional administration: so, Europeans speak of "Galileo markets" and the US government speaks of "GPS markets".

There is friction over constellations. In Europe the question is: might Galileo be mandated?; in the US: is the reception of "foreign" GNSS illegal, immoral, un-American? The current view is that of governments and diplomats: separate control, spheres of influence, geo-political competition for dominance.

But most users of satellite navigation and timing now look at the world completely differently. See, for example, the screen of the Sony smartphone, an Android, in London, shown in Figure 13. If you look carefully you can see that it is receiving 7 GPS satellites, but also 7 GLONASS and 3 Beidou. These all contribute to the GNSS position fix. To this phone, Galileo and GPS are each just 30 satellites among what may soon be 140. All those satellites are either GPS-like or WAAS-like. The differences between the constellations are of compelling interest to Geeks and to the governments who have paid for them. But most users have simply never heard of "Galileo" or "Beidou", and nor do they care. They call them all "GPS"! So a government that mandates a single system is denying its citizens the benefits of today's GNSS chips that already use multiple constellations. Which world-view will prevail: individual constellations or this world GNSS?

Figure 14

On the left of Figure 14 we see the satellites being received by the smart-phone in Figure 13. But then a low-powered jammer is switched on close by. In a few seconds (the right-hand picture) all the signals have disappeared: GPS, GLONASS and Beidou! I suggest: we are already in the "Era of GNSS". The constellations now all live together – and as here, they die together; they have simply become components of a single GNSS.

I suggest that the time has come to stop focussing on constellations, whether satellite or terrestrial, and instead find ways to deliver to users world-wide the resilient PNT they need and deserve. Technically we can do that. But to implement it requires political will and wisdom. So, we need something else, and we need it urgently and nationally and internationally. It is this: a clear way ahead to that goal, a path, a course, a direction, a flight-plan for: the navigation of navigation.

Sveučilište u Rijeci
POMORSKI FAKULTET U RIJECI
FACULTY OF MARITIME STUDIES RIJEKA
University of Rijeka

University of Zagreb
Faculty of Transport
and Traffic Sciences

Royal Institute of Navigation
Science Technology Practice

10th
Annual
Baška GNSS
Conference

EMERGING TECHNOLOGIES IN E-NAVIGATION

Gareth Wimpenny, Alan Grant

The General Lighthouse Authorities of the United Kingdom and Ireland
E-mail: Gareth.Wimpenny@gla-rrnav.org

Abstract

The International Maritime Organisation's (IMO) e-Navigation concept covers a wide range of technologies and approaches, aimed at keeping the mariner safe and aiding the master's decision making on the bridge. Resilience of key information is a highlighted concern with a recognised need for resilient positioning, navigation and timing (PNT) information. This paper introduces two emerging technologies being considered to support the introduction of e-Navigation.

The first element introduced in this paper is the concept of using Wi-Fi networks to position vessels through the use of existing 2.4 and 5.2 GHz Wi-Fi transmissions, installed to offer internet access and thereby used as signals of opportunity.

The second is linked to maritime safety information and considers an update to the existing NAVTEX system used at sea. NAVTEX is limited to broadcasting short text messages, while a new approach called NAVDAT is able to provide significantly more information and can be targeted to vessels over a wide geographical area.

Such information could include new messages over and beyond the current Maritime Safety Information (MSI) and potentially include GNSS authentication data.

Key words: *Wi-Fi, NAVDAT*

1 POSITIONING USING WI-FI NETWORKS

1.1 Overview

A fundamental part of e-Navigation is the provision of resilient PNT, acknowledging that all positioning systems are vulnerable and that a combination of dissimilar systems is required. One area which seems to have received little focus is the use of Wi-Fi signals for positioning a vessel. While Wi-Fi positioning is commonly associated with locating objects and people indoors, the concept can be moved outside and function at longer ranges, especially in ports and harbours where large numbers of Wi-Fi access points are being installed to enable mariners to access the internet.

Positioning can be accomplished either by calculating the angle or time difference of arrival of Wi-Fi transmissions, or a simpler system may be used based on comparing actual Wi-Fi signal strengths observed with that predicted by model or previously determined empirically, known as 'fingerprinting'. It is recognised that any use of Wi-Fi information will have a limited operational area. It is recognised that such a system would be used to provide a backup to the primary means of navigation, typically GNSS, or to provide sanity/integrity checks. Wi-Fi could provide additional information where the risks to navigation are greater, for example within ports and port approach areas.

The following work investigates two approaches, starting with modelling Wi-Fi signal strength using the 'Two Ray Ground Refection' model. It then reports on preliminary trials measuring Wi-Fi signal strength at sea using commercial off the shelf (COTS) Wi-Fi hardware.

1.2 Two Ray Ground Reflection Model

The conventional means of positioning using Wi-Fi data is to use fingerprinting which is where the received signal strength is compared to previously known values (Goldsmith 2005). This works well indoors where walls and other infrastructure attenuates the signal over a short distance.

When considered outside in port areas, the signals attenuate more slowly, leading to large areas of common signal strength values.

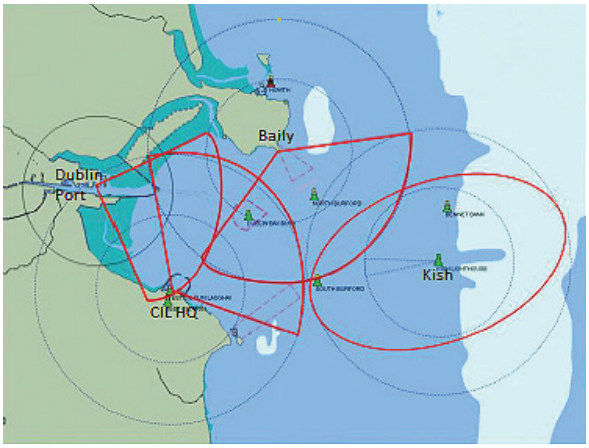

Figure 1 An image indicating approximate coverage of the Wi-Fi access points located around the port of Dublin, known as the Dublin Bay Digital Diamond (DBDD).

An example of this was observed using the Dublin Bay Digital Diamond (DBDD) where a number of Wi-Fi access points have been installed around the port to provide internet access (Figure 1). Initial trials recording the signal strength when measured on a vessel traversing the port have shown that accuracies in the order of 300 m or more could be calculated from a single access point. Such accuracies may be useful, but additional information may be used to enhance this. One such approach is to consider the two ray ground model to investigate if features from the propagation of the transmission can help improve the resulting position accuracy.

The Two Ray Ground Reflection model takes into account both a direct ray between transmitter and receiver as well as a reflected ray from the sea surface. This is represented by Figure 2 (Henniges 2012).

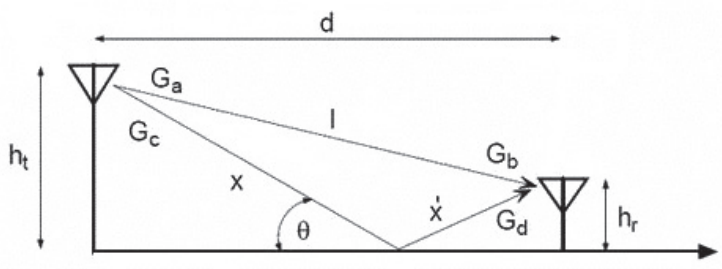

Figure 2 Two Ray Ground Reflection Model

In Figure 2, d is the distance between transmitting and receiving antennas and h_t and h_r are the heights of the transmitting are receiving antennas respectively. The received power is given by P_{Rx} where:

$$P_{Rx} = P_{Tx}\left(\frac{\lambda}{4\pi}\right)^2 \left|\frac{\sqrt{G_L}}{l} + \frac{\Gamma\sqrt{G_R}\, e^{-\Delta\phi}}{x + \acute{x}}\right|^2 \quad (1)$$

P_{Tx} = Power at the transmitter

λ = Wavelength

Γ = Ground reflection coefficient

l = Path length of direct signal

x = Path length of reflected signal, first part

$\acute{x}$ = Path length of reflected signal, second part

$\Delta\phi$ = Phase difference between the two received signal components, given by:

$$\Delta\phi = \frac{2\pi(x + \acute{x} - l)}{\lambda} \quad (2)$$

G_L and G_R are the gains from direct and reflected signals respectively and are given by:

$$\sqrt{G_L} = \sqrt{G_a + G_b} \quad (3)$$

$$\sqrt{G_R} = \sqrt{G_c + G_d} \quad (4)$$

The Two Ray Ground Reflection model has been successfully used to model signal reflections from the sea surface (ITU 2010a). The model shows multipath interference between the direct and reflected rays results in a distinctive pattern of nulls in signal strength, an example of which is shown in Figure 3, for which ht = 30 m, hr = 10 m, λ = 0.1228 (2.442 GHz, Wi-Fi channel 7). The antenna gains, ground reflection coefficient and transmitter output were all set to 1. Nulls are more frequent close to the transmitting antenna with the number of nulls decreasing as distance increases.

From the equation for P_{Rx}, it can be seen that received signal strength is a function of transmission wavelength λ and signal path lengths, l, x and $\acute{x}$ which are in turn a function of antenna heights h_t and h_r. The effect of varying antenna height upon nulls in signal strength is shown in Figure 4.

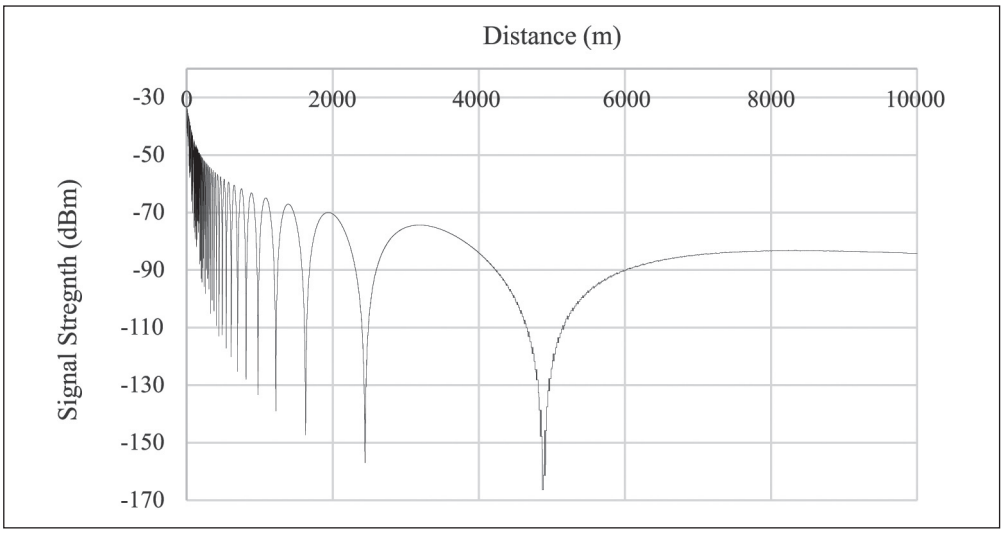

Figure 3 Signal strengths shown using the Two Ray Ground Reflection Model

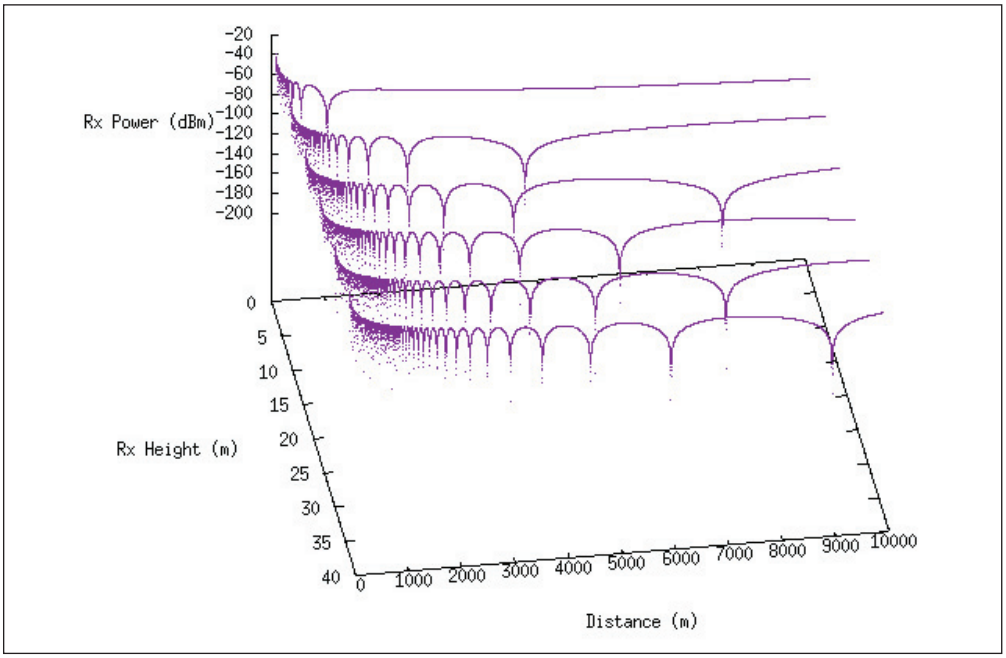

Figure 4 Effect of receiver antenna height on signal strength for a Wi-Fi signal with wavelength 0.1228 m (2.442 GHz, Wi-Fi channel 7). Plot shows receiver antenna heights of 2, 9, 16, 23, 30 and 37 m. All other parameters are as in Figure 3.

This is a three dimensional graph showing six signal strength plots with the receiving antenna at six different heights. It can be seen that the number and position of nulls in signal strength varies with antenna height, with lower antenna height leading to fewer nulls at distance and vice versa.

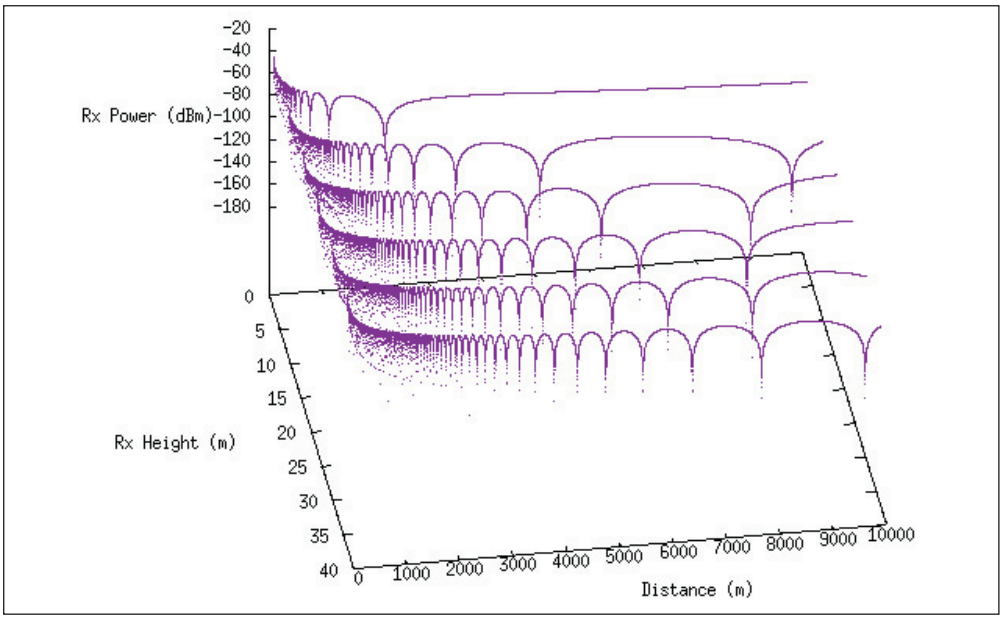

Figure 5 Effect of receiver antenna height on signal strength for a Wi-Fi signal with wavelength 0.0572 m (5.24 GHz, Wi-Fi channel 48). Plot shows receiver antenna heights of 2, 9, 16, 23, 30 and 37 m. All other parameters are as in Figure 4.

Figure 5 is also a three dimensional graph, identical to Figure 4 with the exception that it shown transmissions at the 5.24 GHz Wi-Fi frequency. It can be seen that the higher frequency gives rise to an increase in the number of nulls seen. Furthermore, the nulls seen at 5.24 GHz have a different spacing to those seen at 2.442 GHz.

The model suggests that using a variety of Wi-Fi frequencies and antenna heights, a rich variation in spacing and positioning of nulls in signal strength may be achieved. A vessels position may then be derived by determining the presence of a null. Such a technique could be used to enhance the positioning resolution given by fingerprinting when there are few signal sources available. It is acknowledged however, that changes in sea state will affect the reflectivity of

the sea surface and so affect the depth and positioning of nulls described by the Two Ray Ground reflection model.

1.3 Positioning using the two Ray Ground Reflection Model

To investigate the existence of nulls in Wi-Fi signal strength a series of trials were conducted. These trials aimed to investigate the potential for positioning using commercial off the shelf (COTS) Wi-Fi hardware, typical of equipment which may be used by the mariner for access to the internet when in port. Trials were conducted on vessels as they conducted their normal operations.

1.3.1 Dublin Bay trials

Trial data was obtained from the Commissioners of Irish Lights as a vessel conducted surveys in the Dublin Bay area. It is understood Wi-Fi signal strength measurements were made using a laptop computer connected to a Wi-Fi antenna mounted externally on the vessel. Signal strength data was recorded from one of the 2.4 GHz Wi-Fi access point located within the bay.

Signal strength data obtained from these trials is shown in Figure 6, alongside modelled data from the Two Ray Ground Reflection Model.

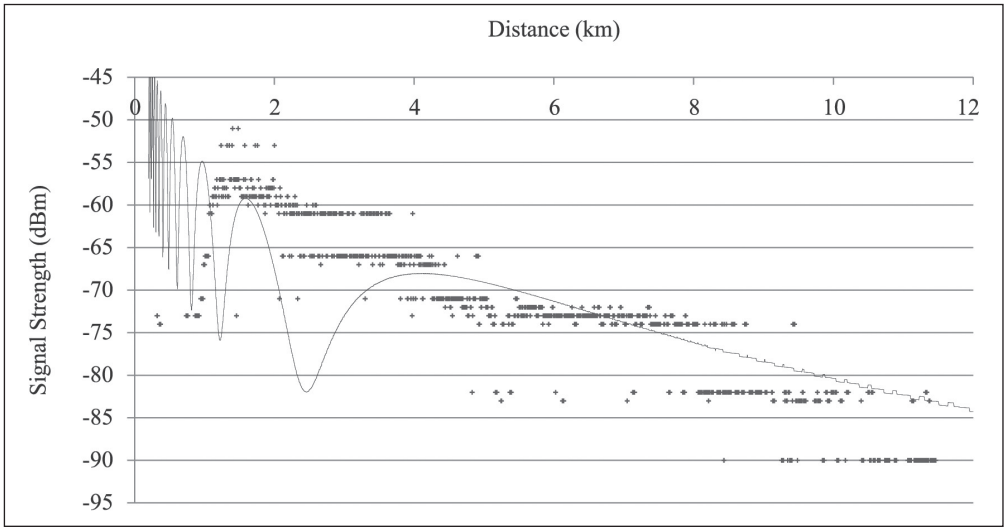

Figure 6 Dublin Bay Wi-Fi signal strengths shown experimentally (dotted points) and by the Two Ray Ground Reflection Model (solid line).

It can be seen from Figure 6 that Wi-Fi signals are recorded at ranges approaching 12 km from the access point. Empirical signal strength data is however, quantised into several bands by the COTS equipment used to record signal strength data. Due to this quantisation, this data does not have the resolution to accurately indicate position based on signal strength, as the quantisation adds to the position error. This suggests that difficulties may be encountered using some COTS equipment to accomplish received signal strength based positioning. No nulls in empirical signal strength can be seen and the empirical data gives a poor fit to the model, the cause for this is yet to be determined, but it's likely to be due to sea state and movement of the vessel which are not considered in the model.

1.3.2 Harwich trials

Further trials were conducted in Harwich to investigate the use of other Wi-Fi receiver equipment from the point of establishing whether the quantisation observed previously is normal. A 2.4 GHz Wi-Fi access point was installed at the end of Trinity Pier, at approximately 2.5 m above sea level. The signal strength from this access point was monitored on board a Trinity House vessel as it conducted routine operations. The receive equipment was installed at the vessels bow, approximately 4.5 m above sea level.

Wi-Fi signals were received using a laptops built-in Wi-Fi chipset and antenna to see if such a configuration could be used by the mariner. Signal strength data was recorded on the laptop using a Linux shell script making use of the 'iwconfig' and 'iwlist' functions. These functions permitted access to the Wi-Fi chipset allowing a direct reading of (the uncalibrated) Wi-Fi signal strength measured in dBm. This approach was selected to enable access to the raw signal strength data.

Data obtained experimentally is shown in Figure 7 alongside modelled data from the Two Ray Ground Reflection model.

From Figure 7 it can be seen that the use of a Wi-Fi access point, with an omni-directional antenna 2.5 m above sea level, results in no signals recorded at ranges over 2 km. The empirical signal strength data appears noisy and could be due to multipath interference, sea state or, due to small movement of the laptop computer, the changing polarisation of the laptops built in antenna causing signal attenuation.

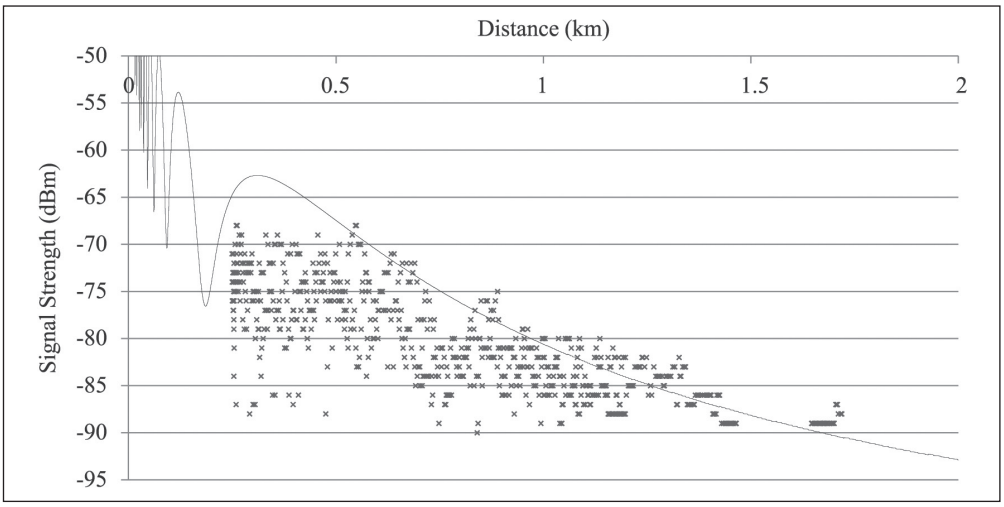

Figure 7 Harwich Harbour Wi-Fi signal strengths shown experimentally (dotted points) and by the Two Ray Ground Reflection Model (solid line).

It does show that the data is not quantised which is an important consideration for both the fingerprinting and two ray model approaches.

The vessel did not sail any closer than approximately 200 m to the Wi-Fi access point so no data is available to verify the existence of nulls suggested by the Two Ray Ground Reflection model at these ranges. This was unfortunate, due to the use of a vessel of opportunity, and will be addressed in future trials. It can be seen however that at ranges greater than 200 m, that there may be coarse agreement between the maximum signal strengths recorded empirically and that shown by the model which may be used in the future in a method yet to be defined.

1.4 Future work

This work has investigated positioning using only the 2.4 GHz Wi-Fi band and has not considered the effect of varying antenna heights on nulls in received signal strength. Nor has it considered multiple access points or the combination of approaches.

It is aimed to repeat trials shown in this work and make use of a dedicated vessel so as to avoid the gap in coverage seen at 0-200 m. Such trials will also investigate the influence of varying antenna height on received signal strength

shown by the Two Ray Ground Reflection Model as well as investigating positioning using signals in the 5.2 GHz Wi-Fi band and from multiple antennas. Finally trials of the fingerprinting approach using combinations of antennas and access to raw Wi-Fi data will be considered.

2 NAVDAT

2.1 Current NAVTEX service

The existing NAVTEX service broadcasts maritime safety information (MSI) to vessels using a medium frequency (MF) direct text printing service. NAVTEX is a component of the Global Maritime Distress and Safety System (GMDSS) and is regarded as a primary means of disseminating MSI. Carriage of a NAVTEX receiver is a compulsory requirement for all vessels bound by the IMO Safety Of Life At Sea (SOLAS) convention (IMO 2011).

NAVTEX broadcasts are one-way, made from multiple terrestrial stations around the world to vessels within broadcast range. Broadcasts are made in English at 518 kHz with each stations broadcast time(s) scheduled to avoid mutual interference. Additionally, broadcasts may also be made at 490 kHz or 4209.5 kHz providing local inshore information and/or broadcasts in a local language. Each NAVTEX station may use a different transmission power and antenna system, therefore the working range of each station will vary. By using transmission powers of 1 kW by day and 300 W by night however, broadcasts are typically quoted as having a working range of 460 km (250 NM). NAVTEX has a 100 bit/s bitrate, effectively limiting NAVTEX to simple text only broadcasts. For this reason, NAVTEX is regarded by some as using a dated technology. The limitations of the low bitrate provide little scope for an improved NAVTEX service.

2.2 NAVDAT outline

A new approach, called NAVDAT has been developed which also provides one-way broadcasts from terrestrial stations to vessels within range. A frequency of 500 kHz has been allocated to NAVDAT by the International Telecommunication Union (ITU) on a worldwide basis. NAVDAT takes advantage of a bandwidth of 10 kHz and uses Quadrature Amplitude Modulation (QAM) to achieve a theoretical bitrate of 12 to 25 kbit/s (depending on QAM modulation technique) (ITU 2012). NAVDAT is therefore suitable for transmission of a larger volume of data than NAVTEX, including the ability to transmit image files and graphical data

to users as well as plain text. The larger bandwidth also gives the ability to transmit messages to an individual vessel (identified via Maritime Mobile Service Identity (MMSI)) or group of vessels in addition to the general broadcast. The ability to transmit encrypted and digitally authenticated (signed) messages also exists.

At the time of writing no maritime organisations provide a NAVDAT service and the only NAVDAT transmissions have been as part of experimental trials. The IMO is however, currently discussing the overhaul of the GMDSS with the possibility of including NAVDAT (IMO 2013). It is suggested that should the IMO make this recommendation NAVDAT services will proliferate.

2.3 Potential uses of NAVDAT

NAVDAT could be used to broadcast almost any conceivable data from shore to ship without recourse to satellites, limited only by the 12 to 25 kbit/s bandwidth and MF broadcast range. NAVDAT therefore has a wide range of potential uses. The IMO has listed some potential services, over and above replacing the existing NAVTEX service (IMO 2012). Some examples taken from this IMO paper include:

- Broadcasting weather information in the form of ocean-maps (e.g. isobaric maps) or digital data;
- Transmission of information relating to vessel traffic service including vessel traffic service pictures, recommended routes and speed and temporary exclusion zones;
- Transmission of information related to maritime signalling including operational status of AtoN; and
- Transmission of information relative to search and rescue at sea including area and search pattern.

Further to the above, providing NAVDAT broadcasts are securely authenticated, NAVDAT may itself be used to provide security updates to e-Navigation services. In particular, NAVDAT could be used to disseminate and update public encryption keys required to secure e-Navigation services and GNSS authentication data.

Other potential uses of NAVDAT include controlling or reprogramming remote Aids to Navigation (AtoN). For example, a secure NAVDAT broadcast could be used to instruct a remote Automatic Identification System (AIS) beacon to broadcast a new virtual AtoN indicating the position of a wreck.

2.4 Demonstrations of NAVDAT

NAVDAT trials have been published by the ITU (ITU 2010b) and IMO (IMO 2015). The IMO document describes tests in which NAVDAT transmissions consisting of MSI, weather forecasts and other information in the form of images and text were transmitted in an XML format and displayed on a ship borne NAVDAT terminal.

The use of NAVDAT to automatically update the vessel's Electronic Navigation Chart (ENC) using a correction file in the International Hydrographic Organisation (IHO) S-57 standard was also shown. By using NAVDAT to display graphical information to the mariner and to automatically pass data to other systems (in this case, the ships ECDIS) the IMO document demonstrates two of the key benefits of NAVDAT.

2.5 Relevance of NAVDAT to the GLA

The GLA are interested in NAVDAT as a potential component of e-Navigation communications as it has the potential to be used in command and control type applications, as well as to provide safety critical information to the mariner. In addition, there will be a need for authenticated, or secure, communications to convey positioning service updates, augmentation data, and service integrity information. Although NAVDAT has not been designed for these services, such use can be perceived if authentication can be provided over large distances; PNT data may follow.

3 CONCLUSIONS

3.1 Positioning using Wi-Fi networks

With the introduction of more Wi-Fi access points around ports and harbours the opportunity is there to use such signals for positioning. Two approaches have been considered to date, fingerprinting and the use of a Two Ray model. Trials with both have shown limitations and further work is needed to investigate what can be done to resolve them.

It was noted that some Wi-Fi hardware can quantise the reported signal strength measurements which significantly affects the performance of both approaches. It is not clear yet whether this is an industrial norm, but an approach has been developed to gain access to the raw unquantised data.

Trials showed that while the received data did not show any nulls as predicted by the model, the signal strength dropped in line with the model. It is felt that the noisy signal strengths measurement during the Harwich trial could be due to sea state, movement of the ship or changing antenna polarisation.

Further work is required to establish the suitability of using nulls in Wi-Fi signal strength shown by the Two Ray Ground Reflection model for positioning.

3.2 NAVDAT

It is suggested that NAVDAT, due to its higher bandwidth and greater flexibility can be considered as a natural successor to the existing NAVTEX service. NAVDAT broadcasts appear well suited to providing MSI in a more intuitive and user friendly format and will not be limited to plain text transmissions.

NAVDAT has secured radio frequencies from the ITU and is being considered by the IMO as part of the modernised GMDSS. Therefore it is considered as only a matter of time before NAVDAT transmissions will become available and new services are provided. The higher bandwidth available to NAVDAT permits the broadcast of authenticated data which may in turn be used to provide security updates to e-Navigation services, enabling many different potential services, providing benefits to the mariner and service providers alike.

Acknowledgments

The authors would like to express their gratitude to the Commissioners of Irish Lights for its help collecting data used to support the results shown in Figure 6.

REFERENCES

Goldsmith, A. (2005) *Wireless Communications*, Cambridge: Cambridge University Press.

Henniges, R. (2012) Current approaches of Wi-Fi Positioning. Service-Centric Networking seminar.

International Maritime Organization (IMO). (2011) MSC.1/Circ.1403: Revised NAVTEX Manual. London: IMO.

International Maritime Organization (IMO). (2012) NAV 58/INF.17: *Digital system for broadcasting maritime safety – and security – related information*. London: IMO.

International Maritime Organization (IMO). (2013) *Report of the 8th meeting of the IMO/ITU EG*. London: IMO.

International Maritime Organization (IMO). (2015) NCSR 2/INF.4: NAVDAT-based maritime safety related information broadcasting tests conducted in China. London: IMO.

International Telecommunication Union (ITU). (2010) ITU-R M.2202: *Maritime broadband wireless mesh networks*. Geneva: ITU.

International Telecommunication Union (ITU). (2010) *Report ITU-R M.2201: Utilization of the 495-505 kHz band by the maritime mobile service for the digital broadcasting of safety and security related information from shore-to-ships*. Geneva: ITU.

International Telecommunication Union (ITU). (2012) Recommendation ITU-R M. 2010: *Characteristics of a digital system, named Navigational Data for broadcasting maritime safety and security related information from shore-to-ship in the 500 kHz band*. Geneva: ITU.

Sveučilište u Rijeci
POMORSKI FAKULTET U RIJECI
FACULTY OF MARITIME STUDIES RIJEKA
University of Rijeka

University of Zagreb
Faculty of Transport
and Traffic Sciences

Royal Institute of Navigation
Science Technology Practice

10th
Annual
Baška GNSS
Conference

IMPROVING AVAILABILITY OF THE EGNOS SYSTEM IN ALGERIA FOR DUAL FREQUENCY

Lahouaria Tabti, Salem Kahlouche

Center of Spatial Techniques, Department of Geodesy
Avenue de la Palestine BP 13, 31200 Arzew, Algeria
E-mail: thouaria@yahoo.fr

Abstract

Satellite Based Augmentation System (SBAS) is a navigation system that supplements Global Navigation Satellite Systems (GNSS) providing a more accurate and reliable navigation service than GNSS alone, and also provides the high level of integrity required for most aviation navigation operations.
The existing SBAS signals are broadcast from a geostationary satellite using the L1 frequency, future SBAS satellites will also broadcast a service on the L5 frequency using a signal similar in design to the L5; This new L5 signal will provide an additional service that makes use of the civil signals at the L1/L5 frequencies.
The new GPS signals L1/L5 will allow civil users to remove the ionospheric delay in the pseudo-ranges. This will have a large impact on the SBAS, as the ionospheric delay is currently the largest error.
In This work we used the SBAS Simulator2 including dual-frequency developed by European Space Agency (ESA) to analyze the coverage of APV1, LPV 200 and APV2 services in terms of the availability.
In Algeria, we observed that the EGNOS system provides a good coverage to the north, against; to be moving towards our south coverage decreases.
Simulations show that dual frequency GPS user has better availability in Algeria, than the availability for a single frequency EGNOS user.

Key words: *GPS, EGNOS, availability, L1/L5*

1 INTRODUCTION

Every satellite-based wide area augmentation system (SBAS), as the European system EGNOS (European Geostationary Navigation Overlay Service), does provide ranging signals transmitted by GEO satellites, differential corrections on the wide area and additional parameters aimed to guarantee the integrity of the GNSS user. SBAS shall provide the following information:

- Satellite orbit and clock corrections to the existing satellite navigation services (GNSS and GEO), as well as the estimation of errors associated to satellites or User Differential Ranging Error (UDRE).
- Ionospheric corrections for a given grid of points, as well as the estimation of errors associated to ionosphere or Grid Ionospheric Vertical Error (GIVE).
- Tropospheric corrections. Satellite orbit/clock corrections and ionospheric corrections are dynamically modeled. The SBAS shall communicate the user the corrections that are available to be used by the receiver. The information of the models is packed on messages to be sent to the user. On the other hand, tropospheric corrections are statically modeled, which means that corrections are tabulated and the information does not depend on any external behavior but the user position (a mean troposphere is assumed).

1.1 Aviation navigation requirements

The Federal Aviation Administration's objective in using GPS is to provide enhanced services and reduce infrastructure cost for aircraft navigation. To do so, the Required Navigation Performance (RNP) for accuracy, integrity, availability, and continuity must be met. These four parameters are defined as follows:

- Accuracy corresponds to the difference between the measured and the real position, speed or time value.
- Integrity refers to the confidence the user is able to have in the calculation of the position. Integrity includes a system's capacity to provide confidence thresholds as well as alarms in the event that anomalies occur.
- Continuity defines a system's ability to function without interruption throughout the operation the user wants to carry out (for example landing a plane). Continuity is the probability, from the moment that the accuracy and integrity criteria are fulfilled at the beginning of an operation that they continue to be fulfilled throughout that operation's entire duration.

- Availability is the percentage of time in which, over a certain zone geographical area, the accuracy integrity and continuity criteria are fulfilled (CNES 2011).

1.2 EGNOS extension in the MEDA Region

At present, in the mission of EGNOS, the provision of services for MEDA (MEDiterranean Area: Morocco, Algeria, Tunisia, Egypt, Israel, Jordan, Palestine, Lebanon, Syria and Turkey) are foreseen. This extension will improve simultaneously the performances over the core EGNOS and MEDA service areas, creating new markets in emerging countries.

The main function of the Ranging and Integrity Monitoring Station (RIMS) is to collect measurements from GPS satellites and to transmit these raw data every second to the Central Processing Facilities (CPF) of each Mission Control Centres (MCC). The current RIMS network comprises 39 RIMS sites located over a wide geographical area. Figure 1 shows the geographical distribution of the RIMS already in operation (ESSP 2015).

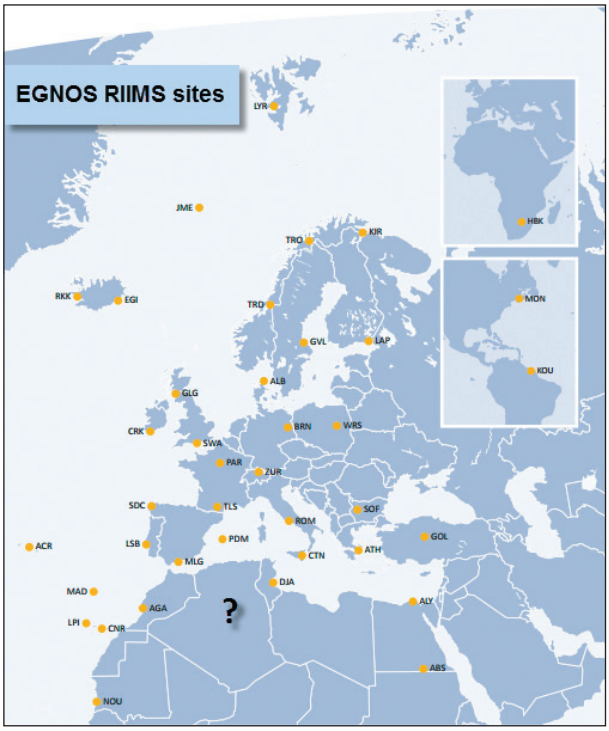

Figure 1 EGNOS reference stations

1.3 Use of Dual Frequency

The usage of dual civilian frequencies (L1 and L5) is an attempt to address the largest delay estimation in the EGNOS system (ionospheric delay), the need for better improvement of its error estimation and correction was raised. This need lead to the potential use of both L1 and L5 frequencies together which would improve the performance for GPS users by allowing them to estimate and correct/mitigate the ionospheric errors.

This is done in a way through which the GPS dual frequency receiver would be directly involved in estimating the ionospheric delay and applying its error factor to the pseudo-range measurements for each line of sight GPS satellite without any help needed from the EGNOS system. There is another major advantage from using the dual frequency system which is its relative immunity against unintentional interference. So if one of the signal frequencies has been jammed, we will still have visual and measurements from the second signal from the same satellite (Zayan & Rehan 2011).

For an L1/L5 dual-frequency GPS/EGNOS user, the weighting matrix W, is a diagonal matrix and the inverse of the i^{th} diagonal element is given by the variance for the corresponding satellite, $\sigma^2_{i,dual}$ as calculated in equation:

$$\sigma^2_{i,dual} = \sigma^2_{i,flt} + \sigma^2_{i,air,\,\text{L1-L5}} + \sigma^2_{i,trop} \qquad (1)$$

where $\sigma^2_{i,flt}$ is the fast and long-term degradation confidence, which is the confidence bound on satellite clock and ephemeris corrections, $\sigma^2_{i,air,\,\text{L1-L5}}$ is the L1/L5 dual-frequency airborne receiver error confidence, which is the confidence bound on ionospheric-free receiver measurements for an L1/L5 dual-frequency GPS/EGNOS user.

Note: Because the calculation of $\sigma^2_{i,air,\,\text{L1-L5}}$ already considers both the L1/L5 dual-frequency user ionosphere range error confidence and the airborne multipath and noise error confidence, there is no need for additional terms accounting for these errors in Equation (1) and $\sigma^2_{i,trop}$ is the tropospheric error confidence, which is the confidence bound on residual tropospheric error (Shiun 2010).

2 SBAS SIMULATOR SIMULATION RESULTS

2.1 Constellation sigma values

Constellation sigma values contain error over bounds related to specific constellation.

2.1.1 Satellite error bound for single frequency mode

For the single frequency mode the overall satellite residual is computed as:

$$\sigma^2_{i,sf} = \sigma^2_{i,flt} + \sigma^2_{i,UIRE} + \sigma^2_{i,air,sf} + \sigma^2_{i,tropo} + \sigma^2_{i,RIMS} + \sigma^2_{i,system} \quad (2)$$

where: $\sigma_{i,sf}$ is the total satellite error over bound for single frequency, $\sigma_{i,flt}$ is the fast and long-term degradation confidence, $\sigma_{i,UIRE}$ is the variance of ionospheric correction errors, $\sigma_{i,air,sf}$ is the air residual for single frequency specified in equation (3), $\sigma_{i,tropo}$ represents the square of tropospheric correction residual error is be obtained using MOPS model (CNES 2011), $\sigma_{i,RIMS}$ is the error contribution from RIMS, and $\sigma_{i,system}$ is the overall constellation system error.

The $\sigma_{i,air,sf}$ is computed as:

$$\sigma^2_{i,air,sf} = \sigma^2_{i,noise,sum} + \sigma^2_{i,multipath} \quad (3)$$

$$\sigma^2_{i,noise,sum} = \sigma^2_{i,noise} + \sigma^2_{i,clock} + \sigma^2_{i,orbit} \quad (4)$$

2.1.2 Satellite error bound for dual frequency mode

For the dual frequency mode the overall satellite residual is computed as (User Manual 2015):

$$\sigma^2_{i,df} = \sigma^2_{i,DFC} + \sigma^2_{i,iono} + \sigma^2_{i,air,df} + \sigma^2_{i,tropo} + \sigma^2_{i,RIMS} + \sigma^2_{i,system} \quad (5)$$

where $\sigma_{i,DFC}$ is the model variance for dual frequency residual error as specified in equation(6), $\sigma_{i,iono}$ is the ionospheric residual error for dual frequency services as specified in equation (7), $\sigma_{i,air,df}$ is the air residual for dual frequency specified in equation (8), The $\sigma_{i,DFC}$ is computed as:

$$\sigma^2_{DFC} = \begin{cases} [(\sigma_{DFRE}) \cdot (\delta_{DFRE}) + \varepsilon_{ce} + \varepsilon_{er}]^2, & \text{if } RSS_{DFC} = 0 \\ [(\sigma_{DFRE}) \cdot (\delta_{DFRE})]^2 + \varepsilon^2_{ce} + \varepsilon^2_{er}, & \text{if } RSS_{DFC} = 1 \end{cases} \quad (6)$$

The $\sigma_{i,iono}$ is computed as:

$$\sigma_{iono} = 10^2 \text{ cm} \times F_{pp} \tag{7}$$

where F_{pp} is defined in MOPS.

The $\sigma_{i,air,df}$ is computed as:

$$\sigma^2_{i,air,df} = f^2_{dual}\,\sigma^2_{i,noise,sum} + f^2_{dual}\,\sigma^2_{i,multipath} \tag{8}$$

where f_{dual} is dual frequency factor defined as:

$$f_{dual} = \sqrt{\frac{f_1^4 + f_5^4}{(f_1^2 - f_1^2)^2}} \tag{9}$$

where f_1 is the first frequency and f_5 is the second frequency.

2.2 Analysis and simulation

The criterion of this research is to compare the coverage of availabilities in Algeria versus the horizontal and vertical alert limit (HAL and VAL) under the different cases. The simulation tool used is the SBAS Simulator 2 including dual- frequency developed by European Space Agency (ESA). The following parameters were used to measure EGNOS system performance in flight operations:

- Date 03/10/2015; EGNOS satellite monitoring status for each satellites GPS as function of the precision indicators (UDREI) is given in Figure 2.

The monitoring status of each of these satellites GPS in function of UDREI, it's given by:

- UDREI < 12: SV satellite is used by EGNOS.
- UDREI = 12, 13: Although not considered as unhealthy, satellites with UDREI ≥ 12 cannot be used for all services. UDREI = 14: SV unmonitored.
- UDREI = 15: SV unhealthy.
- The satellites that are not in EGNOS GPS mask are also represented in the figure.

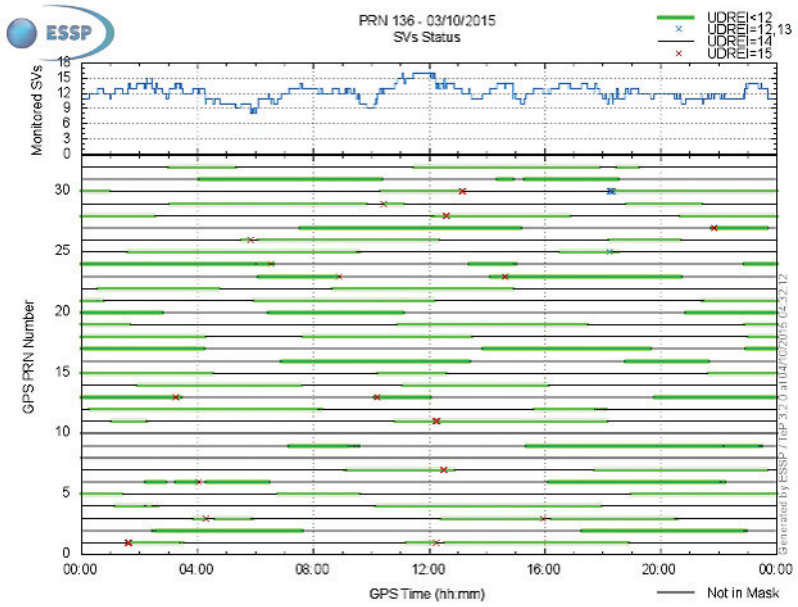

Figure 2 GPS satellites monitoring statues on 03/10/2015 (ESSP; 2015)

- The area covered is [-10, 15] degree in longitude and [15, 40] degree in latitude (to allow coverage for all country: Algeria);
- RIMS Network: RIMS stations used in the simulation is based on operational stations in 2015 which are in total of 39 (ESSP), presented in figure 1;
- σ_{UDRE} and σ_{DFRE} is determined by the interpolation; is set the value which is based on number of RIMS that monitor a specific satellite. The model used to calculate the ionospheric error (GIVE) is based on an interpolation which depends on current RIMS stations;
- Availability simulation computes the availability for a defined service level. In this simulation we consider three services: APV1 (HAL = 40 m, VAL = 50 m), LPV 200 (HAL = 40 m, VAL = 35 m), and APV2 (HAL = 40 m and VAL = 20 m).

The availability of the system is computed by the percentage of time that the horizontal protection level (HPL) is below than the horizontal alert level (HAL) and the user vertical protection level (VPL) is less than the vertical alarm level (VAL).

2.2.1 Horizontal protection level

The simulation result of an L1 single-frequency is shown in left of Figure 3, the simulation results of an L1/L5 dual-frequency is shown in right of Figure 3.

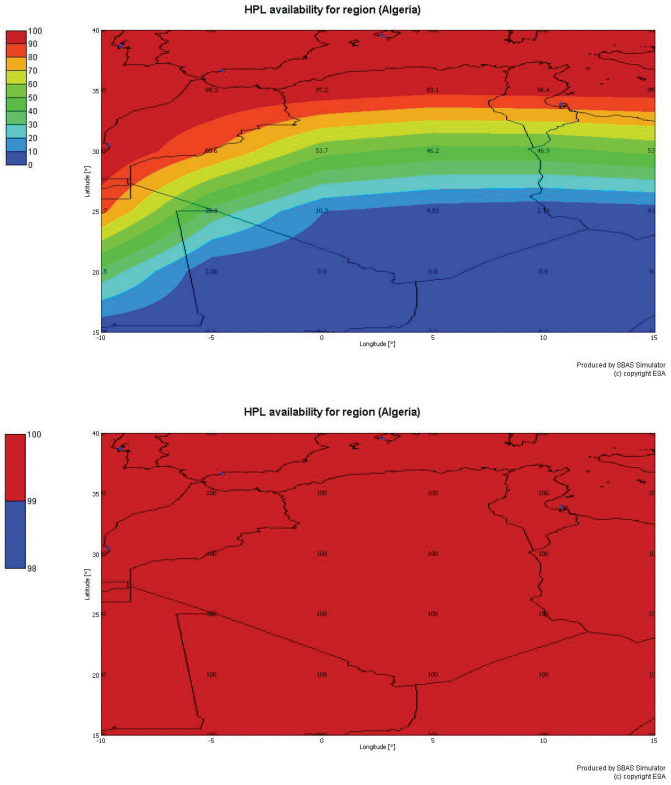

Figure 3 EGNOS horizontal availability performances with L1 frequency in the left and with L1/L5 frequency in the right (HPL < HAL = 40 m)

The simulation results show that an L1/L5 dual frequency for all the service is 100% in Algeria, as summarized in Table 1.

Table 1 EGNOS horizontal availability with single and dual frequency for all services

φ: Latitude λ: Longitude Services & Frequency		25° [0° 5°]	30° [0° 5°]	35° [0° 5°]
All services	L1	[4.83 10.3]	[46.2 53.7]	[93.1 97.2]
	L1/L5	100%	100%	100%

2.2.2 Vertical protection level

The simulation results for the L1/L5 dual-frequency are shown in the right of figures 4, 5 and 6. Right of Figure 4 is the APV1 coverage simulation result, which shows that an L1/L5 dual-frequency has 100% of the time that VPL lower than VAL in Algeria. Left of figures 4, 5 and 6 shows the VPL availability for an L1 frequency in Algeria.

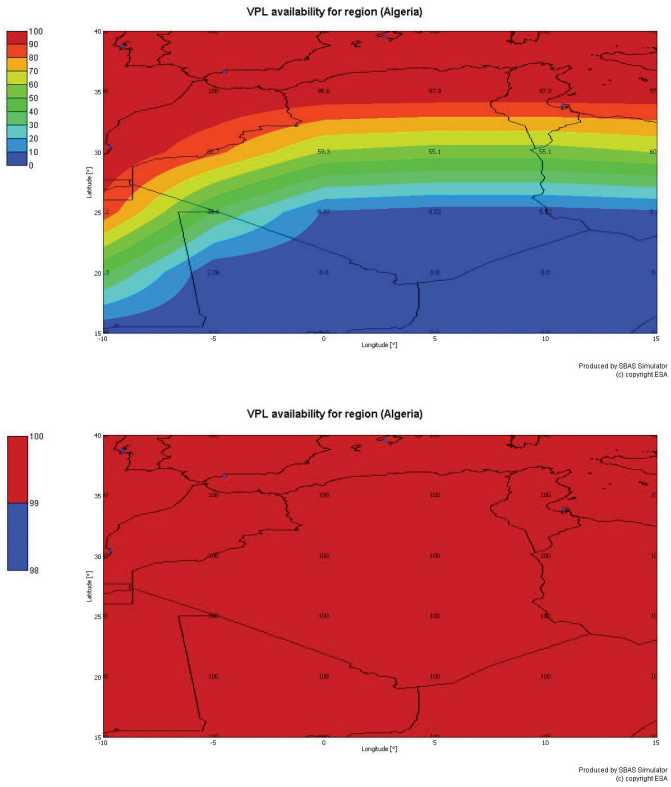

Figure 4 EGNOS vertical availability performances with L1 frequency in the left and with L1/L5 frequency in the right for APV1 service (HPL < HAL = 50 m)

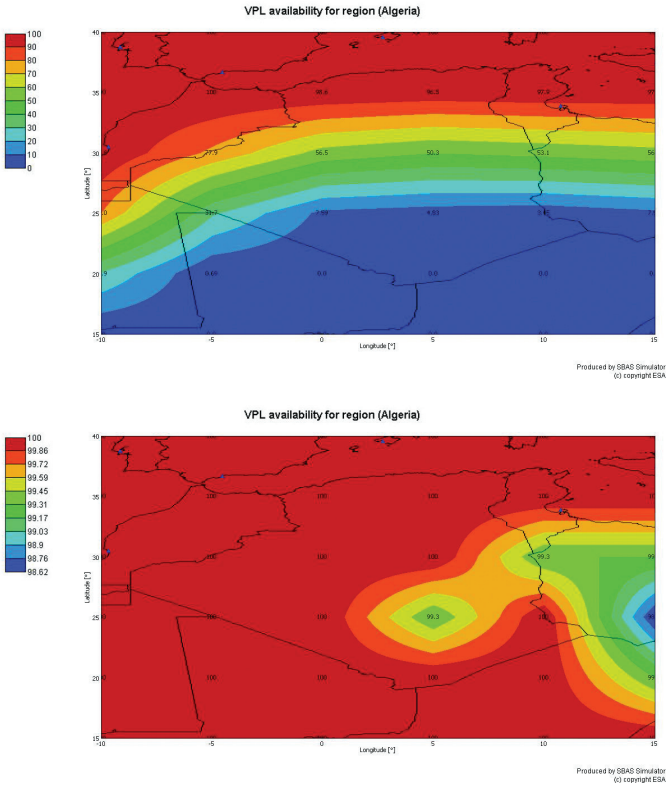

Figure 5 EGNOS vertical availability performances with L1 frequency in the left and with L1/L5 frequency in the right for LPV 200 service (HPL < HAL = 35 m)

Comparing Figure 4, Figure 5 and Figure 6, it is evident that in the case of a single frequency, we see that EGNOS covered the north of Algeria, this coverage is ensured by the European stations.

The L1/L5 dual-frequency user case has a better time availability than the L1 single-frequency case. A summary of these results simulations are presented in Table 2.

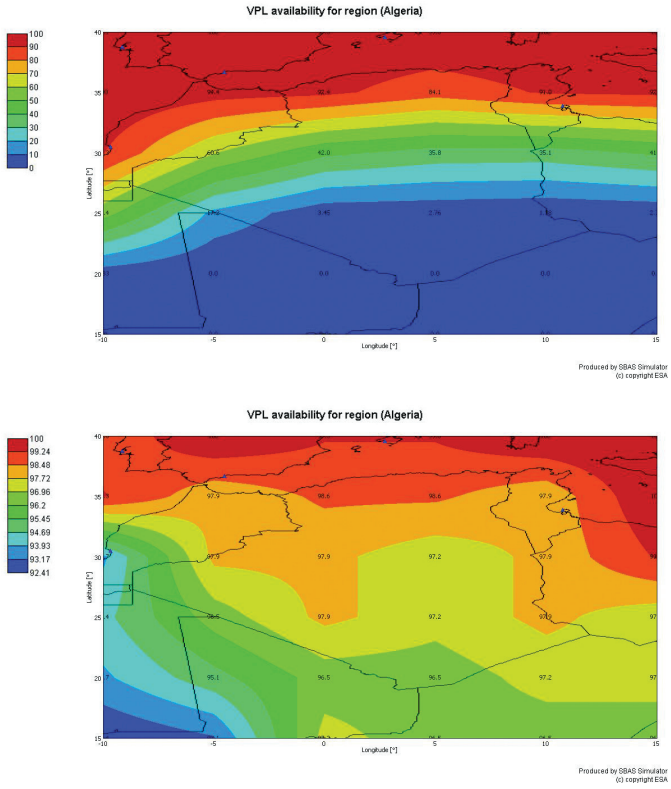

Figure 6 EGNOS vertical availability performances with L1 frequency in the left and with L1/L5 frequency in the right for APV2 service (HPL < HAL = 20 m)

Table 2 EGNOS vertical availability with L1 and L1/L5 frequencies for all services

Service & Frequency \ φ: Latitude, λ: Longitude		25° [0° 5°]	30° [0° 5°]	35° [0° 5°]
APV1 VAL = 50 m	L1	[5.52 8.97]	[55.1 59.3]	[97.9 98.6]
	L1/L5	100	100	100
LPV 200 VAL = 35 m	L1	[4.83 7.59]	[50.3 56.5]	[96.5 98.6]
	L1/L5	[99.3 100]	100	100
APV2 VAL = 20 m	L1	[2.76 3.45]	[35.8 42.0]	[84.1 92.4]
	L1/L5	[97.2 97.9]	[97.2 97.9]	98.6

For all single-frequency simulation results, the coverage of APV1, LPV 200 and APV2 in center of Algeria ($\varphi < 30°$) is less than 60%. When comparing the VPL contours, the L1/L5 dual frequency user case has a better time availability than the L1 single-frequency user case.

Table 2 shows that both APV1 and LPV 200 availability is nearly 100% for dual frequency, and even APV 2 availability goes beyond 97%.

In Algeria, the coverage is slightly better with 39 stations using L1/L5 because we can directly estimate the ionospheric delay. This direct use of dual frequency will be more accurate and offer higher availability. This coverage can be improved if a RIMS station is installed in center of Algeria.

3 CONCLUSION

This study evaluates the performance of dual-frequency GPS in term of EGNOS availability (which is used to determine the service coverage) that depends to the single or dual GPS frequencies and includes the following cases:

- Case 1: APV1 (HAL = 40 m, VAL = 50 m);
- Case 2: LPV 200 (HAL = 40 m, VAL = 35 m);
- Case 3: APV 2 (HAL = 40 m and VAL = 20 m).

The new signals on L5 enhance the availability of the augmented GPS system for aviation. The nominal performance with two signals increases availability to 100% for the APV1 and LPV200 approach in Algeria.

The difference between the availability obtained with EGNOS dual frequency and single frequency is decreased for services associated with a smaller VAL.

The implementation of RIMS station in Algeria allow to receive the corrections transmitted by the EGNOS system and will certainly benefit from the advantages offered by this system in particular in the center and south of Algeria, in terms of accuracy, availability, integrity and reliability.

REFERENCES

Azoulai L., Neri Airbus P. (2012) SBAS Error Modelling for Category I Autoland

ESSP (2015) https://egnos-user-support.essp-sas.eu/new_egnos_ops/gps_egnos

Salós Andrés, C.D. (2012) Integrity monitoring applied to the reception of GNSS signals in urban environments, Theses of Doctor, Institut National Polytechnique de Toulouse (INP Toulouse).

Shiun Jan. S. (2003) Aircraft landing using a modernized Global positioning system and the Wide area augmentation system, Theses of Doctor, Stanford university.

Shiun Jan. S. (2010) Vertical Guidance Performance Analysis of the L1-L5 Dual-Frequency GPS/WAAS User Avionics Sensor. Sensors ISSN 1424-8220, www.mdpi.com/journal/sensors

User Guide for EGNOS Application Developers (2011) ED 2.0, 15/12/2011, CNES, ESA.

User Manual, Upgrade of SBAS Simulator (2015) Iguassu Software Systems. Ref: SBAS-SIM-MANUAL. Issue: 1 Rev.: 2, Date: 19/08/2015.

Zayan, D., Rehan, M. (2011) Parametric Study on Wide Area Augmentation System for GPS Accuracy Enhancment. International Journal of Computer Applications (0975–8887). Volume 28, No. 9.

Sveučilište u Rijeci
POMORSKI FAKULTET U RIJECI
FACULTY OF MARITIME STUDIES RIJEKA
University of Rijeka

University of Zagreb
Faculty of Transport
and Traffic Sciences

Royal Institute of Navigation
Science Technology Practice

10th
Annual
Baška GNSS
Conference

GEOLOCATION USING GOOGLE VISION API

Adnan Ramakić[1], Diego Sušanj[2], Kristijan Lenac[2]

[1] University of Bihać, Rectorate, Bosnia and Herzegovina

[2] University of Rijeka, Faculty of Engineering, Rijeka, Croatia
E-mail: klenac@riteh.hr

Abstract

In this paper we present an approach for geolocation using Google Vision API. Google Vision API is one of many different kinds of Cloud solutions offered today by large companies in the IT industry. It is part of Google Cloud Platform and it uses powerful machine learning models and enables developers to analyse images and their content.

Using mentioned technology, we have developed and tested a method that estimates a geographic location of an object from the results obtained from Google Vision API when applied on a set of images of landmarks in the vicinity of the object.

Key words: *Internet of Things (IoT), Google Cloud Platform, Google Vision API, geolocation*

1 INTRODUCTION

In this work we address the problem of identifying the geographical location of a person or device by means of a service in the Cloud called Google Vision API. Google Vision API is part of Google Cloud Platform. It uses powerful machine learning models which can be applied by users on their photos or images to analyse their content. The capability of recognizing known natural or artificial landmarks while providing their location can be harnessed for geolocation of objects of interest. This is particularly interesting in the context of Internet of Things (IoT) where network-connected devices and systems automatically use such services to provide personalized experience to users.

This work is divided as follows. First the Internet of Things (IoT) is described with reference to the model relevant to the proposed method. After that, Google Cloud Platform and Google Vision API are introduced and described. A solution for geolocation using mentioned technologies is presented next. Finally, the results of the testing are shown and conclusions are drawn.

2 INTERNET OF THINGS

The Internet of Things (IoT) is widely used term which today can encounter in different aspects of human life. IoT term is defined by Kevin Ashton in 1999, and his roots can be traced back to the Massachusetts Institute of Technology (MIT), from work at the Auto-ID Centre. This group was working in the field of networked radio frequency identification (RFID) and emerging sensing technologies (Evans 2011).

IoT represents the use of intelligently connected devices and systems. This devices and systems use different embedded sensors and actuators to obtain the data. For ordinary people this can be solution that can improve different aspects of daily life like security, health, energy efficiency, education and more, while for enterprises IoT can be used to improve decision-making and productivity in manufacturing, retail and so on (GSM 2014).

The Internet Architecture Board (IAB) is in 2015 released a guiding document for networking of smart objects which contain a framework of four common communication models which use IoT devices. This models are (IS 2015):

- Device – to – device,
- Device – to – Cloud,

- Device – to – Gateway,
- Back – End Data – Sharing model.

In first case, device – to – device model, two or more devices are directly connected and communicate between one another. Device – to – Cloud model represents a model where IoT device connects directly to a Cloud service like an application service provider. Device – to – Gateway (device-to-application-layer gateway (ALG) model) model is communication model where IoT device connects through an ALG service as a conduit to the cloud service. The fourth model represents a communication architecture which provides a way for export and analyse smart object data from cloud service in combination with other data, from other sources (IS 2015).

3 GOOGLE CLOUD PLATFORM

Google Cloud platform is built from set of physical assets (computers, hard disks, virtual machines) that are contained in Google's data centres whose location is in global region. These regions include Central US, Western Europe and East Asia. Regions consist a collection of zones which are isolated within the region and these zones are identified by name (GCD 2016). Figure 1 shows the relationship between global scope, regions and zones.

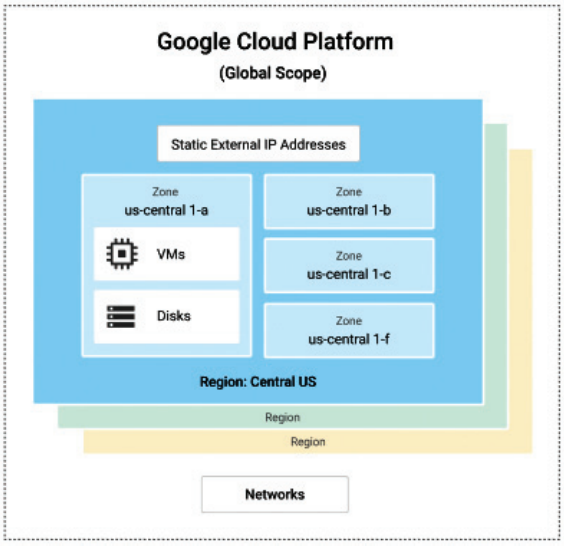

Figure 1 The relationship between global scope, regions and zones (GCD 2016)

In the next section the commonly used services will be described. These services are:

- Computing and hosting services,
- Storage services,
- Networking services,
- Big Data services.

Google Cloud Platform has a possibility for computing and hosting where users can choose to work with a managed application platform, leverage container technologies or build their own cloud-based infrastructure (GCD 2016). Figure 2 shows elements of computing and hosting services. These elements are App Engine, Container Engine, and Compute Engine.

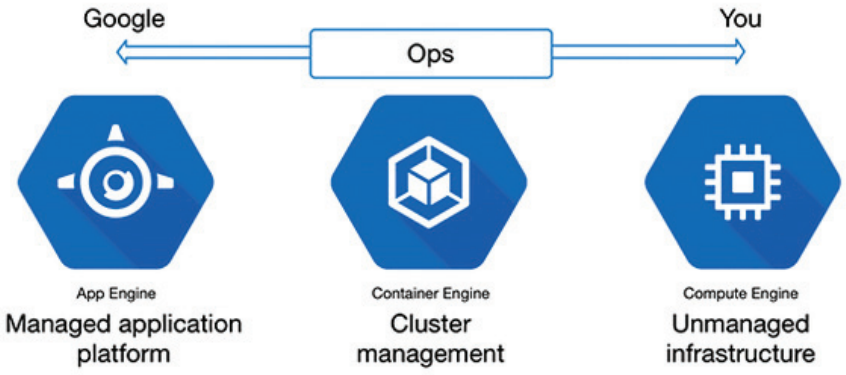

Figure 2 Google Cloud Platform, Computing and hosting (GCD 2016)

Google App Engine is a platform as a service (PaaS) Cloud Platform. Google Container Engine is based on open source Kubernetes system, where users can create and manage groups of Compute Engine instances, called Clusters, declare the requirements for Docker containers, use Google Container Registry for secure, private storage of Docker images, create pods, create and manage replication controllers, create and manage services, create an external network load balancer etc. (GCD 2016) More information on Kubernetes and related terms can be found in (Kubernetes 2016). Compute Engine provides infrastructure as a service (IaaS). With Compute Engine users can use virtual machines (VMs) called instances for building the application. They can choose the preferred operating systems, to which global regions and zones to deploy

resources, development stacks, languages, frameworks and so on. Also users can create instances from public or private images, use Cloud Platform storage technologies or third-party technologies, use Google Cloud Launcher to quickly deploy pre-configured software packages, use SSH (Secure Shell) to connect directly to instances and so on (GCD 2016).

Storage services of Cloud Platform provide an SQL database in Cloud SQL, NoSQL data storage (Cloud Data store and Cloud Bigtable), consistent, scalable, large-capacity data storage in Cloud Storage, persistent disks on Compute Engine etc. (GCD 2016). More about storage services can be read in (GCPa 2016).

In networking services, App Engine manages networking, Container Engine uses the Kubernetes model while Compute Engine provides a set of networking services. These services enable traffic load-balancing, creating DNS records, and connecting a user's network to Google's network (GCD 2016).

Big data services are part of Cloud Platform which are used to process and query big data in the Cloud (GCD 2016).

More about the other services and detailed information can be found in (GCPb 2016).

In the following section Google Vision API, part of Google Cloud Machine Learning services, will be described.

4 GOOGLE CLOUD VISION API

Google Cloud Vision API is a particularly interesting part of Google Cloud. It uses powerful machine learning models to enable developers to analyse images and their content. Google Vision API can detect individual objects and faces in images, find and read words within images, classify images into different categories and much more (GCPc 2016). How it works can be tested on Official Page of Google Cloud Platform listed under (GCPc 2016). In Figure 3 a result of analysing the image with Google Vision API is shown.

As shown in Figure 3 the accuracy of recognition for the Vukovar Water Tower which is contained on analysed image is 98%. The location information for the detected landmark is also provided. Google Vision API shows also some other information under ribbons which can be seen in Figure 3 (e.g. Text detected in the image).

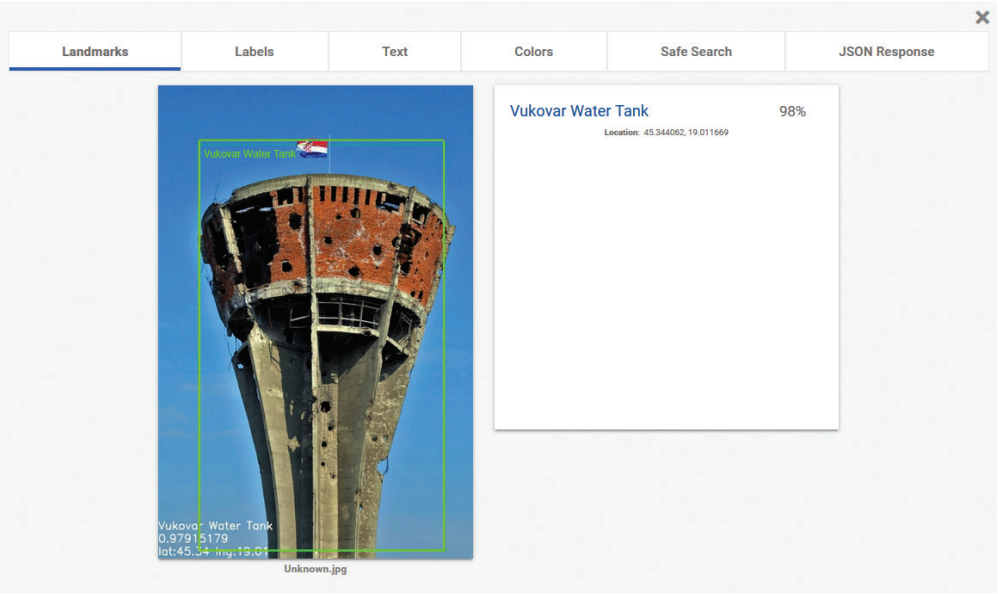

Figure 3 Result of the image analysing with Google Vision API

The pricing list for using Google Vision API is defined according to units per month. It is shown in Table 1.

Table 1 Price based on units per month (According to table shown in (GCPc 2016) on a day 16.01.2017)

Price per 1,000 units, by monthly usage				
Feature	**1 – 1,000 units/month**	**1,001 – 1 Million units/month**	**1 – 5 Million units/month**	**5 – 20 Million units/month**
Label Detection	Free	$1.50	$1.50	$1.00
OCR	Free	$1.50	$1.50	$0.60
Explicit Content Detection	Free	Now free with Label Detection		
Facial Detection	Free	$1.50	$1.50	$0.60
Landmark Detection	Free	$1.50	$1.50	$0.60
Logo Detection	Free	$1.50	$1.50	$0.60
Image Properties	Free	$1.50	$1.50	$0.60

In the next chapter a proposed method for objects geolocation using the Google Vision API is presented.

5 PROPOSED SOLUTION

The method proposed in this paper uses the information on the environment around the user and/or device to identify their geographical location. Example of such information are photos of important historical and natural landmarks. To facilitate the recognition process and increase the likelihood of Google Vision API correctly recognizing the landmark the user should take multiple pictures containing features that are unique to the location that is to be recognized. Each image can then be uploaded and processed in multiple ways, all dependent on Google Vision API.

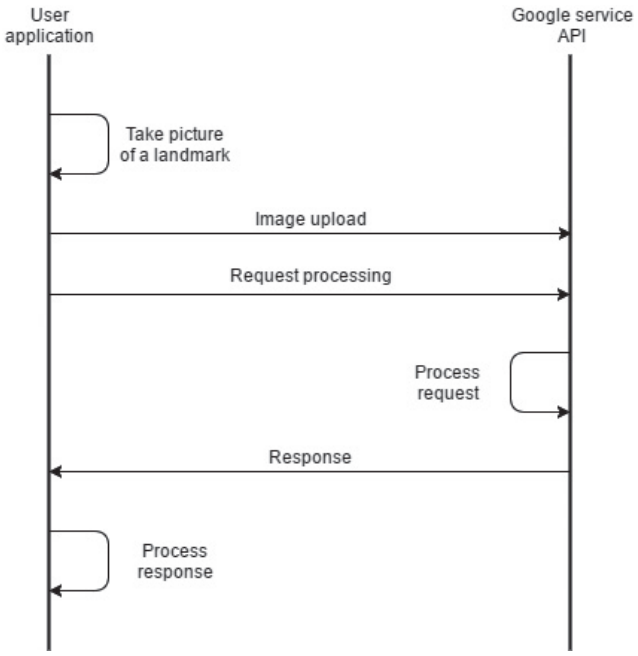

Figure 4 Proposed processing solution

As shown in Figure 4, a simple usage scenario involves the user taking a picture of a landmark and uploading it through a mobile or desktop application to be processed using Google Vision API. After processing the image, the server returns a response to the user as a text message in a JSON format. Afterwards, local client parses the received message and reads the relevant fields to determine the geographical location of the landmark in the picture. This method can be

used both with images taken while off-line, i.e. not connected to the Internet, and then uploaded when the connection to the Cloud service becomes available or in a live mode if the clients have the Internet access when taking the pictures. The processing is usually pretty fast, so we could call this a pseudo real-time operation, and it mostly depends on speed or quality of the device's Internet connection. Using Google Storage to store the pictures reduces time, because uploading is done prior to any processing, and the image is transferred over much faster network between Google services. While testing the proposed method we didn't have any problem with slow response, even with lower speed mobile data connection to Internet.

5.1 Uploading images

Images can be uploaded on Google Cloud Storage which offers a unified object storage, primarily for developers and enterprises, from data serving to data analytics and data archiving. Google Cloud is optimal for live data, like video streaming and frequently accessed content like web sites and images (GCS 2016). For our purpose, Google Cloud Storage offers ease of access and processing as the user only needs to use adequate link to his project bucket and image name (for example – *gs://<your-project-bucket>/landmark.jpg*).

Another method for uploading images is based on base64 encoding (Josefsson 2006). Each image is read from local storage, encoded using base64 encoding and uploaded with a request to Google Vision API instance.

5.2 Processing modes

Google Vision API supports two basic types of processing: single image and batch processing. In single image processing mode, the user uploads a single base64 encoded image or sends a link to his Google Storage bucket as part of the request.

In batch mode, the user sends multiple images, or links, as part of single request.

In this phase we can define which type of features we are looking for. For example, we can execute image content analysis, text detection and optical character recognition, face detection, landmark detection or company logo recognition. We can ask for multiple responses for the same image, and they will be sorted in a descending order based on the score and the correctness of the exact selection.

5.3 Responses

Google Vision API returns a structured response in a JSON format containing, in case of batch processing, image names and data about the image. In case of landmark detection Google returns the following data for each image: the position described with latitude and longitude, a score value for the correctness of detection, the image coordinates of the bounding box around the detected landmark and a description, usually the name of the detected landmark.

6 RESULTS

Testing of this method included one hundred images divided in two sets of fifty images. The first set, called 'Existing images', consisted of images downloaded from the Internet, while the second set, called "New images", consisted of the images we took in live mode while testing the method or images taken from our private set of photos. The typical content present in the images were historical and cultural landmarks around Europe, often but not exclusively from Croatia.

The results confirmed our initial presupposition regarding Google machine learning algorithms, i.e. images downloaded from the Internet had a higher success rate than our personal images. The results can be seen in Table 2.

Table 2 Test result

	Existing images	**New images**
Positive	43	34
Negative	7	16
False positive	0	0

In Figures 5 – a, b, c, d, e, and f some examples of detected landmarks are shown. In all cases in the bottom left corner can be seen the information on the landmark, the likelihood and its latitude and longitude. In Figure 5e in particular the image is pictured from inside out which resulted with a lower likelihood. Also interesting is the result on image in Figure 5d where the algorithm detected only a part from the front wall of the landmark. In Figure 5f images of the church of Saint Jacob in Šibenik from different angles and with different conditions resulted with different likelihoods.

Figure 5 Detected landmarks on existing images from internet a) Dubrovnik, b) Water Tank in Vukovar, c) Diocletian's Palace from Split, d) Euphrasian Basilica from Poreč, e) Arena from Pula, f) church of Saint Jacob in Šibenik and on new images g) Motovun City Gate and h) Azure Window

7 CONCLUSION

In this work we studied the potential of using a Google Vision API, part of Google Cloud Platform, for geolocation. Using a hands on type of research we tested the image processing capabilities of the Google Vision API and looked at functionalities it provides. By analysing the technical background of used techniques we learned how it works, what are the current limitations and how it can be used for geolocation purposes. We proposed a method that can be used to identify the geographical location of the user and/or device by uploading the images containing the information on the environment around the user to Google Vision API. The proposed method and testing results also apply to newly growing Internet of things (IoT) paradigm. The described services can easily be used in one of IoT' s typical communication models.

The accuracy of the method depends on multiple factors, including the number of uploaded images, the content of the images, lightning and weather conditions, and of course it is highly dependent on Google Vision API performance which in turn depends on having a large and ever growing learning dataset which Google is building. Currently good results can be expected with highly popular landmarks and places.

REFERENCES

Evans, D. (2011) The Internet of Things, How the Next Evolution of the Internet Is Changing Everything, Cisco Internet Business Solutions Group (IBSG). (www.cisco.com/c/dam/en_us/about/ac79/docs/innov/IoT_IBSG_0411FINAL.pdf)

Google Cloud Documentation (GCD). (2016) (https://cloud.google.com/docs/)

Google Cloud Platform (GCPa). (2016) Choosing a Storage Option (https://cloud.google.com/ storage-options/)

Google Cloud Platform (GCPc). (2016) Google Vision API (https://cloud.google.com/vision/)

Google Cloud Products. (GCPb) (2016) (https://cloud.google.com/products/)

Google Cloud Storage (GCS). (2016) (https://cloud.google.com/storage/)

GSM Association. (2014) Understanding the Internet of Things (IoT) (www.gsma.com/connectedliving/wp-content/uploads/2014/08/cl_iot_wp_07_14.pdf)

Internet Society (IS). (2015) The Internet of Things: An Overview: Understanding the Issues and Challenges of More Connected World. (www.internetsociety.org/sites/default/files/ISOC-IoT-Overview-20151014_0.pdf)

Josefsson, S. (2006) RFC 4648: The Base16, Base32, and Base64 Data Encodings.

Kubernetes Official Page (2016) (http://kubernetes.io/)

Sveučilište u Rijeci
POMORSKI FAKULTET U RIJECI
FACULTY OF MARITIME STUDIES RIJEKA
University of Rijeka

University of Zagreb
Faculty of Transport
and Traffic Sciences

Royal Institute of Navigation
Science Technology Practice

10th
Annual
Baška GNSS
Conference

VERNAL EQUINOX TEC BEHAVIOUR IN CORRELATION WITH GPS COORDINATES' DEVIATIONS

David Brčić, Barbara Pongračić, Serdjo Kos

Faculty of Maritime Studies, University of Rijeka, Rijeka, Croatia
E-mail: brcic@pfri.hr

Abstract

Satellite positioning signals' ionospheric delay presents major single cause of GPS L1 performance degradation, caused by Total Electron Content (TEC) dynamics. Depending on nature of the particular event, TEC processes differ in several timescales, ranging from sudden solar events, solar cycle timescale and storm time periods. In long term, it is assumed that TEC behaviour is governed by Solar Ultra-Violet (UV) flux. TEC regularities have already been modelled, GPS ionospheric model being one of them. Characteristic TEC patterns have been observed in the area of Northern Adriatic (middle latitude region), being the motivation for the conducted research. Three vernal periods were analysed. Computed ionospheric delay was compared with the Klobuchar model. Although TEC showed gradual decrease following the solar cycle decline, several events caused its redistribution and peaking. Simultaneously, latitude and longitude coordinates' deviations were calculated both with and without ionospheric model correction. Preliminary results showed measurable correlation between ionospheric delay and coordinate deviations' residuals. Performance of the ionospheric model was discussed in terms of ionospheric delay description, pseudorange corrections and coordinate error mitigation. Modelled and un-modelled coordinate deviation patterns showed measurable correlation in quiet and unsettled periods. During the storm period, trends of patterns showed significant difference in observed values, as discussed. Results are outlined in the final chapter, together with planned continuation of the research.

Key words: *total electron content, ionospheric model, coordinate deviation patterns, Northern Adriatic Region*

1 INTRODUCTION

Ionospheric TEC acts as a major cause of satellite positioning signals delay (Parkinson & Spilker, Jr. 1999, Hernandez-Pajares, Zornoza & Subirana 2005, Subirana, Zornoza & Hernandez-Pajares 2013). It passes through different ionospheric layers, causing the signal deflection from straight geometric path (Petrovski & Tsujii 2012, Subirana, Zornoza & Hernandez-Pajares 2013, Feynman, Leighton & Sands 2011), prolonging the actual path. TEC dynamics can be described as production, distribution, movement and loss of free ionospheric electrons. Global distribution and state of the ionosphere are affected by geophysical effects, including (Mendillo 2006, Klobuchar 1988, Rishbeth 1988):

- Changes in chemical composition of different ionospheric layers,
- Alterations of neutral winds and,
- Diurnal changes in electric fields which initiate ionization processes along geomagnetic field lines, as well as thermal energy expansion in high latitude areas.

Geomagnetic activity can be described with *Kp* and *Dst* indices. *Kp* index indicates strength of geomagnetic storms and disturbances in the horizontal component of geomagnetic field. It is derived from mean standardized values of 13 geomagnetic observatories on mid-latitudes. *Kp* values range from 0 to 9, with 0 being calm and 5 or more indicating geomagnetic storm (NOAA 2016a). *Dst* index is an index used to represent equatorial geomagnetic activity measuring equatorial electrojet. Geomagnetic storm is indicated by sudden rise of *Dst* values followed by a sharp decrease with great negative values (Sugiura & Kamei 2016).

TEC can be defined as the total number of electrons along the signal path contained in a column with square meter cross section (Subirana, Zornoza & Hernandez-Pajares 2013):

$$STEC = \int N(s)ds \tag{1}$$

Where:

STEC – slant TEC; *N* – electron density; *s* – signal path length.

The lowest ionospheric delay values are present when satellite elevation angle is 90° (Klobuchar 1987, Subirana, Zornoza & Hernandez-Pajares 2013, Petrovski & Tsujii 2012). TEC is expressed in TEC units where 1 TECU = 10^{16} electron/m^2 or approximately 16 cm (0.54 ns) of range error at GPS L1 frequency (Subirana, Zornoza & Hernandez-Pajares 2013, Parkinson & Spilker, Jr. 1999, Hernandez-Pajares, Zornoza & Subirana 2005). STEC is dependable on the satellite elevation which is corrected by estimation of vertical TEC above given point on the surface of the Earth. TEC dynamics are being affected by the solar cycle (Mendillo 2006, Klobuchar 1988) which is currently declining after its 2013-2014 maximum (NOAA 2016c). Diurnal TEC values are under influence of solar radiation and solar zenith angle causing greater values during daytime (Parkinson & Spilker, Jr. 1999, Klobuchar 1983). Annual maximum values are observed during equinoxes when solar radiation is perpendicular to the equator (Klobuchar 1988, Rishbeth 1988). For GPS single frequency users, Klobuchar ionospheric model is used to estimate the ionospheric delay (Klobuchar 1975, Klobuchar 1983). TEC is calculated in a point obtained by the intersection between the satellite signal path and average height of the ionosphere (350 km). Night-time correction is constant at value of 5 ns (9.24 TECU), while day-time correction is modelled as a cosine curve with peak at 14:00 local time. Slant factor is calculated as elevation function for each satellite (Klobuchar 1987):

$$F = 1 + 16(0.53 - E)^3 \qquad (2)$$

Where:

F – slant factor; E – satellite elevation.

Cosine curve is defined by amplitude, period and phase depending on α_n and β_n coefficients, generated by observation date and mean solar flux and transmitted in the navigation message (Ovstedal 2002).

GPS positioning performance degradation in the elaborated area is the subject of constant research (Brčić, Kos & Filjar 2012, Kos, Barić & Brčić 2015, Brčić, Filjar & Kos 2014). In the proposed paper, TEC dynamics have been analysed during main space weather (geomagnetic) conditions in the area of the Northern Adriatic, comprising several days' observations. Several TEC diurnal patterns were noticed, as it will be presented. During same periods, GPS horizontal coordinates' deviations were analysed in the area. Horizontal positions were computed both with and without employment of the ionospheric model, making

two types of obtained positions' datasets. Analyses of modelled and un-modelled positional values showed different patterns, depending on geomagnetic activity which took place. Deviations were further compared with residuals calculated as differences between computed and modelled TEC values, expressed in seconds of delay. Results and findings are presented in the concluding chapter, together with preferred activities as continuation of the research.

2 METHODOLOGY

Positioning data from three IGS stations were collected: Bolzano, Medicina and Graz (Figure 1) (IGS 2016a), in order to gather results applicable in regional terms. GPS positioning files (RINEX.pos) were calculated and archived using RTKLIB open source program package, employing observation and navigation files. Ionospheric correction was settled by employing standard ionospheric model, coefficients of which were taken from diurnal navigational messages. Other standard methods and algorithms were settled as follows: static positioning mode, L1 frequency (single) positioning solution, 15° elevation mask, broadcast ephemeris, continuous ambiguity resolution and tropospheric model (Saastamonien).

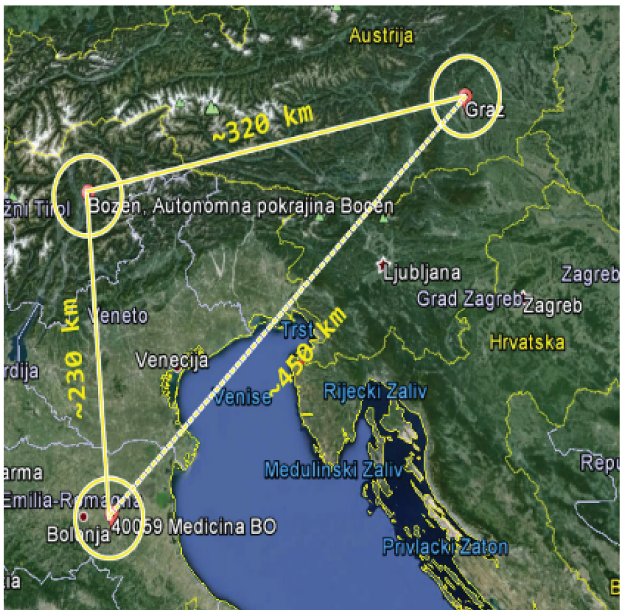

Figure 1 Position of IGS stations: Bolzano, Medicina and Graz.

Vernal equinoxes were selected for analysis due to mutual perpendicular position of the solar terminator and the equator. Periods of 9 consecutive days in years 2014, 2015 and 2016 were elaborated, with geomagnetic conditions described with *Kp* and *Dst* indices. Coordinate deviations were monitored as responses to TEC behaviour.

During selected period in 2014 *Kp* values varied between 0 and 3 and *Dst* values between -20 and 22 nT. *Kp* values during vernal equinox period in 2015 reached values up to 7.7 with decrease in *Dst* values to -223 *nT*. During the same period in 2016 *Kp* and *Dst* retained their moderate values. Vernal equinox periods during 2014, 2015 and 2016 were characterized as quite, severe and unsettled geomagnetic conditions respectively (Kamide & Chian 2007, NOAA 2016b). On Figure 2, time series of both geomagnetic indices through analysed periods are shown.

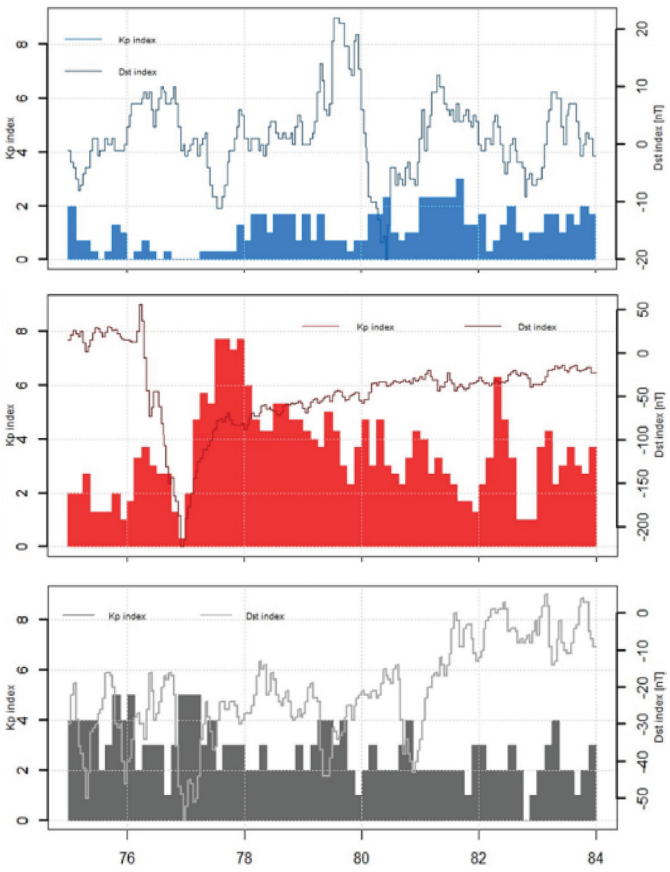

Figure 2 Values of Kp and Dst indices during vernal equinox periods in 2014 (top), 2015 (middle) and 2016 (bottom).

TEC values were calculated by using dual frequency GPS measurements from all IGS stations. Measured phase differences were smoothed with code differences, after which they were levelled again using code differences in order to correct TEC values. After Differential Code Biases (DCB) correction, it is assumed that all frequency-dependent quantities except ionospheric delay were satisfactory eliminated. Geometry-free combination and elimination of error due to instrumental biases were made using Rinex-GPS-TEC software. Similar TEC patterns were present on all locations, thus only Bolzano data were processed. This was confirmed by calculating residuals of TEC values in 2014 and 2015, as shown on Figure 3.

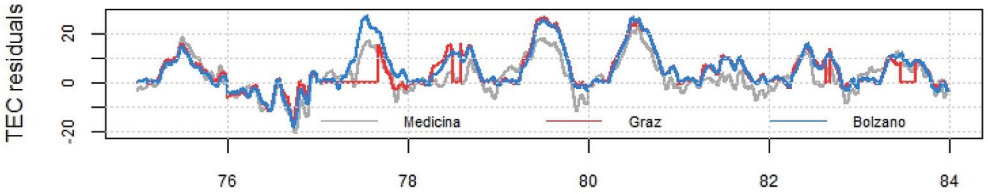

Figure 3 TEC residuals for Medicina, Graz and Bolzano between 2014 and 2015.

Residuals, expressed in seconds, between TEC values retrieved by Klobuchar's correction model of ionospheric delay and ionospheric TEC values were calculated to be modelled in correlation with coordinate's deviations. TEC values from Klobuchar's correction model of ionospheric delay were calculated using coefficients contained in and transmitted by GPS satellite navigational messages on daily basis in standardized RINEX format (IGS 2016a) and according to Klobuchar's correction model of ionospheric delay algorithm (Klobuchar 1975). Overall TEC values have negative trend due to declining solar cycle and with diurnal peak values during daytime. Greatest diurnal TEC values were observed during the 76th day in 2015 when geomagnetic disturbance occurred (NOAA 2016d). On Figure 4, calculated and modelled TEC are presented during observed periods, showing TEC patterns in three consecutive years.

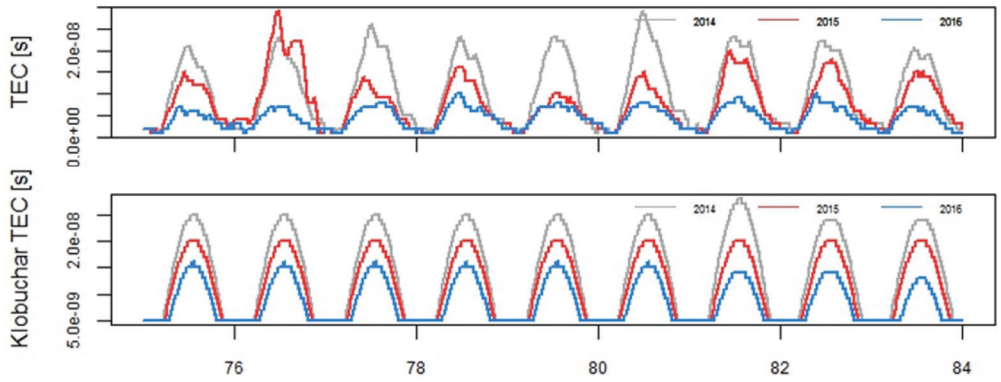

Figure 4 Calculated TEC time series in seconds' equivalents (upper image) and modelled ionospheric delay (lower image) through elaborated periods.

GPS coordinates' deviations were calculated with the reference to the mean position:

$$\Delta\varphi = (\varphi_c - \varphi_M) \times 60 \times 1852\ (m) \tag{3}$$

$$\Delta\lambda = \frac{(\lambda c - \lambda M)\cos\varphi_M \pi}{180}\ (m) \tag{4}$$

where $\Delta\varphi$ – northing error (m); φ_c – calculated/measured latitude (°); φ_M – mean latitude (°); $\Delta\lambda$ – easting error (m); λ_c – calculated/measured longitude (°); λ_M – mean longitude (°).

Due to insufficiently accurate position of Bolzano IGS station available (IGS 2016b), coordinates' deviations were calculated from the mean position during all three periods. Coordinates' residuals were calculated as differences between deviations obtained with and without applied correction model:

$$\varphi_{residual} = \Delta\varphi_{on} - \Delta\varphi_{off}(m) \tag{5}$$

$$\lambda_{residual} = \Delta\lambda_{on} - \Delta\lambda_{off}(m) \tag{6}$$

where $\varphi_{residual}$ – latitude residual value (m); $\Delta\varphi_{on}$ – Klobuchar-modelled latitude deviation (m); $\Delta\varphi_{off}$ – un-modelled latitude deviation (m); $\lambda_{residual}$ – longitude residual value (m); $\Delta\lambda_{on}$ – Klobuchar-modelled longitude deviation (m); $\Delta\lambda_{off}$ – un-modelled longitude deviation (m).

3 INTERPRETATION OF RESULTS

Latitude deviation from the mean value was most evident in 2015. During all periods, longitude had smaller deviations in comparison with latitude, as presented on Figure 5. Positions obtained with applied Klobuchar's model showed less deviation from the mean value.

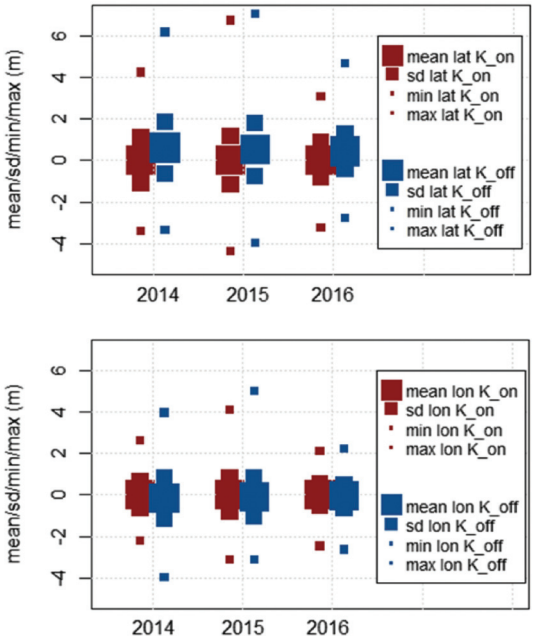

Figure 5 Latitude and longitude deviation statistics: mean value, standard deviation and minimal and maximal values.

Coordinates' deviation residuals were similar during 2014 and 2016. In both years there was recognizable residual pattern. Longitude residuals were mainly positive while latitude residuals had mostly negative values. In 2015 there was no such pattern; during the geomagnetic disturbance both coordinates had negative residuals. It is also noticeable that longitude residuals returned to normal values faster than latitude residuals.

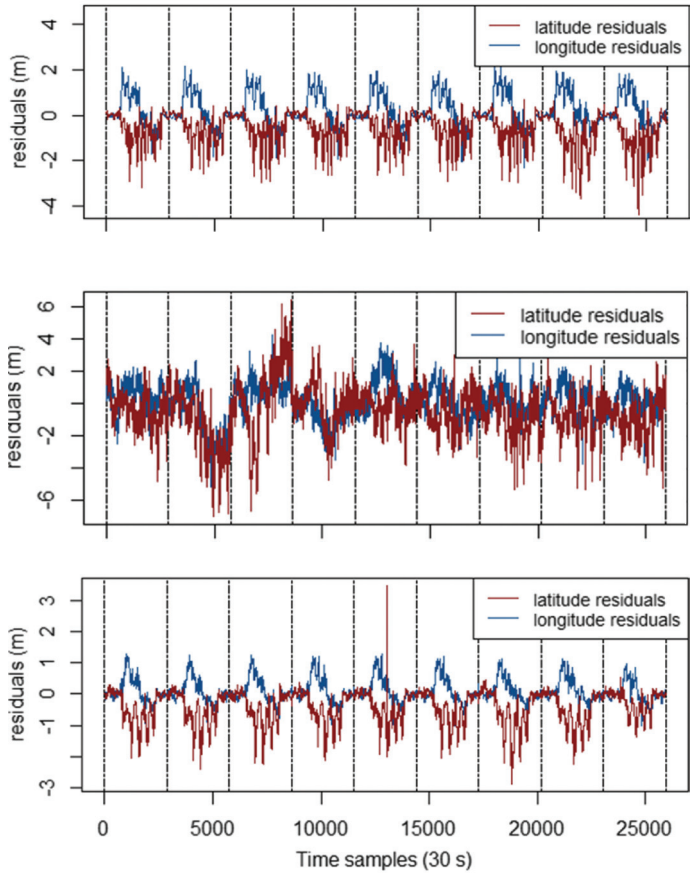

Figure 6 Latitude and longitude coordinates' deviation residuals through observed periods in 2014 (top), 2015 (middle) and 2016 (bottom).

TEC residuals were negative during 2015 and positive in 2014 and 2016, except during day 80/2014 (Figure 7). For the next day, Klobuchar coefficients were changed (Figure 4) and residuals returned to positive values. During geomagnetic disturbance both TEC residuals and coordinates' deviations were negative.

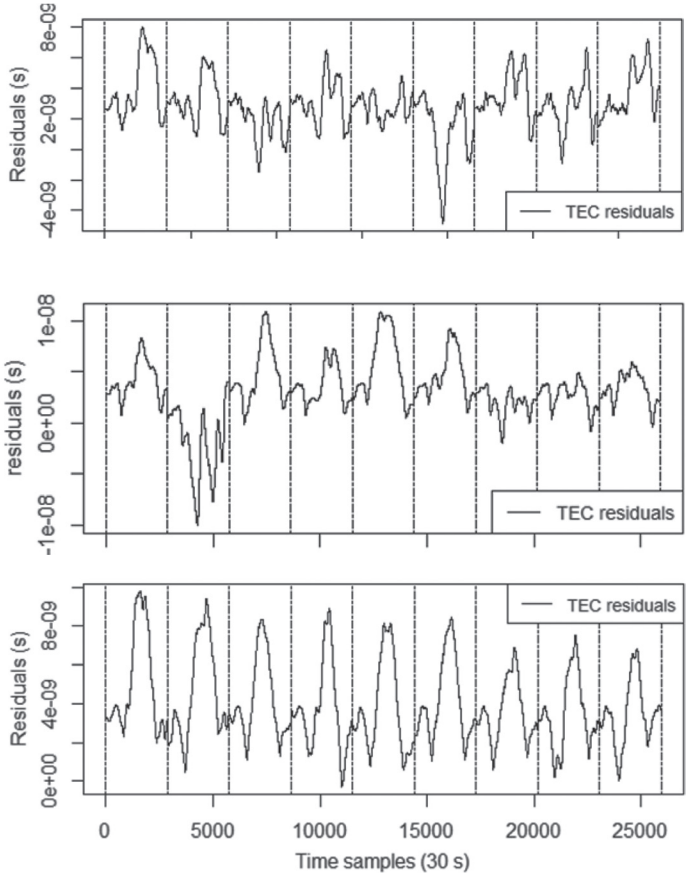

Figure 7 TEC residuals during observed periods in 2014 (top), 2015 (middle) and 2016 (bottom).

There was less dispersion in coordinates' deviations during 2014 and 2016 than in 2015. Longitude deviations were centred on approximately zero, while latitude deviations differed. Conducted linear regression showed low R-squared values in 2015 meaning that multi-variable regression and non-linear correlation model should be applied. On Figure 8, bivariate histograms (hexagon binning) representing modelled and un-modelled latitude and longitude deviations are shown.

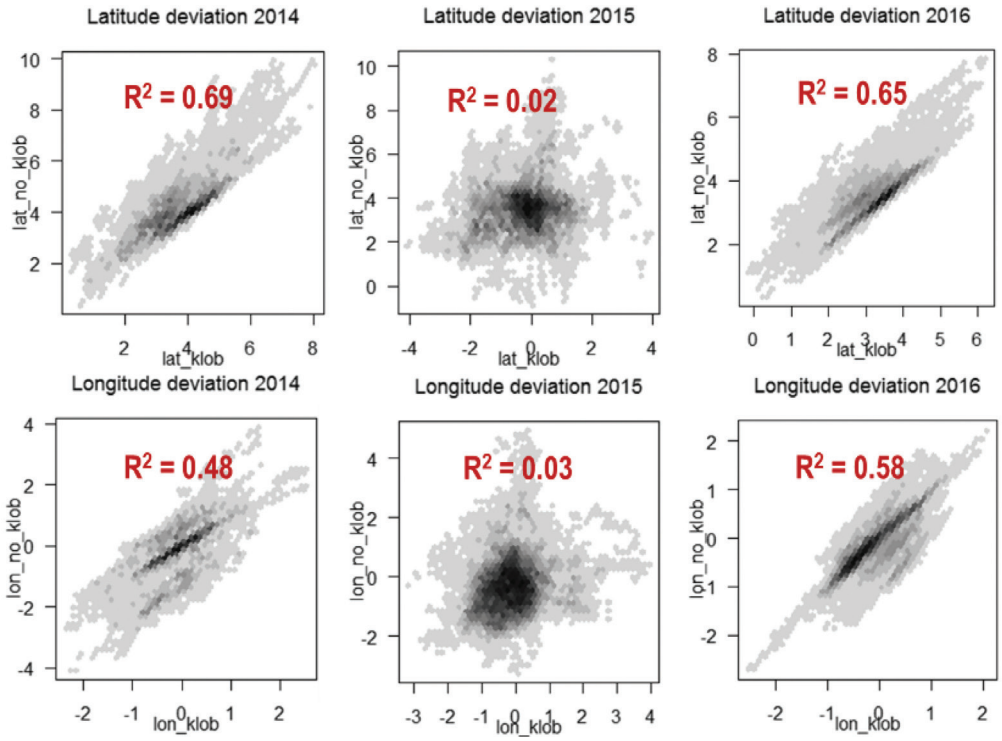

Figure 8 Hexbin plots of latitude and longitude deviations, showing r-squared coefficients between modelled and un-modelled values during observed periods. The number of points falling in each hexagon is plotted in grayscale proportional to the counts (a darker plot represents greater count).

Pearson's and Spearman's correlation methods were used to determine possible linearity between variables, i.e. coordinates' residuals and TEC residuals. Pearson's correlation coefficients were greater for longitude residuals and TEC values but relatively weak (0.32). For geomagnetic conditions in 2015 Pearson's coefficient for longitude residuals and TEC values was -0.08. Latitude residuals with TEC values showed more correlation using Spearman's correlation method with correlation coefficients of -0.72 in 2016. When comparing correlation coefficients for latitude and longitude residuals with TEC residuals it has been noticed that Spearman's correlation coefficients were more significant. Longitude and TEC residuals had negative correlation coefficients during severe geomagnetic conditions in 2015. Correlation results are presented in Table 1.

Table 1 Pearson's and Spearman's coefficients for latitude and longitude residuals with TEC and TEC residuals values.

2014				
	TEC		TEC residuals	
	Pearson	*Spearman*	*Pearson*	*Spearman*
Latitude residuals	-0.595958958	-0.6776599	0.116142	0.15650009
Longitude residuals	0.1934686	0.1879289	0.3383002	0.36992266
2015				
	TEC		TEC residuals	
	Pearson	*Spearman*	*Pearson*	*Spearman*
Latitude residuals	-0.34787505	-0.35085458	0.20202758	-0.03491978
Longitude residuals	-0.08521554	0.0334332	-0.30042874	-0.17449550
2016				
	TEC		TEC residuals	
	Pearson	*Spearman*	*Pearson*	*Spearman*
Latitude residuals	-0.72381814	-0.77823157	0.50750006	0.45324032
Longitude residuals	0.32484957	0.27352732	0.07605711	0.08966107

During each observed period a single day was analysed, representing specific period characteristics: quiet, unsettled and severe geomagnetic conditions. During geomagnetic disturbance on 76th day of 2015 correlation coefficients were significantly lower than coefficients regarding whole period in 2015. Also, correlation coefficients were negative (coordinates' residuals with ionospheric TEC values, modelled TEC values and TEC residuals) when comparing with 76th day of 2014 and 2016. The best correlation was noticed during 76th day in 2016.

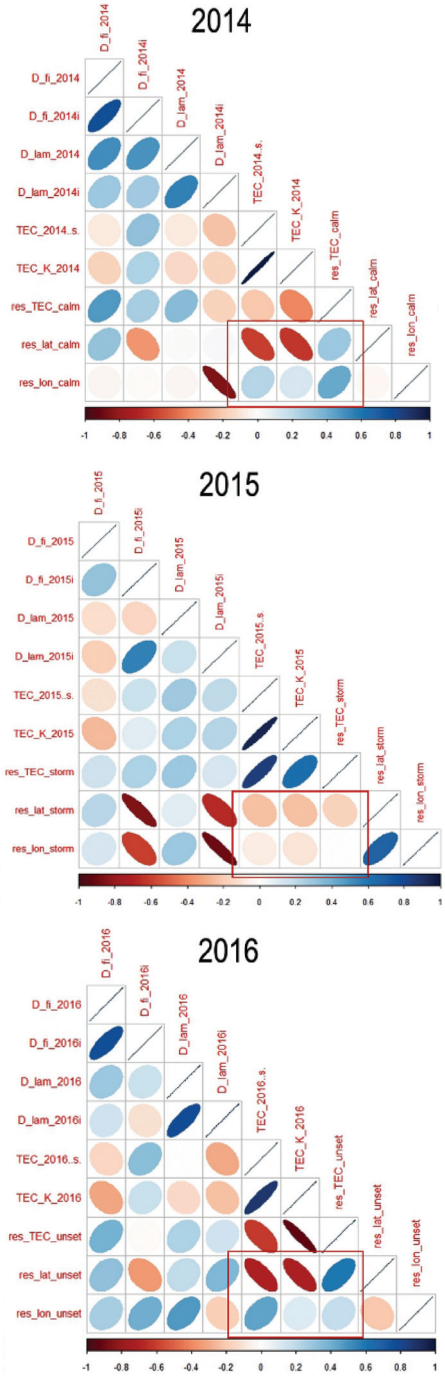

Figure 9 Correlation matrices between positioning and TEC observables, and residuals for a day 76 in 2014 (top), 2015 (middle) and 2016 (bottom).

As for daily TEC patterns, several types were observed, as already identified in (Kos, Barić & Brčić 2016); 'standard' pattern with one TEC peak, a pattern with two peaks during the day, and a pattern with three peaks, occurring before, at and after the culmination of the Sun.

4 CONCLUSIONS AND FURTHER WORK

Similarities in TEC values and residuals regarding three chosen locations confirmed that disturbance occurred during 2015 had influence on regional basis. Due to its geographical location and availability of data, Bolzano IGS station was chosen as representative station. By processing data from three consecutive years, representing three levels of geomagnetic/space weather activity it has been noticed that TEC values were decreasing which was being followed by its modelled values, in accordance with declining solar cycle. Minimal TEC values were the same for all three years during night time period. Daily maximum values showed significant difference. Diurnal TEC pattern as described with Klobuchar model was rarely noticed. The most commonly observed TEC daily pattern was in the form of two cosine curves next to each other, latter being truncated and constant till the end of the day (in night hours). Coordinates' deviations showed distinctive patterns during 2014 and 2016. Longitude coordinates' deviations showed more resilience than latitude, despite the fact that longitude acts as more complex coordinate due to the rotation of the Earth. When comparing coordinate deviations and statistical results of modelled and un-modelled coordinate's deviation, during storm time period there were no larger deviations regarding coordinates' values. Modelled and un-modelled coordinates' deviations showed better results and in 2015 barely any similarity in their behaviour.

Results can be interpreted in various ways. During geomagnetic disturbances (2015), modelled and un-modelled coordinates' deviations haven't shown similarities when compared to quiet (2014) and moderate (2016) geomagnetic activity behaviour. Klobuchar model was less successful during this period. Comparing residuals, it was noticed that during 2015 both coordinates tended to have a negative direction, i.e. south and west – unlike during periods in other years. During 2015 there was weak correlation, both for coordinates' deviation residuals with TEC and TEC residuals values. Also, longitude had weaker correlation coefficients than latitude. Research will be continued regarding other periods and other stations (other mid-latitude stations in combination with polar and equatorial stations) with emphasis on longitude coordinates' deviation.

Acknowledgments

Research activities presented in this paper were conducted under the research project Research into the correlation of maritime-transport elements in marine traffic: Satellite navigation segment, supported by the University of Rijeka, Croatia. Authors appreciate, compliment and support the access to open software packages and tools used in the presented research: *R*, *R Studio* and *Rattle*, *RTKLIB* and *Rinex-GPS-TEC*.

REFERENCES

Brčić, D., Filjar, R. & Kos, S. (2014) On identification of local GPS ionospheric delay anomaly in the Adriatic Sea area. *Proceedings of the 34th International Conference on Transportation Systems (KOREMA)*. Dubrovnik, Hrvatska, 5–9. 11. 2014. pp. 112–115.

Brčić, D., Kos, S. & Filjar, R. (2012) A case of degraded GPS performance during a short-term ionospheric disturbance in Northern Adriatic. *Proceedings of the 6th Global Navigation Satellite Systems Vulnerabilities and Solutions Conference*. Royal Institute of Navigation, London, UK; The Nottingham Geospatial Institute, University of Nottingham, UK & University of Rijeka, Faculty of Maritime Studies. Baška, Hrvatska, 21–24. 5. 2012. pp. 23–35.

Feynman, R. P., Leighton R. B. & Sands, M. (2011) The Feynman Lectures on Physics. New York: Basic Books.

Hernandez-Pajares, M., Zornoza J. M. J. & Subirana, J. S. (2005) *GPS Data processing: code and phase Algorithms, Techniques and Recipes*. 2nd edition. Barcelona: Centre de Publicacions del Campus Nord, UPC.

International GNSS Service (IGS) (2016) IGS Station List (Online). Available: https://igscb.jpl.nasa.gov/network/list.html

International GNSS Service (IGS). (2016) (Online). Available at: ftp://igs.ensg.ign.fr/pub/igs/data/

Kamide, Y. & Chian A. C. L. (Eds.) (2007) *Handbook of the Solar-Terrestrial Environment*. New York: Springer Science and Business Media.

Klobuchar, J. A. (1975) A First-Order, Worldwide, Ionospheric, Time-Delay Algorithm. *IPL Project No. 4643*. Hanscom: Air Force Cambridge Research Laboratory. p. 25.

Klobuchar, J. A. (1983) Ionospheric Effects on Earth-Space Propagation. *Environmental research paper No. 866*. Hanscom: Air Force Geophysics Laboratory. p. 33.

Klobuchar, J. A. (1987) Ionospheric Time-Delay Algorithm for Single-Frequency GPS Users. *IEEE Transactions on Aerospace and Electronic Systems*. 23 (3). pp. 325–331.

Klobuchar, J. A. (1988) Ionospheric corrections for timing applications. *Proceedings of the 20th Annual Precise Time and Time Interval (PTTI) Application and Planning Meeting*. (On CD) pp. 193–204. Vienna (VA), 07-09.12.1988. Washington DC: Naval Observatory.

Kos, S., Barić, M. & Brčić, D. (2015) Discrepancies between predicted and final IGS ionospheric maps in the Northern Adriatic region. *Proceedings of the 9th Annual Baška*

GNSS Conference. The Royal Institute of Navigation, London & University of Rijeka, Faculty of Maritime Studies. Baška, Hrvatska, 10-12.5.2015. pp. 35–52.

Mendillo, M. (2006) Storms in the ionosphere: Patterns and processes for total electron content. *Reviews of Geophysics*. 44 (4). p. 47.

NOAA SWPC (2016) *Geomagnetic Kp and Ap indices*. (Online). Available at: http://www.ngdc.noaa.gov/stp/GEOMAG/kp_ap.html

NOAA SWPC (2016) *Solar cycle progression*. (Online). Available at: http://www.swpc.noaa.gov/products/solar-cycle-progression

NOAA SWPC (2016) *Space weather scales*. (Online). Available at: http://www.swpc.noaa.gov/noaa-scales-explanation

NOAA SWPC (2016) *Weekly overview-Space weather highlights 16 March – 22 March 2015*. (Online). Available at: http://www.swpc.noaa.gov/products/solar-cycle-progression

Ovstedal, O. (2002) Absolute positioning with single-frequency GPS receivers. *GPS Solutions.* 5 (4). pp. 33–44.

Parkinson, B. & Spilker, J. J. (1999) Global Positioning System: Theory and Applications. Volume I., Washington, DC: AIAA.

Petrovski, I. i Tsujii, T. (2012) *Digital Satellite Navigation and Geophysics: A Practical Guide with GNSS Signal Simulator and Receiver Laboratory*. Cambridge: Cambridge University Press.

Rishbeth, H. (1988) Basic physics of the ionosphere: a tutorial review. *Journal of the Institution of Electronic and Radio Engineers*. 58 (6). pp. S207–S223.

Subirana, J. S., Zornoza J. M. J. & Hernandez-Pajares, M. (2013) *GNSS Data processing, Volume I: Fundamentals and algorithms*. Noordwijk: ESA Communications.

Sugiura, M. & Kamei, T. (2016) On Dst index (description in the IAGA Bulltetin No 40). (Online). Available at: http://wdc.kugi.kyoto-u.ac.jp/dstdir/dst2/onDstindex.html.

Sveučilište u Rijeci
POMORSKI FAKULTET U RIJECI
FACULTY OF MARITIME STUDIES RIJEKA
University of Rijeka

University of Zagreb
Faculty of Transport
and Traffic Sciences

Royal Institute of Navigation
Science Technology Practice

10th
Annual
Baška GNSS
Conference

A CHARACTERISATION OF GNSS POSITIONING ERROR VECTOR BEARING DURING THE INTENSE SPACE WEATHER DISTURBANCE

Nenad Sikirica[1], Marko Ševrović[2], Renato Filjar[3,4]

[1] Polytechnic Hrvatsko Zagorje Krapina, Krapina, Croatia

[2] Faculty of Transport and Traffic Sciences, University of Zagreb, Zagreb, Croatia

[3] Faculty of Maritime Studies, University of Rijeka, Rijeka, Croatia

[4] Faculty of Engineering, University of Rijeka, Rijeka, Croatia
E-mail: renato.filjar@gmail.com

Abstract

Satellite navigation is enabling technology for a growing number of technology and socio-economic applications. A robust and accurate assessment of the GNSS positioning performance is required in order to assist the definition of Quality of Service for GNSS-based applications, and to allow for the identification of GNSS positioning performance deterioration. Here the Positioning Error Vector Bearing (PEVB) is introduced as a new indicator of GNSS positioning performance is proposed, that efficiently and accurately indicates GPS positioning performance deterioration due to geomagnetic effects.

Key words: *GNSS positioning performance, Positioning Error Vector Bearing (PEVB), space weather disturbance*

1 INTRODUCTION, AIM AND MOTIVATION

Satellite navigation has already been established as a fundamental enabling technology for a growing number of technology, scientific, industrial and socio-economic applications.

In general, space weather and ionospheric disturbances appear as the major single natural contributor to the GNSS positioning service quality deterioration (Davis, 1990, Canon *et al.* 2013). Thus, there is a growing need for an accurate assessment of the GNSS positioning performance and the reliable indication and identification of the approaching GNSS positioning performance deterioration caused by space weather and ionospheric effects.

Here we argue that the consideration of the GNSS positioning error in the sense of a vector rather than a scalar factor significantly improves identification of the influence of the space weather on the GNSS positioning performance. This hypothesis is challenged in the case scenario of the 2015 St Patrick's Day space weather event, where the time series analysis shows a clear signature of the space weather effect on positioning error vector bearing time series.

The manuscript concludes with the discussion of the sources of the signature and potential utilisation in forecasting the short-term forecasting and post-process analysis of the space weather effects on GNSS positioning performance.

2 PROBLEM DESCRIPTION AND PREVIOUS RESAERCH

Development of the GNSS-based and enabled applications requires the reasonable assurances of the quality of position estimation performed using the GNSS signals-in-space, since every anomaly in GNSS-base position estimation immediately affects the quality of GNSS-based applications (Thomas *et al.* 2011).

A wide research area has been established since the emergence of GNSS with the aim to methodically and systematically describe the causes of and the processes behind the GNSS position estimation errors (Sanz Subirana *et al.* 2013, Jin 2012). The GNSS position estimation error budget was identified in qualitative sense in the early days of the US-operated GPS system. Still, the robust models of the casues and processes of the GNSS position estimation error remain the aim of the current research in the field (Thomas *et al.* 2011).

Among the open question in the subject is the quest of identification of the principal indicators of the positon estimation error processes and their mapping to GNSS positioning performance.

A methodology for GNSS position estimation error determination has been appropriately established for a variety of GNSS-based applications. (Petrovski and Tsujii 2012) and (Petrovski 2014) summarised the general approach in GNSS position estimation error determination, based on common practices recommended in GNSS operation documents released by GNSS operators (operators of GPS, GLONASS, Beidou and Galileo systems). (Zandbergen & Barbeau 2011) gave a detailed outline of the GNSS position estimation error determination procedure, as seen from the perspective of mobile GNSS-based applications. (SaPPART 2016) presented a systematic and generalised methodology for the GNSS positioning performance assessment for road transport (including the Intelligent Transport Systems). (Thomas *et al.* 2011) systematically categorised a wide range of GNSS-based applications according to the requirements for the GNSS position estimation accuracy.

All the approaches assume the scalar nature of the GNSS position estimation errors, with the over-all GNSS positioning error budget due to natural sources shown in Table 1.

Table 1 An outline of the GNSS positioning error sources, a compilation after (Petrovski & Tsujii 2012), (Sanz Subirana *et al*. 2013), and (Jin 2012)

Error source by the nature of operation	Characteristic range	Mitigation method
1. Satellite and control segment		
Satellite ephemeris (orbit) error	(0.5 – 10) m	corrections
Satellite clock error	(0.5 – 10) m	differentiation
2. Propagation effects		
Ionospheric delay	(5– 150) m	corrections, modelling, differentiation
Tropospheric delay	(2 – 10) m	corrections, modelling, differentiation
3. User segment errors		
User receiver noise	(1 – 5) m	statistical signal processing, if necessary
Multipath error	(5 – 60) m	aerial characteristics and positioning, statistical signal processing in base-band domain

Those have been addressed and mitigated in the sense in the sense of un-correlated (statistically independent) processes, deriving the knowledge on the nature of GNSS position estimation errors from the dynamics of scalar position estimation errors time series in northing, easting and height directions.

Processes that generate the GNSS position estimation error have been identified during GPS/GNSS error budget assessment, and described in general (global) terms. A good overview of the mathematical models describing both the User Equivalent Range Errors (UERE) and Geometric Degradation of Precision (GDOP) components of the GNSS position estimation error can be found in a number of references, such as (Sanz Subirana *et al.* 2012).

The effects of ionospheric/space weather disturbances are of particular interest, since the GNSS ionospheric error remains the single most influential contributor to the over-all GNSS position estimation error. Although physical models of the GNSS ionospheric error generation have been established on the global level, the relationship between the parameters describing the space weather conditions and the GNSS positioning performance remains complex, thus preventing the development of the reasonably simple mathematical model that would allow for identification and forecasting of potential GNSS positioning performance deterioration.

3 A NOVEL PERSPECTIVE OF GPS POSITIONING ERROR DESCRIPTION WITH POSITIONING ERROR VECTOR BEARING

The GPS positioning error is a three-dimensional vector by its nature, given by its three components, as depicted in Figure 1. Alternatively and more commonly, the over-all GPS position estimation error may be determined by three components in geographical reference framework: the northing, easting, and vertical (height) ones.

The GPS positioning performance is considered differently in various GPS applications, depending on the number of mobile dynamics degrees of freedom. For instance, the majority of road traffic-related GPS applications are not concerned with the height determination error, rendering the planar (horizontal) GPS positioning error relevant only (Figure 2).

Here a novel perspective of the GPS positioning error description that includes the Positioning Error Vector Bearing (PEVB) is proposed. Furthermore, it is argued that the analysis of the PEVB dynamics, as an indicator of GPS position estimation quality, reveals the impact of the ionospheric effects on GPS positioning accuracy, thus rendering the PEVB a robust indicator of GPS positioning performance deterioration.

The GPS Positioning Error Vector Bearing is defined in horizontal plane, using the known GPS northing. e_n, and easting, e_e, error components, respectively, as denoted in (1).

$$PEVB = \tan^{-1}\left(\frac{e_n}{e_e}\right) \tag{1}$$

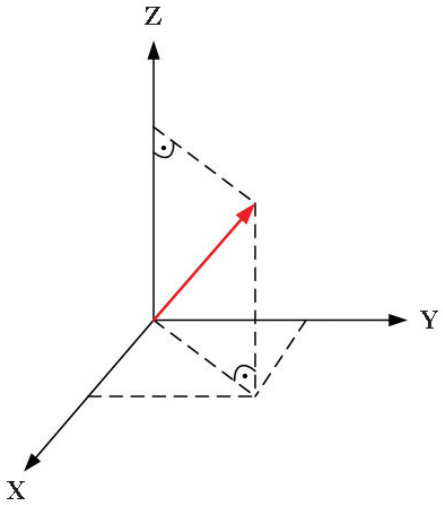

Figure 1 Definition of the GPS Positioning Error Vector Bearing (PEVB)

Definition of the GPS PEVB was given with the planar GPS applications concerned (most of the road traffic, maritime and location-based telecommunications applications fulfil the presumption). However, the generalised form that encompasses the third dimension (height) may be introduced for advanced purposes (air navigation, scientific applications etc.). It will be shown in the remaining part of this manuscript that the consideration of the planar GPS PEVB is sufficient to indicate the deterioration of the GPS positioning performance.

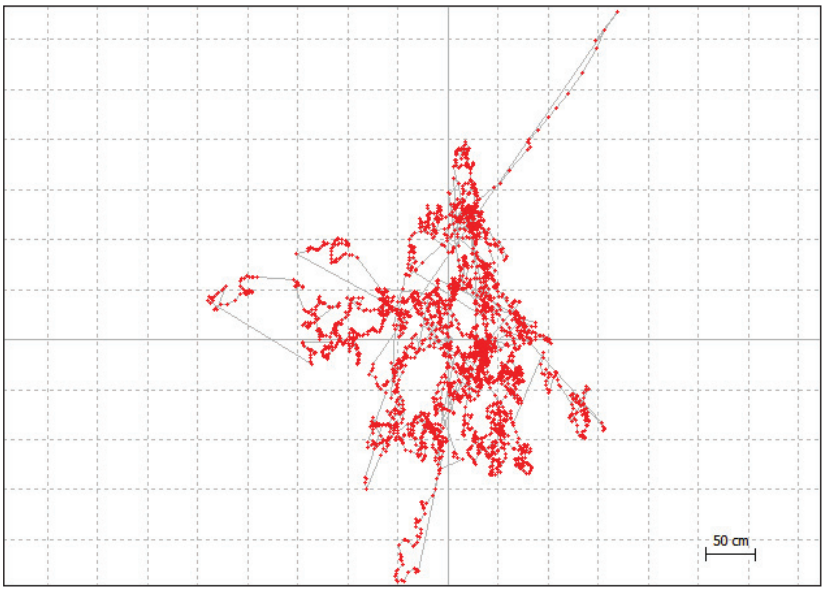

Figure 2 A daily set of GPS positioning errors, as observed at Padua reference GPS station in Padua, Italy

4 VALIDATION METHODOLOGY

The GPS PEVB concept for GPS positioning deterioration indication is demonstrated using the particular case of sudden deterioration of a geomagnetic and ionospheric storm, with the experimentally collected GPS pseudoranges. Ionospheric and geomagnetic storms are single most influential causes of GPS positioning performance deterioration (Canon 2013).

4.1 The 2015 St Patrick's Day event description

The fast-developing geomagnetic storm occurred on 17 March, 2015, on the traditional St Patrick'S Day, thus immediately acquiring the name of the 2015 St Patrick's Day space weather event (Jacobsen & Andalsvik 2016).

The storm in question resulted from the sudden solar discharge occurred on 15 March, 2015, as depicted in Figure 3 by time series of satellite-based solar radiation in various spectra. The geomagnetic storm outbreak is evident from the planetary Kp index records, indicating the intensity of the geomagnetic field disturbance, as shown in Figure 4.

A transition period between the solar and geomagnetic filed disturbances of around two days should be noted.

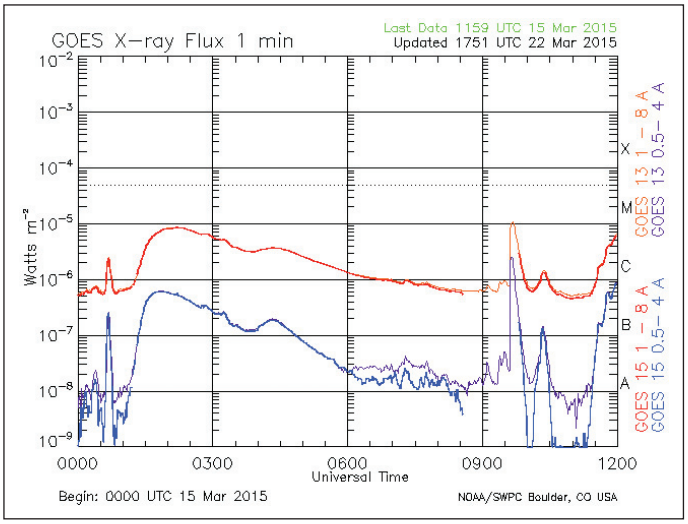

Figure 3 Space weather environment that caused the 2015 St Patrick's Day geomagnetic storm

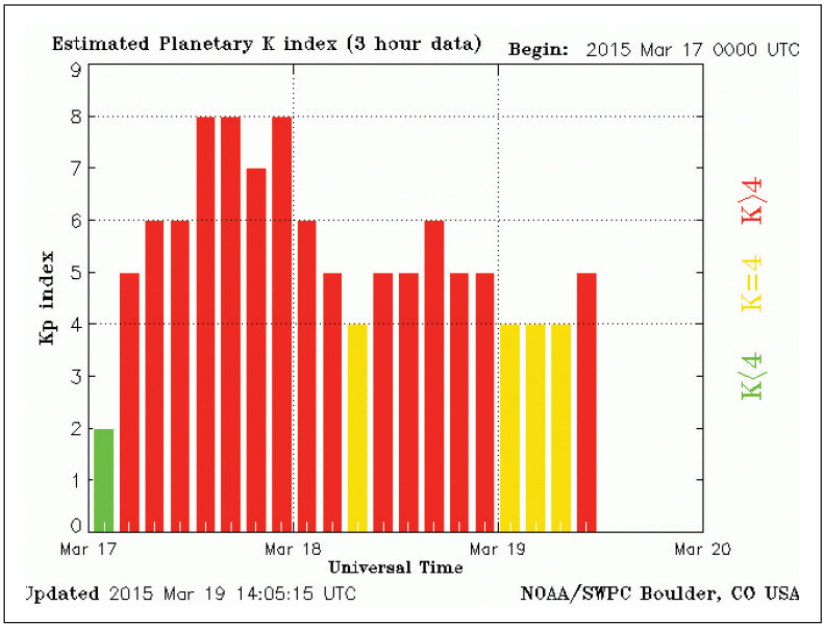

Figure 4 Planetary Kp index during the 2015 St Patrick's Day geomagnetic storm (Source: NOAA)

4.2 GPS positioning observations

GPS positioning observations used in this research were taken from the internet-based International GNSS Service (ICG) archive of GNSS observations. The database comprises 24-hours observations of GPS pseudoranges with 30 s-sampling interval, navigation messages, and (where possible) meteorological conditions and the other relevant information and observations sets. Observations are taken at the global network of stationary reference stations and stored in a specific data RINEX format. The GPS pseudoranges and navigation messages collected at the reference station in Padua, Italy (Figure 5) were used in this research. The choice of the Padua reference station was taken after consideration of the data quality record and due to its proximity to the Adriatic Sea area, a region with intense air, maritime and road traffic, as a potential benefiters of the research.

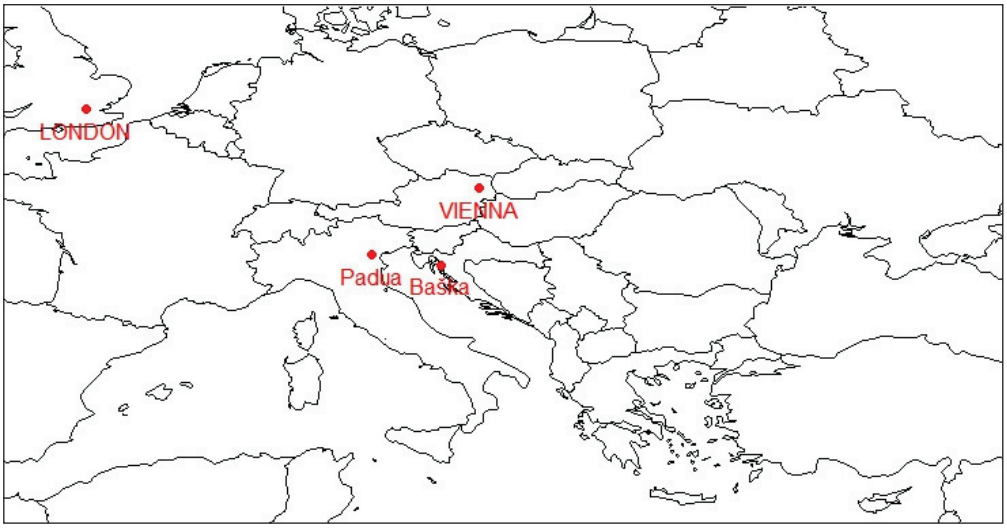

Figure 5 Position of the IGS reference station in Padua, Italy

5 RESEARCH RESULTS

The GPS positioning performance was analysed using the simulation approach based on the GPS pseudoranges observed at the IGS reference station in Padua, Italy on 15 March, 2015 (day 74, two days before the storm outbreak, used as the control case scenario) and on 17 March, 2015 (day 076, the day of the storm

outbreak). RTKLIB (Takasu 2013), an open-source GNSS Software Defined Radio (SDR) receiver configured to act as a commercial-grade single frequency GPS receiver, in a post-processing mode generated time series of GPS positioning northing, and easting errors in respect to the true position of the IGS reference station in Padua, Italy. Time series of positioning errors were analysed using the software developed by one of us (Filjar) in the R programming environment for statistical computing (R Development Core Team 2017). Further to this, the R-based software created a time series of GPS horizontal positioning error, as well as of the GPS PEVB. Those were further analysed with the R-based software developed to the purpose.

Time series of PEVB and the absolute horizontal positioning error, respectively, are presented for days 74 and 76 in Figures 6 and 7.

Histograms, as the first estimates of the probability distributions, for PEVB and the absolute horizontal positioning error, respectively, are presented for days 74 and 76 in Figures 8 and 9. Red line indicates the corresponding normal (Gaussian) distribution.

Raw periodograms, as the first estimates of the power spectra, for PEVB and the absolute horizontal positioning error, respectively, are presented for days 74 and 76 in Figures 10 and 11.

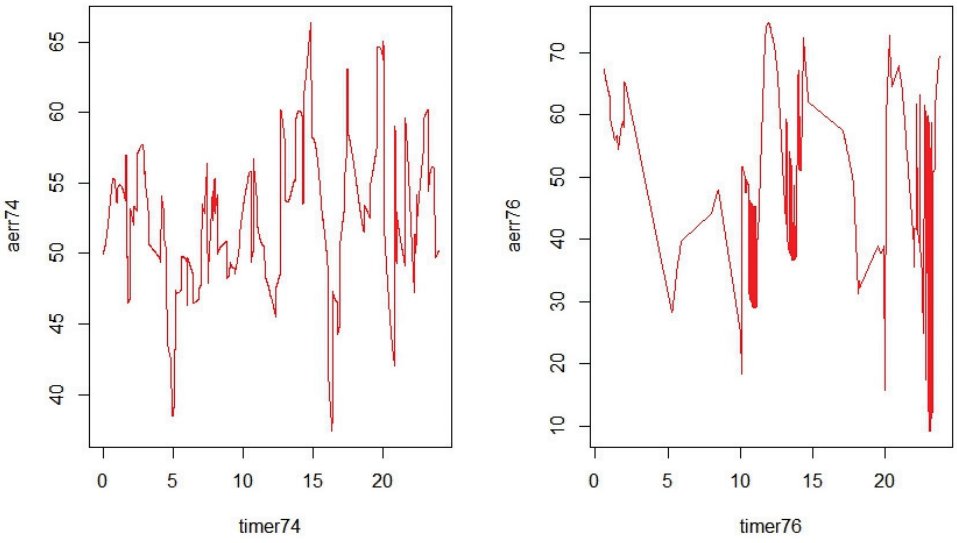

Figure 6 PEVB time series for days 74 (left) and 76 (right) in 2015

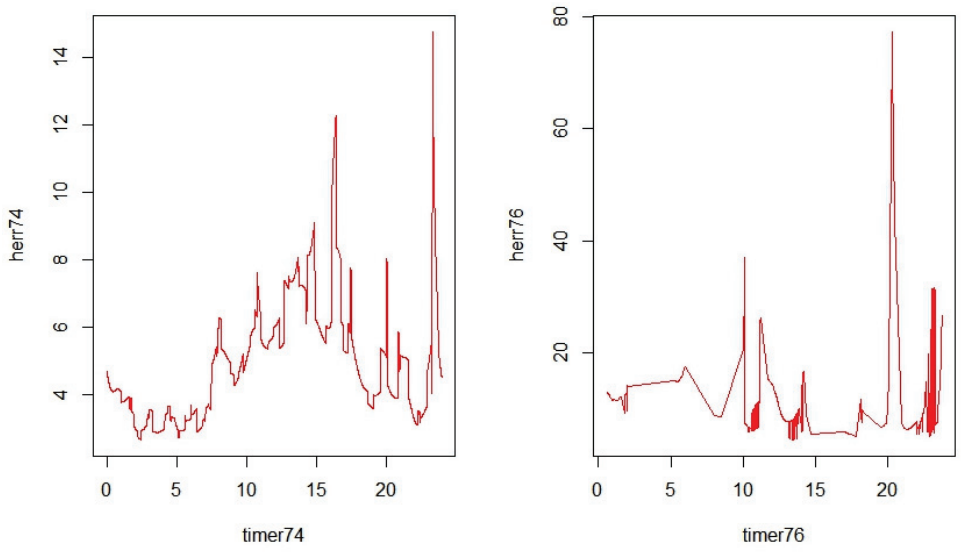

Figure 7 Horizontal positioning error time series for days 74 (left) and 76 (right) in 2015

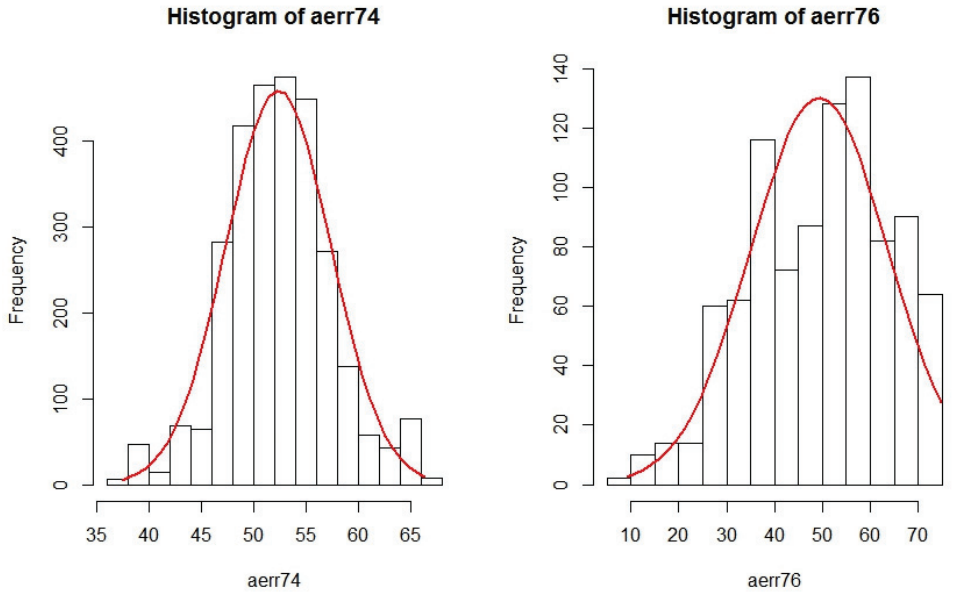

Figure 8 Histograms of PEVB, days 74 (left) and 76 (right) in 2015

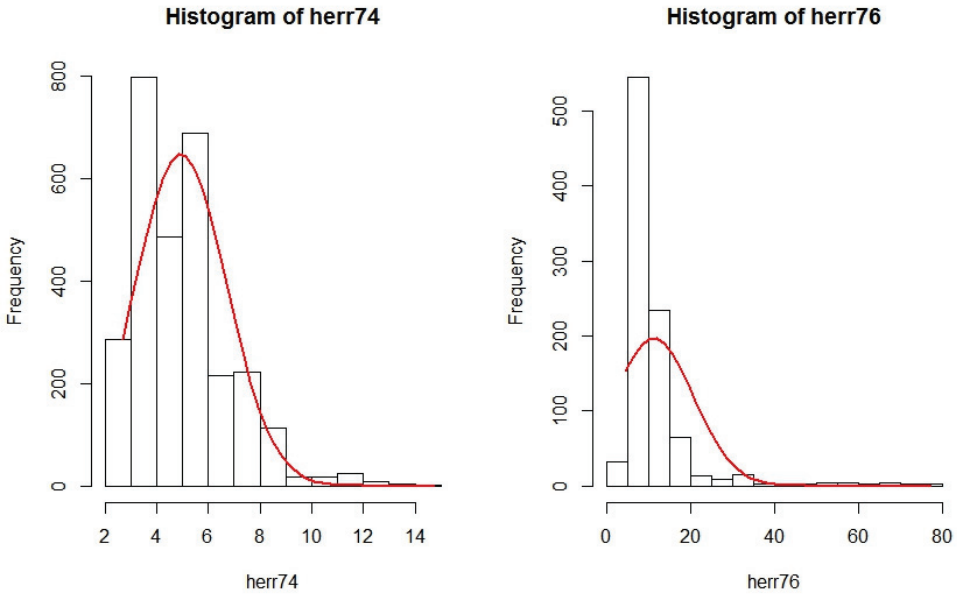

Figure 9 Histograms of horizontal positioning error, days 74 (left) and 76 (right) in 2015

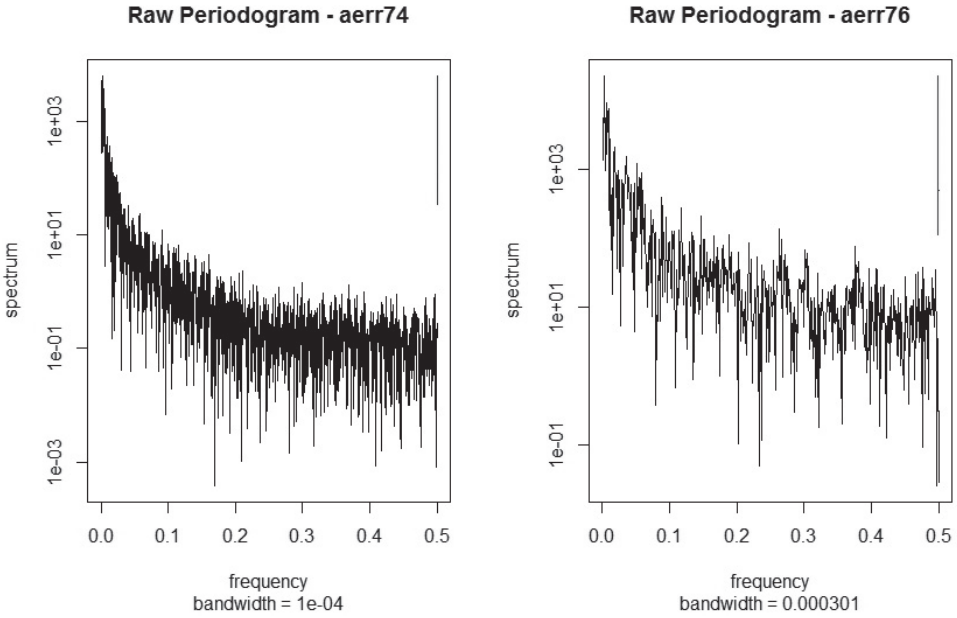

Figure 10 Raw periodograms of PEVB, days 74 (left) and 76 (right) in 2015

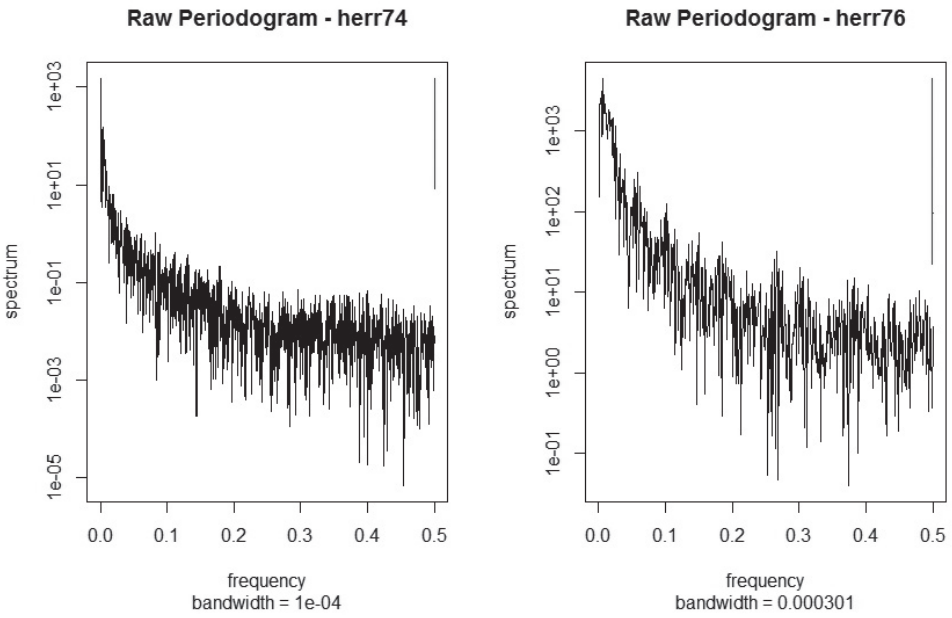

Figure 11 Raw periodograms of the horizontal positioning error, days 74 (left) and 76 (right) in 2015

Current findings call for continuation of the research towards the examination of the opportunities to characterise the other causes of GPS/GNSS positioning deterioration, as well as characterisation of the Quality of Service (QoS) of the GPS/GNSS-enabled applications.

6 CONCLUSION

Growing number of GNSS-based applications require a more thorough description of GNSS positioning performance. Here the Positioning Error Vector Bearing (PEVB) is introduced as a reliable, accurate and efficient indicator of GPS positioning performance. Its value in describing GPS positioning performance and indicating GPS positioning quality deterioration was demonstrated in the case of the 2015 St Patrick's Day geomagnetic storm.

Future work to focus on PEVB dynamics patterns, identifications of the other GPS/GNSS positioning performance deterioration causes, and opportunities to identify developments of GNSS positioning performance deterioration for various applications (incl. personal navigation) from the PEVB time series.

Acknowledgments

The work presented in this manuscript resulted partly from the activities performed within the COST Action TU1302 *Satellite Positioning Performance Assessment for Road Transport*.

REFERENCES

Cannon, P. et al. (2013) Extreme space weather: impacts on engineered systems and infrastructure. Royal Academy of Engineering. London, UK. Available at: http://bit.ly/11OdBNN, accessed on 10 February, 2016.

Davis, K. (1990) Ionospheric Radio. Peter Peregrinus Ltd. London, UK.

Jacobsen, K. S. & Andalsvik, Y. L. (2016) Overview of the 2015 St Patrick's day storm and its consequences for RTK and PPP positioning in Norway. J Space Weater Space Clim, 6, A9, 12 pages. DOI: 10.1051/swsc/2016004

Jin, Sh (editor). (2012) Global Navigation Satellite Systems – Signal. Theory and Applications. InTech. Rijeka, Croatia. Available at: http://www.intechopen.com, accessed on 15 January, 2017.

Petrovski, I. G. (2014) GPS, GLONASS, Galileo and Beidou for Mobile Devices. Cambridge University Press. Cambridge, UK.

Petrovski, I. G. & Tsujii, T. (2012). Digital Satellite Navigation and Geophysics: A Practical Guide with GNSS Signal Simulator and Receiver Laboratory. Cambridge University Press. Cambridge, UK.

R Development Core Team (2017) R: A language and environment for statistical computing. R Foundation for Statistical Computing, Vienna, Austria. ISBN 3-900051-07-0. Available at http://www.r-project.org, accessed on 5 February, 2016.

Sanz Subirana, J. et al. (2013) GNSS Data Processing – Volume I: Fundamentals and Algorithms. European Space Agency (ESA). Nordwijk, The Netherlands. Available at: http://bit.ly/1QV4KAL, accessed on 10 February, 2016.

SaPPART. (2015) Better use of Global Navigation Satellite Systems for safer and greener transport (SaPPART White Paper). COST Action TU1302 Satellite Positioning Performance Assessment for Road Transport (SaPPART). Bruxelles, Belgium. ISBN 978-2-85782-707-8.

Takasu, T. (2013) RTKLIB: An Open Source Program Package for GNSS Positioning. Software and documentation available at: http://www.rtklib.com, accessed on 10 February, 2016.

Thomas, M et al. (2011) Global Navigation Space Systems: reliance and vulnerabilities. The Royal Academy of Engineering. London, UK. Available at: http://bit.ly/1vrIenu, accessed on 10 February, 2016.

Zandbergen, P. A. & Barbeau, S J. (2011) Positional Accuracy of Assisted GPS Data from High-Sensitivity GPS-enabled Mobile Phones. J of Navigation, 64, 381–399.

Sveučilište u Rijeci
POMORSKI FAKULTET U RIJECI
FACULTY OF MARITIME STUDIES RIJEKA
University of Rijeka

University of Zagreb
Faculty of Transport
and Traffic Sciences

Royal Institute of Navigation
Science Technology Practice

10th
Annual
Baška GNSS
Conference

CHARACTERIZATION OF IONOSPHERIC EFFECTS AND INVESTIGATION OF THEIR INFLUENCE ON CURRENT GNSS OBSERVING SYSTEM

Marija Čokrlić[1], Roman Galas[1], Kinga Wezka[1], Norbert Jakowski[2], Mogese Wassaie[3], Baylie Damtie[3]

[1] Technische Universität Berlin, E-mail: marija.cokrlic@tu-berlin.de

[2] German Aerospace Centre – DLR

[3] Bahir Dar University, Ethiopia

Abstract

In Global Navigation Satellite System (GNSS) precise positioning, and especially in real-time, it is crucial to generate messages containing information about permanently varying local state of the ionosphere. Regular variations/changes in ionosphere can be modeled and predicted to a certain extent, whereas irregular ionospheric variations/changes are random and difficult or even impossible to predict.

Technische Universität Berlin (TUB) operates its monitoring station (based on scintillation GNSS receiver Septentrio PolaRxS) in cooperation with Deutsches Zentrum für Luft- und Raumfahrt (DLR), IEEA Paris and Bahir Dar University in Ethiopia where ionospheric anomalies occur more often and are stronger then in the mid-latitude.

For the study presented in this paper, two days,were selected with respect to the global geomagnetic storm index: the one with low- and high geomagnetic activities. Since ionosphere correlates with Earth geomagnetic field, some ionospheric disturbances are expected and detected. Analysis of the ionosphere is done with TUB academic software and influence of the ionosphere onto positioning is presented as well.

Key words: *ionosphere, ionospheric disturbances, TEC, ionospheric scintillation*

1 INTRODUCTION

Ionosphere has critical influence on the trans-ionospheric communication- and navigation systems, and thus it is one of the critical factors that has influence on the Global Navigation Satellite Systems (GNSS). Mitigation of the ionospheric threads is one of the most interesting topics in the research and development area to improve availability, reliability and precision of the GNSS systems.

GNSS signals, passing through the ionosphere, are affected by the free electrons and can be refracted or dispersed. Thus they are carrying ionospheric characteristics and signatures that can be isolated and studied. Because of that and of the relatively low cost of the GNSS receivers, and availability of the data from the already existing continuously operating reference GNSS networks, studying and monitoring of the ionosphere on a global scale and with high spatial- and time resolution become available. From the other side, ionospheric perturbations can degrade accuracy of the positioning for more than hundred meters and even make the PVT (position, velocity and time) estimations impossible or false. Thus information about the state of the ionosphere must be available in real time to enhance availability and to improve navigation accuracy.

We are developing software tools to derive magnitudes of those ionospheric parameters in a very challenging real-time single station mode. Some of the modules, like e.g. calculation of amplitude scintillation index S4, Total Electron Content (TEC) and Rate of TEC (ROT), are already validated and some others, like phase ($\sigma\varphi$) scintillation index, are still in the testing phase. The tools are needed in order to detect and to analyse ionospheric perturbations in real- or near- real time and to investigate if some new approaches for generation of navigation-corrections can be developed. Our main goal is to provide such corrections or at least warning messages on ionospheric irregularities, for near-real-time (or even real-time) single user receiver based processing, like e.g. single station PPP (Precise Point Positioning).

2 TUB-NAVSOLUTIONS ACADEMIC SOFTWARE – IONOTOOLS MODULE

The TUB-NavSolutions GPS university software suite is continuously developing and upgrading. The Software contains several modules, from the pre-processing based on the zero-differenced observables, over single point-positioning to relative positioning (baseline and network solution with undifferenced code- and carrier phase observables). Recently the "ionoTools" module is developed, implemented and it is still upgrading (Čokrlić & Galas 2013).

As an exchange format between the raw data and our processors we are using T-BinEx (Galas & Kohler 2001) binary format developed at Deutsches GeoForschungsZentrum (GFZ) and upgraded at the TUB for ionospheric purposes. Data in proprietary formats of the TOPCON/JAVAD-, NovAtel- and Septentrio receivers as well as in the RINEX are accepted on the input to the T-BinEx converter. Output of the T-binex is standard input for TUB-NavSolutions and the "ionoTools" processor:

- S4 processor for calculating amplitude scintillation,
- TEC (Total Electron Content) processor for calculate carrier phase TEC levelled using code observations,
- ROT (Rate of change of TEC) processor for calculating ROT index, and
- σφ processor for calculating phase scintillation is tested and under implementation.

For easy identification and detection of sudden ionospheric disturbances, the outputs are plotted with Python scripts (Figure 1). All outputs:

- T-BinEx data,
- S4,
- ROT,
- TEC, and
- σφ.

Files, together with the plots are stored in archives. Our algorithms and results were validated with commercial Septentrio software at the station operated at TUB. The "ionoTools" is ready to process in a uniform way data recorded with various precise GPS receivers.

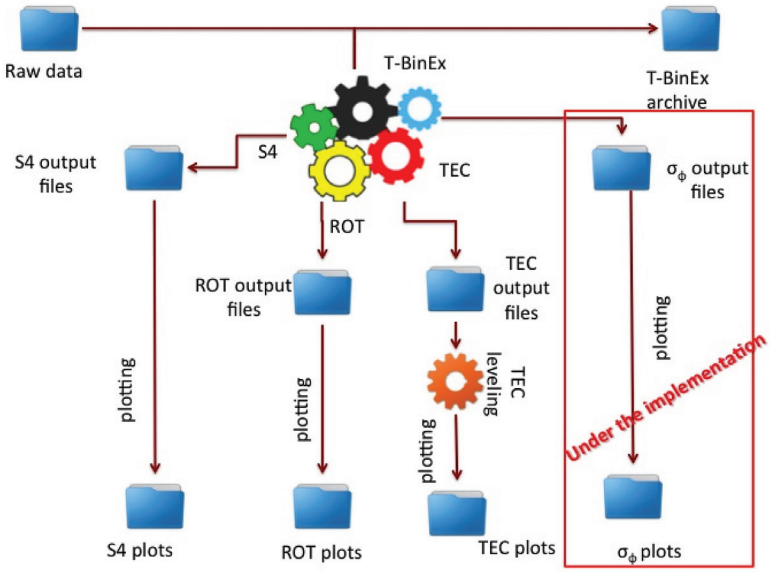

Figure 1 Architecture of TUB-NavSolutions "ionoTools" module

3 SINGLE STATION TEST BED

TUB established a low-maintenaince GNSS continuously operating station in Bahir Dar, Ethiopia. The station is operated in close cooperation with DLR, IEEA and Bahir Dar University in order to study ionospheric gradients in equatorial region. Approximate positions of the stations are depicted in the Figure 2.

TUB station is configured for ionospheric scintillation monitoring:

- currently the code- and carrier phases observables are recorded in 1Hz sampling rate, and
- the I- and Q-amplitudes are recorded with 50Hz sampling rate.

The GNSS data selected for the analysis has been gathered during two days (Figure 3):

- 5th March 2015: with low geomagnetic activities (with Kp index around 2), and
- 17th March 2015: high geomagnetic activities, with Kp index around 8, so called St. Patrick storm.

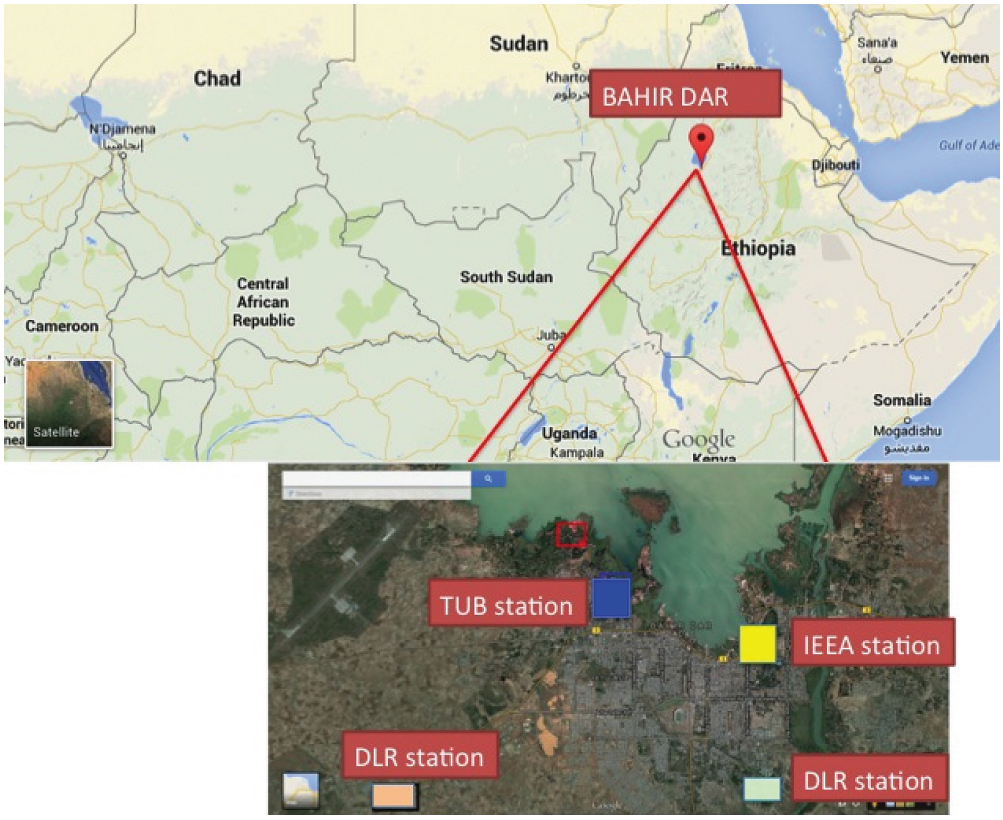

Figure 2 GNSS array being set-up in cooperation with DLR, IEEA and TUB in Bahir Dar, Ethiopia

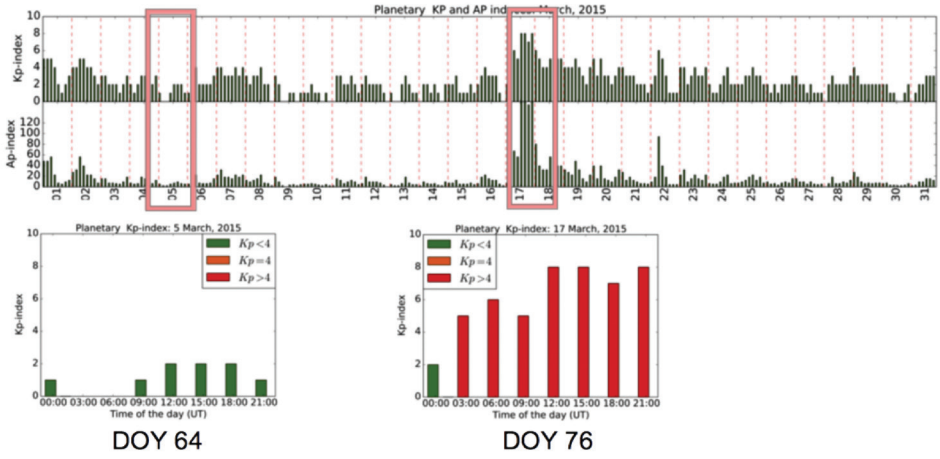

Figure 3 Kp and Ap indices for March 2015

4 RESULTS

Those two selected days of observations gathered in equatorial region have been processed with our TUB-NavigationSolutions software. Some results from specific satellites are presented below in the Figures 4 to 8.

In Figure 4 amplitude scintillation index, ROT and levelled TEC (Jakowski et al., 2011) for satellite PRN 10 on 5th March 2015 when Kp index did not exceed value of 2 are displayed. At approximate 14:00 hours all three displayed values of parameters show disruption.

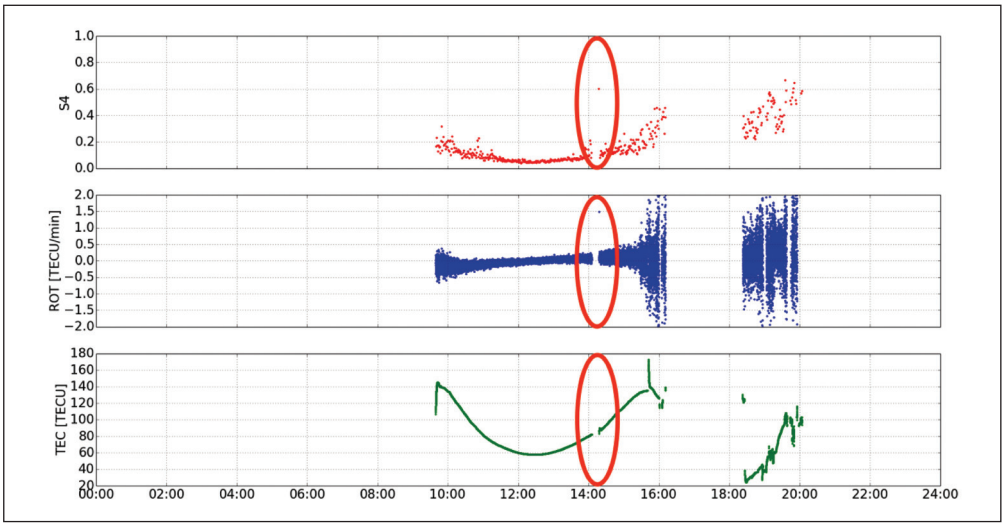

Figure 4 Amplitude scintillation (S4), ROT and TEC for satellite PRN10. Observed at DOY 64 2015 (5th March 2015) at TUB station in Bahir Dar, Ethiopia

Since amplitude scintillation happens suddenly and last for short period of time (couple of seconds), and irregularities we can observe in both, ROT and TEC, we can say scintillation happened at that time.

In the Figure 5 values for the same parameters at the same day for the satellite with PRN 25 are shown. Short period before 20:00 hours and around 22:00 hours in all three plots we can observe ionospheric irregular behaviour and disturbance. In the time series of all values some medium scale-(red circle) and small scale (green circle) travelling ionospheric disturbances (MSTIDs and SSTIDs) are identified lasting from couple of tens of minutes till couple of minutes (Hernandez-Pajarex et al. 2006)

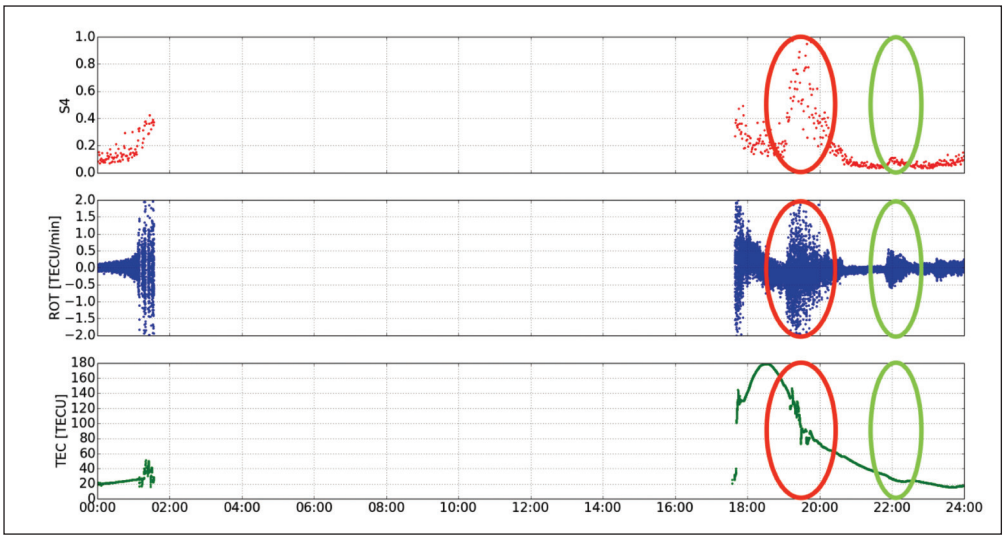

Figure 5 Amplitude scintillation (S4), ROT and TEC for satellite PRN25. Observed at DOY 64 2015 (5th March 2015) at TUB station in Bahir Dar, Ethiopia

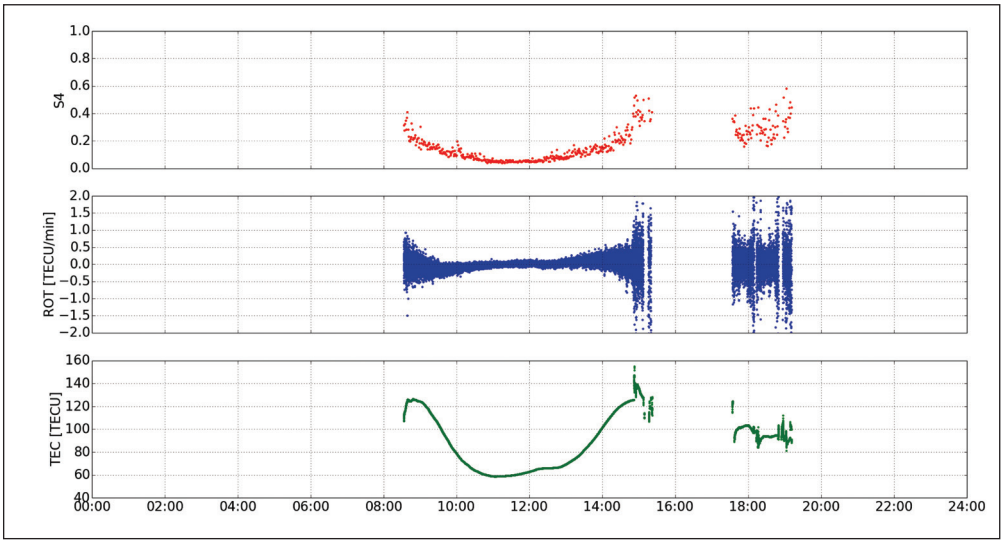

Figure 6 Amplitude scintillation (S4), ROT and TEC for satellite PRN10. Observed at DOY 76 2015 (17th March 2015) at TUB station in Bahir Dar, Ethiopia

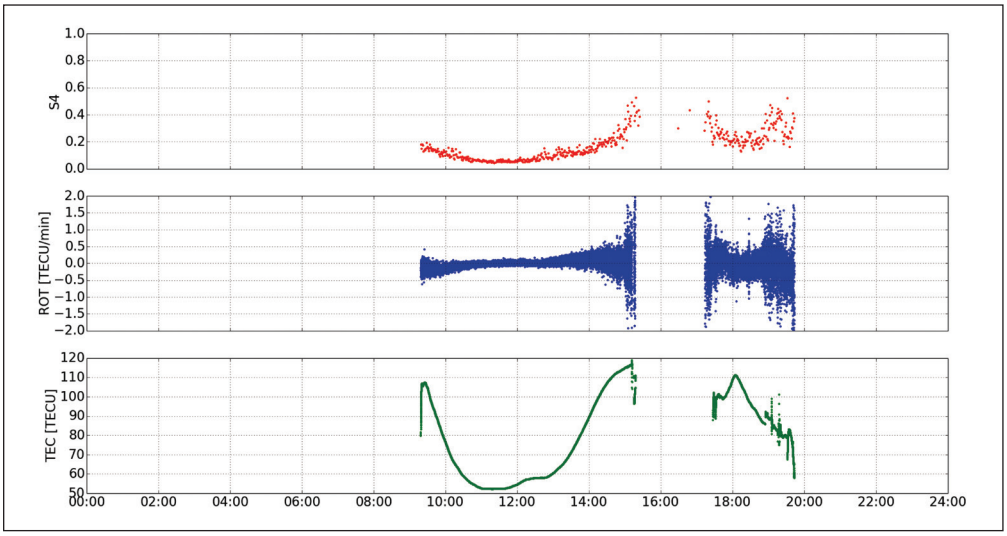

Figure 7 Amplitude scintillation (S4), ROT and TEC for satellite PRN20. Observed at DOY 76 2015 (17th March 2015) at TUB station in Bahir Dar, Ethiopia

Figure 6 and Figure 7 the same values for 17th March 2015 when Kp index was around 8. Figure 6 displays values for satellite with PRN 10 and Figure 7 for satellite with PRN 20. In the both figures no unusual in the ionospheric behaviour can be seen, however we expected perturbations since Kp index was high.

Figure 8 shows amplitude scintillation index S4 for both days: 5th March 2015 (top) and 17th March 2015 (bottom). As expected (equatorial region and sunset period), amplitude scintillation is visible in equatorial region and it is evident at sunset period (Beniguel et al. 2011). It is clear that the most amplitude scintillation events happened on 5th March, while on 17th March 2015 we can observe "normal" amplitude scintillation for the equatorial region.

Figure 9 and 10 show pseudo-kinematic solution on the short- and long baseline. Short baseline (Figure 9) is calculated with IGS TANA station recently established in Bahir Dar and on approximate distance of 14 km from TUB station. With blue colour it is displayed solution from 5th March and red colour represents solution from 17th March 2015. Long baseline (Figure 10) is calculated with IGS station ADIS located in Addis Ababa on approximate distance from TUB station of 318 km.

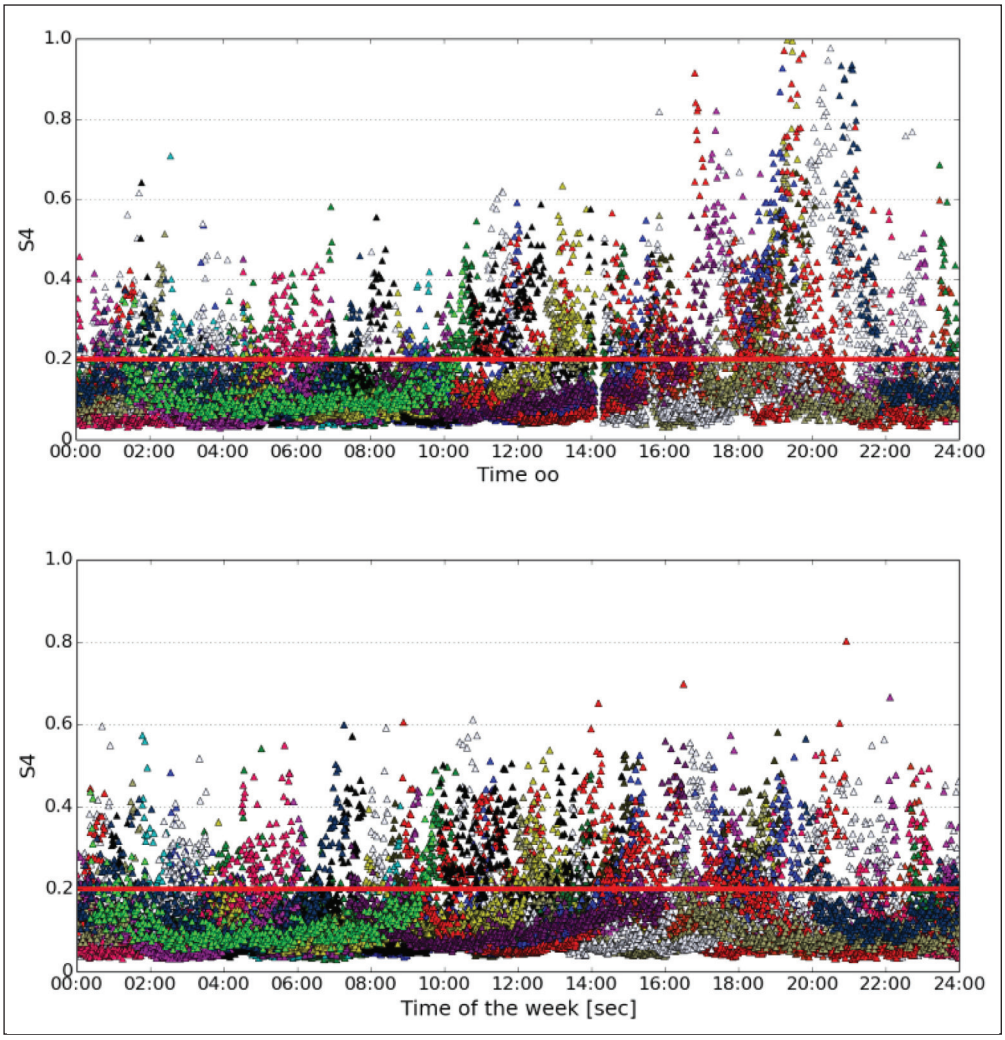

Figure 8 Amplitude scintillation index S4 for DOY 64 (top) and DOY 76 (bottom), 2015 for all satellites at the TUB station in Bahir Dar, Ethiopia

On both figures problems with ambiguity fixing appears shortly after 15:00 hours on the 5th March (DOY 64). The same day we observed high amplitude scintillation and TIDs. Source of the degradation after 9:30 hours is not clear yet and will be investigated. On the 17th March (DOY 76) we are not facing problems with ambiguity fixing like on 5th March.

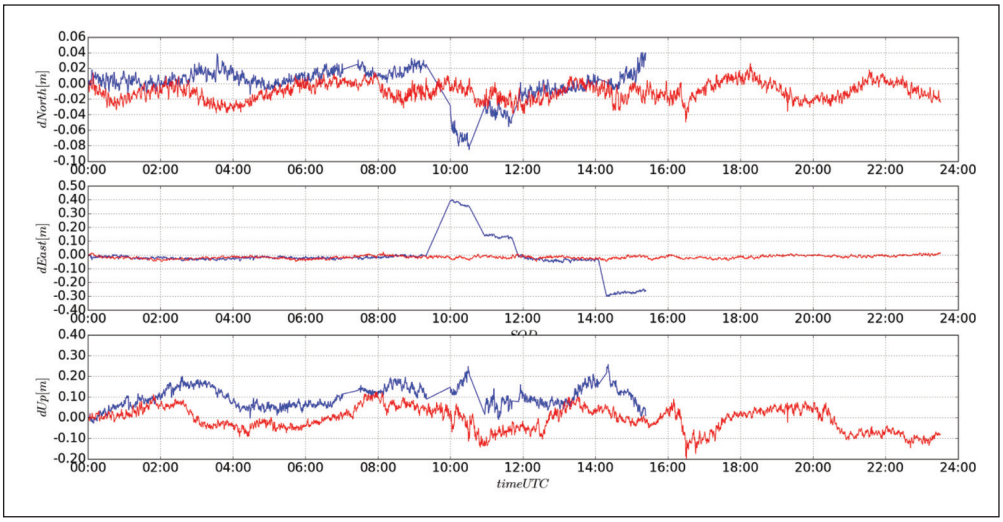

Figure 9 Pseudo-kinematic solution on the baseline TANA(IGS)-TUBD (around 14km) data from the TANA station for DOY 064 are available only from 00:00- 15:28. Blue line represents the day 064, Kp around 2 and S4 index (after 18:00) higher than 6 and red line day 076, Kp around 8 and S4 index is all day lower than 6.

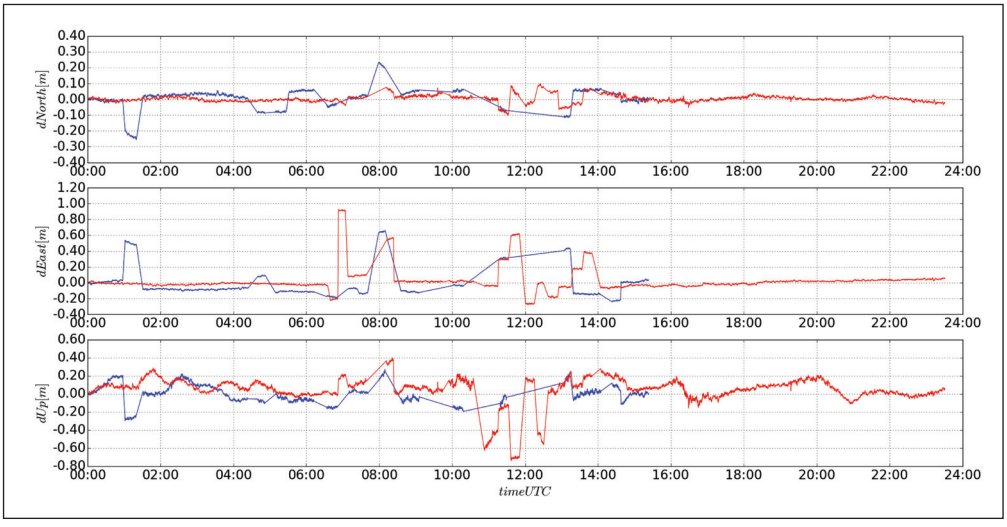

Figure 10 Pseudo-kinematic solution on the baseline ADIS(IGS)-TUBD (around 318km) data from the ADIS station for DOY 064 are available only from 00:00- 15:28. Blue line represents the day 064, Kp around 2 and S4 index (after 18:00) higher than 6 and red line day 076, Kp around 8 and S4 index is all day lower than 6.

5 CONCLUSIONS AND FORTHCOMING ACTIVITIES

We were expecting "anomalies" due to the known correlation of geomagnetic activities with ionospheric disturbances during the 17th March (DOY 76) 2015. However, at the day with lower Kp index (around 2) amplitude scintillation is higher than for the day with higher Kp index (around 8). Those high amplitude scintillations and TIDs could be source of the observed difficulties in fixing carrier phase ambiguities in the Figure 9 and Figure 10. Further, source of poorly fixed ambiguities. Source of the problems in tracking, ambiguity fixing and degradation of the position quality could be ionospheric disturbances. Comparison of the solutions is given in the Table 1.

Table 1 Comparison of two solutions for quiet and disturbed days

Baseline	DOY	N [cm]	E [cm]	U [cm]
Short	64	[+4, -8] |12|	[+40,-30] |70|	[+20,0] |20|
	76	[+2, -4] |6|	~0	[+10,-20] |30|
Long	64	[+20,-30] |50|	[+60,-20] |80|	[+20,-30] |50|
	76	[+10, -10] |20|	[+90,-20] |110|	[+40,-80] |120|

Further raw data analysis is required in order to separate influence of ionospheric scintillation and other effects onto performance of positioning and to investigate surprising results from the comparison of the both days.

Acknowledgments

Part of this research is funded by the FP7 People Programme through the Marie Curie Initial Training Network TRANSMIT – Training Research and Applications Network to Support the Mitigation of Ionospheric Threats.

In addition, acknowledgments are given to Space Weather Application Center Ionosphere (SWACI) operated by German Aerospace Center (DLR) in Neustrelitz.

REFERENCES

Beniguel, Y., Adam, J.-P., Bourdilon, A. & Lassudrie-Duchesne, P. (2011) Ionosphere scintillation effects on navigation systems, Comptes Rendus Physique, vol. 12, pp. 186–191.

Čokrlić, M. & Galas, R. (2013) TUB software tools for monitoring ionospheric irregularities in a single station mode and first results. *Proceedings of the 7th European Conference on Antennas and Propagation (EUCAP 2013)*, Gothenburg, Sweden.

Dierendnock, A. J., Klobuchar, J. & Quyena, H. (1993) Ionospheric scintillation monitoring using commercial single frequency CA code receivers, In Proceedings on the 6th *International Technical Meeting of the Satellite Division of the Institute of Navigation*, ION GPS-93, pp. 333–344.

Galas, R. & Kohler, W. (2001) A binary exchange format for GPS data, Phys. and Chem. Earth, vol. 26, no. 6–8, pp. 645–648.

Hernandez-Pajares, M., Juan, J. M. & Sanz, J. (2006) Medium-scale traveling ionospheric disturbances affecting GPS measurements: Spatial and temporal analysis, Journal of Geophysical Research, vol. 111.

Jakowski, N., Mayer, C., Hoque, M. M. & Wilken, V. (2011) Total electron content models and their use in ionosphere monitoring, Radio Science, vol. 46, pp. 1–11.

Sveučilište u Rijeci
POMORSKI FAKULTET U RIJECI
FACULTY OF MARITIME STUDIES RIJEKA
University of Rijeka

University of Zagreb
Faculty of Transport
and Traffic Sciences

Royal Institute of Navigation
Science Technology Practice

10th
Annual
Baška GNSS
Conference

SATELLITE POSITIONING ERROR MODEL FOR LOCATION – BASED SERVICES

Marin Anđelini, Andrea Lučić, Renato Filjar

Faculty of Engineering, University of Rijeka, Rijeka, Croatia
E-mail: marin.andelini@gmail.com

Abstract

The essence of the location-based services is satellite positioning quality. The errors in satellite positioning are having a direct impact on quality of those services. Among others factors, the Total Electron Content (TEC) in ionosphere is having a big impact on satellite positioning errors. Intensity of Earth's magnetic field affects the electron density in ionosphere, and thus affects the satellite positioning error. By utilisation of methods of statistical analysis and learning, data mining and machine learning, data collected from the reference stations on Earth are transformed into valuable information, thus creating knowledge which is used for decreasing or eliminating the errors in satellite positioning. R and Rattle are emerging as very good tools for data mining for their data analysis possibilities and building of the mathematic models. Error models suggested in this paper are minimising the satellite positioning error, and thus help to maintain and raise the quality of the location-based services.

Key words: *error model, geomagnetic activity, ionospheric delay, total electron content*

1 INTRODUCTION

Contemporary mobile telecommunication networks are offering the base for a number of telecommunication services that are in relation to user's position. Quality positioning is the basis of the quality location-based service. The most common positioning method is a satellite positioning. In satellite positioning an error is accepted, as it is a measurement procedure. What is measured is time needed for a satellite message to be transmitted from the satellite to be received on user's receiver. Ionosphere, as the medium through which this message travels, has the biggest impact on this measurement error. Electron density in ionosphere affects the ability of the satellite signal to breach through it, slowing the signal and thus prolonging the measured time. The way to completely overcome the impact of ionosphere on a satellite positioning is not yet discovered.

As one of the factors that cause ionospheric delay, the impact of the Earth's geomagnetic field is also not completely explored and clear.

The problem and a brief overview of the existing solutions are described in chapter 2. In chapter 3 we present the methods and solution for the problem. The results are explained in chapter 4. Chapter 5 contains the discussion of the results. Conclusion of the work is presented in chapter 6.

2 PROBLEM DESCRIPTION

To overcome the satellite positioning error, the goal is to predict what is the size and type of the error in case the external factors are in a certain state, and correct it. That way, the intelligent system is created, that knows how to reduce the impact of external factors to a satellite positioning.

Some solutions that are more or less reducing the impact the ionospheric delay is having on a satellite positioning are Klobuchar model, NeQuick and EGNOS' ionospheric model. GPS uses Klobuchar model, which corrects about the 50% of the ionospheric range delay (Royal Academy of Engineering, 2001). The problem of Klobuchar's model are anomalies in ionosphere. Galileo uses NeQuick as the ionospheric model (Subirana, Zornoza, Hernandez-Pajares 2013), while EGNOS' ionosphere model optimizes accuracy and integrity by correcting the errors in specific points of the imaginary mesh over the Europe (ESA 2016).

The ionospheric model has to take many factors into account to make a good prediction of the error. Electron density is something that is an input to ionospheric model. The question is what other factors are affecting the changes in electron density in ionosphere. Earth's geomagnetic field is one of them. The problem is to find out how much, and how geomagnetic field affect the TEC, and what effect is this having on the satellite navigation.

3 ERROR MODEL

The goal was, by utilization of methods of statistical analysis and learning in R and Rattle, to develop a satellite positioning error categorization model. The data used was geomagnetic indices from geomagnetic reference station in Grocka, Serbia, the TEC measurements and the actual satellite positions error measurement, gathered from the reference station in Dubrovnik, Croatia.

The actual error data consists of the error in north direction, error in east direction, and height error. Error in east and north directions were combined into single horizontal error and categorized.

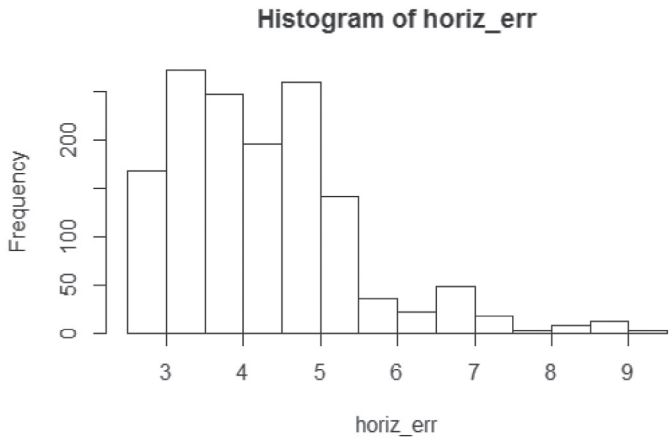

Figure 1 Horizontal error histogram with x axis showing error in meters

Table 1 Categorization of the horizontal errors

Error interval (m)	Categorical value of the error	Number of occurrences by a category
< 2	Very small	0
[2, 4)	Small	687
[4, 6)	Medium	633
[6, 8)	Big	90
> 8	Very big	22

New variable (horizontal error), along with TEC and geomagnetic indices, was used to build the models, using different algorithms. Models were compared and the best were chosen between them.

The outputs of the analysis and modelling are models, error matrix and other numerical quality parameters generated by testing and validation of the models in Rattle, and in the end, analysis and interpretation of the models and their quality.

4 RESULTS

From the correlation analysis, it is obvious that the error is in linear correlation with geomagnetic indices.

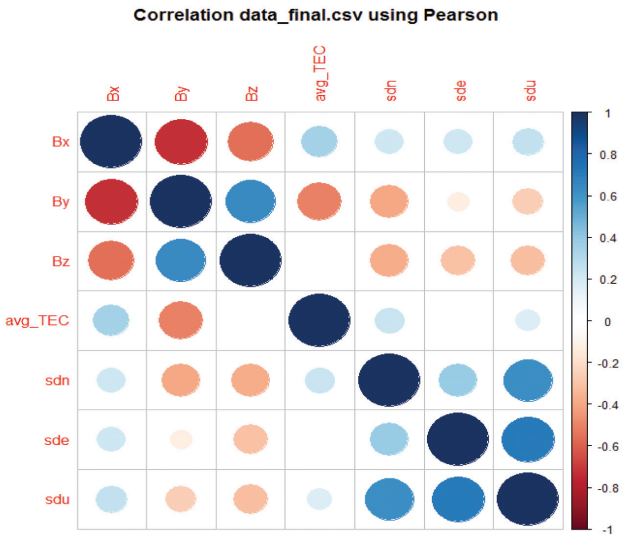

Figure 2 Correlation diagram – Pearson's method (Bx,By,Bz are geomagnetic indices and sdn, sde, sdu are errors in north, east and vertical direction, respectively)

Final error prediction model has the overall error of 6%, but has 80% wrong choices for "very big" errors.

Out-of-the-bag (OOB) estimation showed total error of 7.75%.

Error matrix for the Random Forest model on data_final_horiz_cat.csv

	Predicted				
Actual	small	medium	big	very big	Error
small	0.41	0.00	0.00	0	0.01
medium	0.02	0.47	0.01	0	0.06
big	0.00	0.00	0.06	0	0.07
very big	0.02	0.00	0.00	0	0.80

Overall error: 6%, Averaged class error: 24%

Figure 3 Error matrix

5 DISCUSSION

Intensity of Earth's magnetic field affects the electron density in ionosphere, and thus affects the satellite positioning error.

The 6% total error in model's prediction show great overall accuracy, but the 80% error in predicting "very big" errors is not a satisfying fact. In Table 1, we see that there are very little "very big" errors in the input data, and that could be the reason of lack of accuracy in this horizontal error category, because model could not be "trained" well for this horizontal error category. If similar distribution of errors is common, then this model has very acceptable accuracy, since there were less than 1% of "very big" error in the dataset. Also, the categories of the horizontal error could have been arranged differently, and then the result might be different.

Evaluation of the quality of final model depends on application. In Table 2, we see how high positioning accuracy are needed for road transport applications. For those applications that demand low, or even a medium accuracy, this model can be suitable. For applications that demand high or very high accuracy, this model might not be reliable and robust enough.

Table 2 Road transport demands (Royal Academy of Engineering 2001)

Road transport application	Accuracy
In-car navigation	Low
Selective vehicle priority	Low
Dynamic route guidance	Low
Emergency calls	Low
Fleet management	Medium
Urban traffic control	Medium
Collision avoidance	Medium
Road pricing	Medium
Automated motorway	High
Lane control	Very high
Intelligent speed assistance	Very high

6 CONCLUSION

The analysis showed geomagnetic indices' effect on the satellite positioning error. Final model that was developed using Rattle and R gave good results and can be useful in some applications that do not require high positioning accuracy. In case the input data is truthfully representing the everyday situation, with some rearrangement of the horizontal error categories or their intervals, this model can be used in many applications.

For future work, the model needs to be tested on a larger dataset to check its robustness and then rebuilt if needed.

REFERENCES

European Space Agency (ESA). (2005) EGNOS Fact Sheet. 2: The Ionosphere explained.

Subirana, J. S., Zornoza J. J. & Hernandez-Pajares, M. (2013) GNSS Data Processing, Vol. I: Fundamentals And Algorithms. Noordwijk: ESA Communications.

Thomas et al. (2011) *Global Navigation Space Systems: reliance and vulnerabilities*. London: Royal Academy of Engineering.

Sveučilište u Rijeci
POMORSKI FAKULTET U RIJECI
FACULTY OF MARITIME STUDIES RIJEKA
University of Rijeka

University of Zagreb
Faculty of Transport
and Traffic Sciences

Royal Institute of Navigation
Science Technology Practice

10th
Annual
Baška GNSS
Conference

APPROACHES TO GLONASS TIME ACCURACY IMPROVEMENT

**Petr Bogdanov, Andrei Druzhin,
Tatiana Primakina, Aleksandr Feoktistov**

Russian Institute of Radionavigation and Time, Saint-Petersburg, Russia
E-mail: ser_jey_ant@mail.ru; bogdanov_pp@rirt.ru

Abstract

GLONASS Time is a continuous "paper" time scale which is formed on the basis of GLONASS Main and/or Reserved Central Synchronizers. GLONASS Time is referenced to Russian national time scale UTC(SU) which is generated by State Time and Frequency Reference (STFR). The main approaches used to increase the accuracy of GLONASS Time formation and its synchronization to UTC(SU) are: to increase accuracy characteristics of Central Synchronizers, to increase the accuracy of GLONASS Time synchronization to UTC(SU), and to decrease the error of broadcast to users corrections to GLONASS Time relative to UTC(SU).

Key words: *GLONASS Time, time offset, Central Synchronizer, correction, relative frequency error, synchronization*

1 INTRODUCTION

To provide high-accuracy determination of position, velocity and time for land, marine, air and other kinds of users time scales of all GLONASS space vehicles (SV) are synchronized to GLONASS Time and GLONASS Time is synchronized to Reference Time. National time of Russia UTC(SU) generated by State Time/ Frequency Reference (STFR) is used as GLONASS Reference Time.

Now the accuracy of broadcast GLONASS Time and UTC (SU) meet specified requirements. However, for professional users it is not satisfactory as compared with GPS.

The paper presents the main principles of GLONASS Time generation and its synchronization to UTC(SU) as well as the main approaches that can increase the accuracy of broadcast GLONASS Time and UTC(SU).

2 GLONASS TIME GENERATION

GLONASS Time is generated as a continuous "paper" time scale on the basis of the Main and/or Reserved Central Synchronizers (CS) using the following equation (Bandura, Bogdanov & German 2016):

$$\begin{aligned} \Delta T_{GL}(t) &= \Delta T_{M}(t) + \Delta T^{ph}{}_{M}(t_i) + \Delta T^{fr}{}_{M}(t_j) - \Delta T^{c}(t) = \\ &= \Delta T_{R}(t) + \Delta T^{ph}{}_{R}(t_k) + \Delta T^{fr}{}_{R}(t_l) - \Delta T^{c}(t) - \Delta T_{M-R}(t), \end{aligned} \tag{1}$$

where $\Delta T_{GL}(t)$ – GLONASS Time offset relative to UTC(SU), $\Delta T_{M}(t)$, $\Delta T_{R}(t)$ – Main/Reserved CS time offset relative to STFR time, $\Delta T^{ph}{}_{M}(t_i)$, $\Delta T^{ph}{}_{R}(t_k)$ – corrections for Main/Reserved CS phase steering, $\Delta T^{fr}{}_{M}(t_j)$, $\Delta T^{fr}{}_{R}(t_l)$ – corrections for Main/Reserved CS frequency steering, $\Delta T^{c}(t)$ – correction for controlling GLONASS Time – UTC(SU) offset, $\Delta T_{M-R}(t)$ – offset between Main and Reserved CS time scales.

The main advantage of this GLONASS Time generation method is the simplicity of GLONASS Time generation monitoring. Accuracy characteristics of GLONASS Time generated by this method are completely in compliance with CS accuracy characteristics. Reliability of generated GLONASS Time is provided by backup CS.

Central Synchronizers provide the following accuracy characteristics:

- relative frequency error $\Delta f/f$ below $3 \cdot 10^{-14}$;
- daily frequency instability below $2 \cdot 10^{-15}$.

The backbone of CS is Frequency/Time Keeping Facility (FTKF) including four active Hydrogen Frequency Standards (HFS), a system for internal comparisons and a system for steering frequencies and phases of signals from HFS. HFS which provides the best accuracy characteristics on the results of internal comparisons becomes master standard, the others operate as secondary.

CS time scale is corrected simultaneously with UTC leap second corrections by ± 1 s and, as a result, there is no whole second time offset between GLONASS Time and UTC(SU). However, there is a 3-hour constant offset between GLONASS Time and UTC(SU) due to GLONASS Terrestrial Control Complex operational principles.

Till August 2014 GLONASS Time – UTC(SU) offset was about 400 ns. It met specified requirements but was not satisfactory for time users.

Therefore, on 18th August, 2014 the value of controlling correction $\Delta T^{c}(t)$ was changed to increase the accuracy of GLONASS Time – UTC(SU) synchronization. To keep the specified accuracy of SV – GLONASS Time synchronization the value of daily correction change was 3 ns.

The results of monitoring proved the efficiency of the controlling correction change: GLONASS Time – UTC(SU) offset changed from 392.2 ns (19.08.2014) to 24.4 ns (31.08.2014).

Now the offset of GLONASS Time relative to UTC(SU) is kept within 25 ns.

GLONASS Time – UTC(SU) offset on April 30, 2016 is presented in Figure 1.

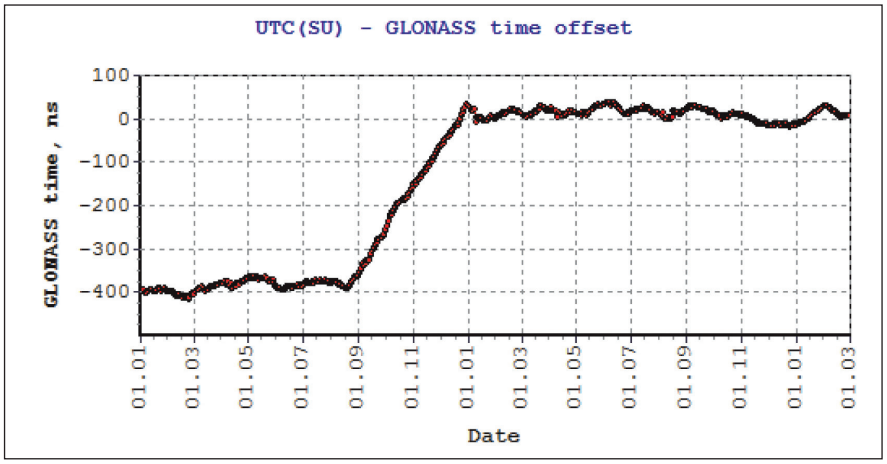

Figure 1 UTC(SU) – GLONASS Time offset

3 GLONASS TIME SYNCHRONIZATION TO UTC(SU)

The offset between STFR and CS time scales is calculated on the basis of their mutual comparisons by the signals from SVs of GLONASS and GPS in differential mode with using "all-in-view" method in accordance with the following equation (Bogdanov & Primakina 2015):

$$\Delta T_{STFR-CS} = \Delta T_{GL(GPS)-CS} - \Delta T_{GL(GPS)-STFR} \quad (2)$$

where $\Delta T_{STFR-CS}(t)$ – CS time scale offset relative to STFR time scale, $\Delta T_{GL(GPS)-CS}(t)$ – CS time scale offset relative to GLONASS/GPS Time, $\Delta T_{GL(GPS)-STFR}(t)$ – STFR time scale offset relative to GLONASS/GPS Time.

Now the error of calculating Main CS – STFR time scale offset is about 8 ns (rms), Reserve CS – STFR time offset 13 ns (rms).

The large error of CS – STFR time offset calculated by GLONASS signals is mostly caused by using Time Transfer Unit (TTU) with single-frequency GLONASS/GPS receiver at CS.

Data on the results of CS – STFR time comparisons by GLONASS/GPS signals are daily transferred to the GLONASS System Control Center where they are used for generating GLONASS Time and calculating corrections to GLONASS Time relative to UTC(SU) which are further uploaded and broadcast to users in navigational signals.

Till August 2014 the error of broadcast corrections for GLONASS Time – UTC(SU) offset contained a systematic component of approximately 200 ns. Therefore, on 18th August, 2014 the generated corrections to GLONASS Time were also changed.

Now the error of broadcast corrections for GLONASS Time – UTC(SU) offset does not exceed 10 ns (rms).

UTC(SU) broadcast by GLONASS is presented in Figure 2.

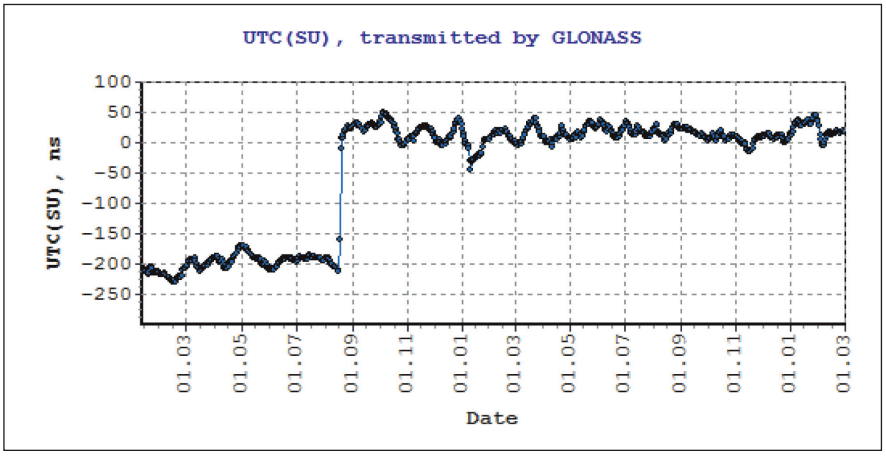

Figure 2 UTC(SU), transmitted by GLONASS

So, now GLONASS provides users with timing service referenced to UTC(SU) with the error below 35 ns without using the broadcast corrections to GLONASS Time and below 10 ns with using the corrections.

4 IMPROVEMENT OF GLONASS TIME GENERATION AND SYNCHRONIZATION TO UTC(SU)

The main approaches used to increase the accuracy of GLONASS Time generation and its synchronization to UTC(SU) are:

- to increase CS accuracy characteristics;
- to increase the accuracy of GLONASS Time synchronization relative to UTC(SU);

- to decrease the error of broadcast to users corrections to GLONASS Time relative to UTC(SU).

The second and the third approaches are going to be realized, first of all, by increasing the accuracy of CS–STFR time scales comparison, so it is planned:

- at the 1st stage to install similar calibrated GLONASS/GPS time receivers at STFR and CS. It can provide the accuracy of calculating time scales offset of about 3 ns;
- at the 2nd stage to use time transfer facilities on the basis of duplex communication links with using satellites in geosynchronous orbits. It can provide the accuracy of about 1 ns.

To eliminate systematic error component of time scale comparisons it is planned to use laser technologies to calibrate the receivers.

5 CONCLUSION

Now the accuracy of GLONASS Time and UTC(SU) broadcast to users meets specified requirements.

As a result of the proposed approaches the following accuracy characteristics of broadcast GLONASS Time and UTC(SU) are planned to be achieved by 2020:

- GLONASS Time – UTC(SU) offset below 4 ns;
- the error of broadcast corrections to GLONASS Time below 2 ns.

REFERENCES

Bandura, A.S., Bogdanov, P. P. & German, E. (2016) Application of New Time Receivers in GLONASS [in press]. Proceedings of the 30th European Frequency and Time Forum. York, UK: EFTF.

Bogdanov, P. & Primakina, T. (2015) GLONASS Time Scale. Proceedings of the 22nd Saint Petersburg International Conference on Integrated Navigation Systems. Saint-Petersburg, Russia: IEEE. pp. 422–428.

Technical co-sponsors

Media coverage